Stony Brook University

The Role of Laminin- Dystroglycan Interactions in the Development and Function of the Blood-Brain Barrier

A Dissertation Presented

by

Michael John Menezes

to

The Graduate School

In Partial Fulfillment of the

Requirements

for the Degree of

Doctor of Philosophy

In

Physiology and Biophysics

Stony Brook University

May 2015

Stony Brook University

The Graduate School

Michael John Menezes

We, the dissertation committee for the above candidate for the

Doctor of Philosophy degree, hereby recommend

acceptance of this dissertation.

Holly A. Colognato, Ph.D. – Dissertation Advisor
Associate Professor, Department of Pharmacological Sciences
Stony Brook University

Raafat El-Maghrabi, Ph.D.– Chairperson of Defense
Research Associate Professor, Department of Physiology and Biophysics
Stony Brook University

Thomas W. White, Ph.D.
Professor, Department of Physiology and Biophysics
Stony Brook University

Styliani-Anna E. Tsirka, Ph.D.
Professor, Department of Pharmacological Sciences
Stony Brook University

This dissertation is accepted by the Graduate School.

Charles Taber
Dean of the Graduate School

The Role of Laminin- Dystroglycan Interactions in the Development and Function of the Blood-Brain Barrier

by

Michael John Menezes

Doctor of Philosophy

in

Physiology and Biophysics

Stony Brook University

2015

The blood-brain barrier (BBB) is a multicellular integrative system that provides a protective interface between the circulatory system and the central nervous system (CNS), serving as a key regulator of neuronal function and physiological homeostasis. At the gliovascular interface, endothelial cells, astrocytes and pericytes are encased in a network of extracellular matrix (ECM) that forms a basal lamina (BL) comprised of ECM secreted by each cell type. Laminins are major constituents of the gliovascular BL where they bind dystroglycan, an adhesion receptor distributed along astrocytic endfeet and the abluminal membrane of endothelial cells. However, the contribution of laminin and dystroglycan to the development and function of the BBB remains unclear. To gain insight into how ECM interactions at the gliovascular interface contribute to BBB development we: (1) inactivated the LAMA2 gene to selectively eliminate

laminin-211 from all cells of the developing brain, and (2) inactivated the DAG1 gene that encodes dystroglycan in neural lineage cells such as astrocytes and neurons. We identified laminin-211 and dystroglycan as novel regulators of the selective permeability of the BBB. We found that LAMA2 and DAG1 expression contribute to the acquisition of cerebrovascular pericyte coverage in the developing brain, functional tight junction morphology, adherens junction composition, and multiple aspects of gliovascular cell-cell and cell-ECM interactions, including glial endfeet architecture. Our findings suggest that laminin-dystroglycan interactions at the gliovascular interface regulate the maturation and function of the BBB. These findings also provide insight into the cellular and molecular changes that occur as a consequence of congenital muscular dystrophies caused by LAMA2 mutations or inappropriate dystroglycan post-translational modifications, which have accompanying brain abnormalities including seizures. Our results indicate a novel role for laminin-dystroglycan interactions in the cooperative integration of endothelial cells, astrocytes, and pericytes in regulating the BBB.

Table Of Contents

List of Figures

List of Abbreviations

α-SMA	alpha-Smooth Muscle Actin
aβ	amyloid beta
AQP4	aquaporin 4
BBB	blood-brain barrier
BEC	brain endothelial cell
BL	basal lamina
BM	basement membrane
BME	beta-mercaptoethanol
CC3	cleaved caspase 3
CD3	common leukocyte antigen
CD31	cluster of Differentiation 31 (endothelial cell marker, ie. PECAM-1)
CMD	congenital muscular dystrophy
CNS	central nervous system
CSF	cerebral spinal fluid
CTX	cerebral cortex
CY3	cyanine3

DAPI	4’,6-diamidino-2-pgenylindole
DGC	dystrophin-associated glycoprotein complex
DMEM	dulbecco’s modified eagle’s medium
DS	donkey serum
EAAT	excitatory amino acid transporters
EC	endothelial cell
ECM	extracellular matrix
FGF-2	fibroblast growth factor 2
GDNF	glial cell line-derived neurotrophic factor
GFAP	glial fibrillary acidic protein
Glut-1	glucose transporter 1
IL-6	interleukin-6
ISF	interstitial fluid
JAM	junctional adhesion molecule
Ki67	MKI67 (cellular proliferation marker)
LAM	leukocyte adhesion molecule
LAT1	large neutral amino acid transporter

MCAO	middle cerebral artery occlusion
MECA32	mouse endothelial cell antigen 32 (i.e. PLVAP)
MMP	matrix metalloproteinase
NS	not significant
PBS	phosphate buffered saline
PDGFR-β	platelet derived growth factor beta
PDL	poly-D-lysine
PECAM1	pan endothelial cell antigen 1
PFA	paraformaldehyde
PLVAP	plasmalemma vesicle associated protein (i.e. MECA32)
SDS PAGE	sodium dodecyl sulfate – polyacrylamide gel electrophoresis
SEM	standard error of the mean
SHH	sonic hedgehog
TBI	traumatic brain injury
TBS-T	tris-buffered saline – tween 20
TCC	triphenyltetrazolium chloride
TCR	T cell receptor

TGF- β	transforming growth factor-beta
TJ	tight junction
VSMC	vascular smooth muscle cells
WT	wild type
ZO-1	zonula occludens

Acknowledgements

It has been said, “Smooth seas do not make skillful sailors.” The seas have not always been always smooth through the almost five years since beginning my graduate school career, and the decade I have spent pursuing higher education. I have encountered challenges at times that have made me question whether I wandered off course. However, the challenges along the way are what make the trip memorable, and allow us to learn and grow as individuals. I am grateful to the numerous people that have helped me become the person I am today.

I would like to thank my supervisor, Dr. Holly Colognato. I appreciate her guidance, and support while providing an incredible amount of freedom to work independently.

I would also like to thank all the past members of the Colognato lab including: Dr. Jenne Relucio, Dr. Thomas Nguygen, Dr. Christopher Eyermann, Dr. Freyja Mc Clenanhan, and Dr. Cindy Leiton and present members of the Colognato lab including: Azeez Aranmolate, Xiwei Shan, Lyl Tomlinson, and Himanshu Sharma. Your friendship made graduate school a great experience.

Finally, I would like to thank my family and friends. I am grateful for your support and guidance that has been critical to my success.

CHAPTER I: GENERAL INTRODUCTION

Physiological role of the Blood-Brain Barrier

The blood-brain barrier (BBB) is a multicellular integrative system that provides a protective interface between the peripheral blood circulation and the central nervous system (CNS), serving as a key regulator of neuronal function and physiological homeostasis. The BBB provides protection to the CNS through two main routes, the cerebral vasculature and the blood-cerebrospinal fluid (CSF) barrier at the choroid epithelium and arachnoid membrane [1, 2].

The BBB regulates the internal environment of the CNS at three levels: physical, transport and metabolic barriers [2]. As a physical barrier the BBB tightly restricts paracellular transport, preventing the passage of molecules and ions. The BBB also physically prevents toxins and pathogens from entering the sensitive environment of the CNS, ensuring an optimal environment for neuronal function. Brain endothelial cells (BECs) contain tight junctions (TJs), specialized proteins to block the passage of substances from the peripheral blood circulation through BECs. The BBB functions as a transport barrier by regulating the delivery of nutrients according to the dynamic biochemical needs of the CNS. BECs and astrocytes express barrier specific transporters such as, glucose transporter-1 (Glut-1), ATP-binding cassette (ABC) transporters such as P-glycoprotein, amino acid carriers including large neutral amino acid transporter (LAT1), and excitatory amino acid transporters (EAAT) [2-4]. To function as a metabolic barrier the BBB contains enzymes that metabolize ATP and neuroactive compounds [2-4]. Enzymatic regulation of the products that enter the CNS allow the BBB to function to segregate pools of central and peripheral neurotransmitters [2-4]. Together the physical,

transport and metabolic barriers act to provide distinct levels of control to the BBB, which confers stringent regulation to the CNS parenchyma.

Cellular components of the BBB

The BBB is formed through the interactions of several cell types within the CNS, including BECs, astrocytes and pericytes, which are encased by the gliovascular ECM (Fig. I-1A, Adapted from Obermeier et al. 2013 [5]) [2, 5]. Each cellular component of the BBB makes an important contribution to barrier function, with dysfunction at each level potentially leading to drastic consequences such as neuroinflammation and neurodegeneration [5].

Endothelial cells

The core element of the BBB is the extensive vascular network of BECs in the CNS. Although BECs may appear similar to ECs in vascular networks of peripheral tissues, BECs are distinct due to the absence of fenestrations, increased density of mitochondria, the absence of high levels of continuous interendothelial TJs, expression of specialized transporters and low rates of endocytosis [2, 3, 5-7]. The barrier features of BECs are not intrinsic but are induced by the CNS environment and exist at all levels of the cerebrovascular network, including penetrating arteries, arterioles, capillaries, post-capillary venules, draining venules, as well as veins [2, 5, 8].

The physical barrier properties of the BBB are mediated through the restriction of paracellular transport by TJs in BECs. TJs form a network of parallel, interendothelial strands of protein that are present between adjacent cells to act as a physical blockade of substances passing through BECs. The main components of TJs include the Claudin family (Claudin-3, -5, 12), Occludin, Junctional Adhesion Molecules (JAM A, B, C) and the Zonula Occludens family

(ZO-1, -2, -3), which are distributed throughout the BEC (Fig I-1B, adapted from Förster et al. 2008 [9]) [2, 10-12]. In addition to TJs, adherens junctions (AJs) such as VE-Cadherin regulate the integrity, permeability and differentiation of the BBB [2, 10-12]. Interestingly, maintenance of specialized features of BECs depends upon factors induced by the environment of the CNS, as *in vitro* BEC cultures lose BBB properties without co-culture of cellular components of the BBB [2, 13]. The loss of BEC barrier features *in vitro* emphasizes the importance of the cellular components of the gliovascular interface in regulating barrier properties.

Astrocytes

Astrocytes are glial cells that regulate a broad array of functions critical to the internal environment of the CNS through astrocytic connections with neurons, axons, oligodendrocytes and blood vessels [2-4]. For example, astrocytes support neuronal function by regulating the osmotic, electrolyte, amino acid and neuronal transmitter homeostasis within the CNS [2, 5]. Astrocytes function beyond mere support cells, however, by actively regulating synapse formation and clearance of axonal material [2, 14-17].

One of the most striking features of astrocytes are their perivascular endfeet that form circumferential processes that ensheath the abluminal membrane of BECs; these endfeet are highly specialized structures that induce and maintain barrier properties [2, 5, 18, 19]. Approximately three decades have passed since the discovery of barrier inducing factors in neural tissue on EC development [5, 8]. Utilizing *in vitro* techniques to co-culture ECs with astrocytes or astrocyte conditioned media it has been observed that astrocytes promote elevated expression of barrier specific transporters, enhance the activity of metabolic enzymes and increase TJ expression by ECs [5, 20]. Various soluble factors secreted by astrocytes have been

identified to increase barrier properties including interlukin-6 (IL-6), glial cell line-derived neurotrophic factor (GDNF) and fibroblast growth factor 2 (FGF-2) [5, 21-23].

Recently attention has shifted to the role of astrocytes in the maintenance rather than formation of the BBB through soluble factors such as Sonic Hedgehog (SHH) and interactions with the renin-angiotensin hormone system by astrocyte secreted angiotensinogen, which is extensively processed and ultimately interacts with the ANG receptor (AT1) expressed on the BECs [5, 24-26]. Cross communication between astrocytes and ECs through SHH and the renin-angiotensinogen hormone system regulates CNS immune quiescence, TJ formation, and TJ processing through the post-translational modification of Occludin and subsequent subcellular localization [5, 24-26].

Astrocytes also secrete ECM molecules that contribute to the extensive network of gliovascular matrix in the parenchymal basal lamina (discussed at length in the following sections). Recent studies that removed the expression of γ1 containing laminins from astrocytes increased the susceptibility of adult mice to spontaneous cerebral hemorrhage, indicating a role for laminin the regulation of the BBB [27]. Further, studies conducted in Chapter II and Chapter III of this dissertation, as well as published in Menezes et al. 2014, describe the extensive developmental role of laminin α2 and dystroglycan in the development and function of the BBB [28].

Pericytes

Pericytes are mural cells that extend long processes along endothelial cells and ensheath the abluminal surfaces of the cerebral vasculature [29, 30]. Vascular coverage by pericytes in neural tissues is significantly higher pericyte coverage of ECs in peripheral tissue, providing early clues to their critical role in the development of BEC barrier properties [5, 31]. Pericytes function to regulate critical vascular functions including vascular stability, regulation of cerebral blood blow through modulation of capillary diameter, and BBB integrity [5, 32].

The role of pericytes in the development and function of the BBB has been studied by manipulating platelet-derived growth factor receptor- β (PDGFR- β), a critical factor for pericyte recruitment. Mice that lack PDGFR-β or its ligand PDGF-β fail to recruit pericytes along the cerebral vasculature, resulting in CNS micro-hemorrhages followed by death during embryonic development [5, 29, 33]. The vasculature of embryos lacking PDGFR-β or PDGF-β has an abnormal distribution of TJ proteins, with increased BBB permeability [29, 34]. Cross communication between pericytes and ECs results in enhanced TJ formation, suppression of EC transcytosis, decreased expression of leukocyte adhesion molecules (LAMs), and facilitated barrier development and function [5, 29]. To study the role of pericytes in the maintenance of BBB integrity in postnatal development, PDGFR-β hypomorphs were generated by deleting tyrosine phosphorylation sites on PDGFR-β or by deleting the ECM retention motif of PDGF-β [5, 31, 35, 36]. Adult PDGFR-β hypomorphic mice exhibited increased cerebral vascular permeability and decreased pericyte coverage along the vasculature [31].

Adhesion between pericyte processes and ECs is regulated through the secretion of transforming growth factor-β (TGF- β) [29, 32]. TGF-β and its receptor TGF-βR2 are expressed

by ECs and pericytes but promote distinct processes that contribute to the regulation of the BBB [29, 32]. TGF- β signaling in ECs promotes pericyte-EC adhesion mediated through N-Cadherin, whereas pericytes respond to TGF-β signaling to increase the production of ECM molecules [29, 32, 37].

The extracellular matrix

The extracellular matrix (ECM) is a complex three-dimensional macromolecular network that envelops cells in various tissues. The ECM provides structural support and coordinates dynamic cellular processes essential for multicellular organisms including adhesion, migration, differentiation, proliferation and survival. The ECM regulates these processes through at least two mechanisms: binding cell surface receptors and the regulation of growth factor availability [38].

Layers of cell surface associated ECM proteins assemble into complex networks to form basement membranes (BMs) or basal lamina (BL) [39]. The major components found in the BL include ECM molecules such as collagens (type IV collagen), glycoproteins (laminins, nidogen/entactin, fibrionectin) and proteoglycans such as heparin sulfate proteoglycans (HSPGs), perlecan and agrin [2, 38, 40-45]. The assembly and organization of ECM components into highly organized, cell-surface associated networks that form BL involves the polymerization of laminin and subsequent associations with type IV collagen networks, nidogen, agrin and perlecan [2, 38, 39].

Laminins

The laminins are a large family of multi-domain, multi-subunit proteins that are major components of the basal laminina. Laminin molecules form large cross, rod or T-shaped heterotrimeric proteins, each consisting of an alpha (α), beta (β), and gamma (γ) subunit [46, 47]. Laminin molecules are named by the combination of α, β, and γ subunits contained within the trimer. For example, laminin-211 contains α2, β1, and γ1 subunits. During laminin translation, each subunit is targeted to the endoplasmic reticulum, forming heterotrimers that are later secreted to the extracellular environment [48, 49]. Laminins composed of different combinations of the five alpha, beta and three gamma subunits gives rise to a large variety of molecules (Fig. I-2A, modified from Domogatskaya et al. 2012 [50]). Through differential composition of various laminin trimmers, cell specific expression confers a high level of control via tissue and environmental specificity, enabling a diverse repertoire of functions.

Laminin molecules share structural features such as coiled-coil, globular and rod-like domains (Fig. I-2A and B, modified from Domogatskaya et al. 2012 and Yousif et al. 2013 [50]). The highly glycosylated α, β, and γ subunits assemble to form laminin trimers through a coiled-coil at the C-terminal (long arm) end and through covalent disulfide bonds between each chain [46, 50-52]. The long arm C-terminal of laminin trimers contains α chain globular (LG) domains, which bind adhesion receptors and other ECM molecules [52, 53]. The α, β, and γ subunits also contain short arm domains that have unique globular domains including the N-terminal (LN), internal (L4) domains, which are separated by EGF repeats (LE) [46, 50-52]. The wide variety of functional domains contained within each laminin molecule confers a wide variety of biological activity beyond structural integrity, such as influencing cellular signaling processes and influencing tissue morphogenesis [46, 54]

Laminin mediated BL assembly

Laminin is essential for the initiation and assembly of the BL into a complex network of stable ECM proteins. Assembly of the BL proceeds through a series of complex steps, that begin with laminin LG domains binding to cell surface adhesion receptors such as integrins, dystroglycan or sulfated glycolipids (SGLs) [38, 51] (Figure II-1A, Adapted from Yurchenco, 2011 [51]). Laminin polymerization then proceeds through interactions mediated through laminin LG domains, which bind integrins and SGLs to orient laminin molecules in an organized sheet configuration [46, 54]. Laminin binding of cell-surface adhesion receptors also initiates cellular processes that alter cytoskeletal organization and signaling events that affect cellular behavior [55]. The nascent BL then undergoes further processing to form a stabilized network of ECM proteins through extensive crosslinking of nidogen to collagen-IV and laminin coiled-coil domains [46, 54]. Additional stability is conferred to the BL through agrin and perlecan, which engage the laminin-nidogen network, adhesion receptors and recruit heparin-binding growth factors [38, 51]. The extensive crosslinking of laminin and collagen-IV networks with ECM proteins such as nidogen, agrin and perlecan confer the structural integrity for the basal lamina in various organs including the brain, heart, kidney and lungs [56-60].

Laminin distribution at the gliovascular interface

At the gliovascular interface four laminin isoforms contribute to the parenchymal and endothelial basal lamina (Fig. I-2B, modified from Yousif et al. 2013 [61]). Individual laminin isoforms are distributed differentially throughout the gliovascular BL, with the parenchymal BL containing laminins-111 (laminin 1, α1β1γ1) and -211 (laminin 2, α2β1γ1) (Fig. I-3A) [62]. The endothelial BL contains laminins-411 (laminin 8, α4β1γ1) as well as -511(laminin 10, α5β1γ1)

(Fig. I-3A) [62]. The parenchymal BL contains laminins secreted from astrocytes and possibly pericytes, whereas the endothelial BL contains laminins from ECs [29, 31, 62, 63]. In capillaries, a composite BL exists in which the parenchymal and endothelial BL merge together into one unit of ECM that contains laminins-211, -411, and -511 [62].

Laminin and barrier function

Laminins of the endothelial BL that serve as ligands for receptors such as integrins and dystroglycan [62, 64-67]. Laminins distributed throughout the endothelial BL are essential for development of the cerebral vasculature; in embryonic development laminin α4 deficient mice have vascular BL defects, vessel dilation and decreased vessel integrity [68]. However, in adult laminin α4 deficient mice vascular development is indistinguishable from wild type counterparts with the exception of an increased expression of laminin α5 ubiquitously throughout the endothelial BL [61, 68, 69]. Through *in vitro* migration assays and *in vivo* Experimental Autoimmune Encephalomyelitis (EAE) experiments, it was elucidated that the role of laminin α5 was an inhibitor of T-cell, neutrophil, and leukocyte extravasation across the BBB during brain inflammation [61, 69]. The inhibitory effect on transmigration of T-cells, neutrophils and leukocytes revealed a novel role for laminin α5 in providing resistance to EAE and highlighted the importance of laminin in the regulation of barrier properties, as well as the therapeutic value of laminin α5 in improving the outcomes of patients suffering pathological conditions where the BBB is compromised [61, 69].

In contrast to endothelial laminins, the function of parenchymal laminins in the regulation of barrier function are less defined. Early studies that utilized dy/dy mice, hypomorphic mutants with reduced but not completely absent expression of laminin α2, revealed no obvious defects in the ultrastructure of the endothelial or parenchymal BL [70]. However, human patients suffering

from mutations in *LAMA2*, which encodes laminin α2, or in genes that encode enzymes needed for dystroglycan post-translational modifications, have congenital muscular dystrophies (CMD) with accompanying brain abnormalities, including seizures, perturbed cortical development and MRI white matter hypointensities, with MRI abnormalities hypothesized to originate, in part due to defects in the BBB [67, 71-76]. In a recent study utilizing mice that lack laminin γ1 expression selectively, using a nestin cre-lox approach to remove laminins-111 and -211, in astrocytes, were reported to have impaired VSMC function resulting in decreased α-SMA levels, decreased arterial constriction and spontaneous hemorrhagic stroke [27]. Interestingly, a separate study that utilized an identical transgenic system reported a lack of laminin expression selectively in astrocytes, reported increased levels of α-SMA associated with the capillary beds, suggesting that laminins can also suppress VSMC maturation [77]. The mechanism by which laminins could either decrease or increase VSMC maturation remains unclear, however these studies clearly highlight laminins as key regulators of VSMCs.

Recently we conducted a study utilizing dy^{3k}/dy^{3k} mice, in which LAMA2 was globally deleted from all cell types, recapitulating the ECM environment of patients with laminin-deficient CMD to understand the role of laminin α2 in BBB development and function. The result of this study are discussed at length in Chapter II, Chapter III and published in Menezes et al. 2014 [28]. We found that in the absence of laminin α2 the development and function of all cellular components of the BBB were significantly impaired. Through postnatal development cerebral vascular pericyte coverage was significantly reduced in LAMA2 mutants [28]. Maturation of BECs and VSMCs were perturbed in LAMA2 mutants, resulting in persistence of embryonic endothelial cell antigens and decreased levels of α–SMA [28]. Additionally we found LAMA2 mutants had reduced levels of selected TJ components, as well as abnormal TJ

morphology [28]. The findings reported in Menezes et al. 2014 identified laminin α2 as a key regulator of barrier function and provide empirical support for the hypothesized BBB defects in patients suffering from CMD [76].

Laminins of the endothelial and parenchymal BL serve as a ligand for dystroglycan, a component of the dystrophin-glycoprotein-complex (DGC) localized at perivascular astrocytic endfeet [65, 78]. Selective disruption of components of the DGC, such as α-dystrobrevin or dystrophin, results in altered AQP4 distribution at glial endfeet (Fig. I-4A, adapted from Waite et al. 2012 [79]) and increased vascular permeability [80, 81]. Studies have explored the role of the DGC by utilizing *in vitro* astrocyte assays to explore the role of laminin binding to dystroglycan in facilitating AQP4 polarization, by forming aggregates of AQP4 channels [78, 82-84]. Adding to the complexity of laminin regulation of barrier function, pericytes themselves reportedly express laminin α2 [31]. In support of this observation, pericyte deficient mice have regions of the vasculature devoid of pericyte coverage that coincide with laminin α2 loss at astrocyte endfeet. This finding suggested that α2–containing laminins may also regulate pericyte-gliovascular interactions such as endfeet positioning along the cerebral vasculature [31].

Adhesion receptors at the BBB

Two main types of matrix adhesion receptors, integrins and dystroglycan, are distributed throughout the gliovascular interface and are thought to regulate both cell-cell and cell-matrix interactions. The adhesion receptors perform two functions: forming a physical link between the ECM and intracellular cytoskeleton of components of the gliovascular interface, and regulating signaling pathways to direct cellular processes [4, 38, 51]. The integrins are a diverse family of transmembrane glycoprotein heterodimers comprised one alpha and beta chain. Integrins bind

ECM ligands, resulting in the activation of signaling pathways [55, 85, 86]. Integrins are expressed on all cell types at the gliovascular interface including ECs [87-90], pericytes [64, 91, 92], and astrocytes [65, 87, 90, 93]. Dystroglycan is an adhesion receptor that consists of two subunits, a highly glycosylated extracellular alpha subunit and a transmembrane beta subunit that connects the receptor to intracellular cytoskeletal components [66, 67]. Dystroglycan is expressed in several cells types of the gliovascular interface, including perivascular astrocyte endfeet and endothelial cells, as well as by other cell types within the CNS including neurons and oligodendroglia [66, 67, 78, 90].

Integrins at the BBB

Integrins act as dynamic regulators of barrier formation through embryonic and postnatal development. During embryonic brain development and vascularization, angiogenic BECs express α4β1 and α5β1 integrins, which bind fibronectin and promote cell proliferation through the MAPK signaling pathway [89, 94]. The expression of integrins changes through postnatal development; in the adult cerebral vasculature BEC differentiation and stabilization are promoted through the interaction of laminin with α1β1 and α6β1 integrin [94]. In BECs the absence of β1- integrin results in down regulation of the TJ components Claudin-5 and VE-Cadherin [95-97]. Through varied ECM ligand presentation and integrin receptor expression, signaling is orchestrated in BECs to facilitate barrier function.

The contribution of integrins in astrocytes, pericytes, and VSMCs has been studied using targeted approaches to remove integrin expression. An astrocyte-specific conditional β1-integrin knockout using a GFAP-Cre resulted in a profound loss of astrocytic derived laminin-111 and -211 organization along the cerebral vasculature, however these mutants had no change

in BBB permeability [98]. A conditional knockout of β1-containing integrins in both pericytes and VSMCs using a PDGFR-β –Cre approach resulted in decreased VSMC differentiation, providing further support for a role for laminin receptor interactions in promoting pericyte and VSMC maturation [64]. These studies highlight the importance of ECM mediated signaling through integrin receptors at the gliovascular interface, which facilitate the development and function of barrier properties.

Dystroglycan and the Dystroglycan-Associated Complex (DGC) at the BBB

Dystroglycan is produced as a single gene product that undergoes subsequent post-translational modifications, resulting in cleavage into discrete non-covalently linked α and β subunits [99]. The extracellular alpha dystroglycan subunit undergoes post-translational N- and 0- linked glycosylation, with the central mucin domain of α-dystroglycan serving as the binding site for laminin G (LG) domains [100]. The transmembrane β-dystroglycan subunit serves as the central component that links alpha-dystroglycan and bound ligands to the cytoskeleton through actin or proteins associated with the dystrophin-glycoprotein-complex (DGC) [79]. The DGC lines perivascular endfeet to facilitate adhesion and polarization of channels to maintain (Figure I-4, Adapted from Waite et al. 2012 [79]).

The complex interplay between the cellular components of the BBB and the ECM of the gliovascular interface is critical for barrier development and function. As discussed, the cell-matrix interactions are facilitated through matrix adhesion receptors expressed along the gliovascular interface, including members of the integrin family and dystroglycan [2]. The function of integrins expressed in ECs [87-90], pericytes [64, 91, 92], and astrocytes [65, 87, 90, 93] have been well characterized in the dynamic regulation of signaling pathways critical for

barrier formation and function in postnatal development, as well as trauma to the BBB such as focal ischemia. In contrast, the role of dystroglycan in the development and function of the BBB is poorly understood [90]. However, in pathological conditions that result in the disruption of the BBB, such as focal cerebral ischemia and Experimental Autoimmune Encephalomyelitis (EAE), dystroglycan expression at the endfeet interface is reduced, suggesting a critical role for Dystroglycan in maintaining BBB integrity and Dystroglycan's potential value towards developing novel therapeutic strategies [43, 101].

At the gliovascular interface, dystroglycan is most well known as the central component of the DGC that lines astrocytic endfeet processes along the cerebrovasculature [78, 102]. At the DGC, dystroglycan binds matrix ligands, forming a physical linkage between the endfeet and the network of ECM at the gliovascular interface. The DGC links intracellular actin cytoskeleton via dystrophin and aggregates channels along astrocytic endfeet via α-dystrobrevin, which physically links aquaporin (AQP4) channels to the complex (Fig. I-4B, adapted from Waite et al. 2012 [79]). Inactivation of the genes that encode either dystrophin or α-syntrophin results in delayed onset edema, altered AQP4 distribution at glial endfeet, altered tight junction levels and morphology, increased cerebrovascular permeability [80, 81, 103-107]. However, the deletion of AQP4 itself does not impact barrier development, suggesting the DGC itself must contribute to other extrinsic cues that facilitate BBB development and integrity [108]. Perturbed barrier function and the regulation of cerebral homeostasis in the absence of dystrophin and α-dystrobrevin warrants further inquiry to elucidate mechanistic insight into how the DGC regulates the cellular development and function of the BBB.

Dynamic alteration of the BBB in pathology

Regulation of the function and integrity of the BBB is perturbed in a wide variety of pathological conditions such as ischemic or hemorrhagic stroke, neurodegenerative disorders such as Multiple Sclerosis (MS), and Alzheimer's disease [3]. Disruption of the BBB associated with pathological conditions often precedes neuroinflammation and neurodegeneration, emphasizing the critical role the BBB plays in maintaining an optimal environment for neuronal function. In pathological conditions the ECM undergoes changes in composition, with some BL components found in the healthy BBB undergoing degradation, while others are upregulated and deposited [2]. Further, changes in the specific adhesion receptors expressed at the gliovascular are dynamically regulated in pathological conditions, enabling cells to respond to the changing gliovascular ECM milieu and direct cellular signaling pathways.

In stroke the cerebral blood flow of the CNS is disrupted by one of two main mechanisms: 1) occlusion of the vasculature, resulting in ischemic stroke or 2) loss of vascular integrity resulting in bleeding and hemorrhage. Disruption of cerebral blood from ischemic or hemorrhagic stroke results in a deficiency of oxygen and nutrients available to the cells within the CNS that rapidly manifests in neurological deficits and cellular death [2, 109]. However, restoration of cerebral blood flow does not mean that the function of CNS tissue will be restored, since BECs undergo ischemic damage due to the transient hypoxia and lack of nutrients [2, 109]. Reperfusion of blood flow to the damaged vasculature also results in increased pressure on damaged BEC and damaged TJs [2, 109]. Stroke therefore results in a multitude of effects including loss of vascular physical integrity, TJ dysregulation, increased BBB permeability, inflammation, as well as broad changes in gliovascular ECM composition including proteolytic degradation of the BL, altered adhesion receptor expression and loss of cell adhesion [2].

The gliovascular ECM undergoes dynamic changes in response to ischemic and hemorrhagic stroke. In response to ischemic stroke, components of gliovascular ECM are rapidly degraded by proteolysis, through the diverse family of matrix metalloproteinases (MMPs) and plasmin [2, 41, 42, 110]. Following stroke, collagen–IV, perlecan and laminins are degraded through the actions of proteases including, MMP-2 or -9, plasmin, or cathepsin-B and -L [2, 42]. Adhesion receptors are dynamically regulated following stroke as studies that utilized focal ischemia found an upregulation in the ECM component fibronectin and increased expression of α5β1 and αvβ3 integrin receptors in BECs, as well as the loss of dystroglycan of astrocytic endfeet [101, 111]. Matrix receptors also respond dynamically to chronic hypoxia, resulting in increased expression of α6β4 integrin and dystroglycan along angiogenic BECS [112].

The loss of BBB function is thought to be a pivotal component of neurodegenerative diseases, with BBB loss preceding and actively contributing to neurological decline [2, 4, 5]. In MS and its animal model EAE, barrier permeability is increased preceding both dramatic increases in neuroinflammation and widespread neurodegeneration [43, 113]. Through the course of EAE leukocytes in the peripheral circulation accumulate in the perivascular space between the endothelial and parenchymal BL of the BBB, forming regions of focal leukocyte accumulation, known as perivascular cuffs [43]. Macrophage derived MMP-2 and -9 are known to cleave dystroglycan, thus facilitating leukocyte infiltration into the parenchyma of the CNS [43, 113, 114]. EAE-mediated leukocyte infiltration triggers neuroinflammation and degeneration of neuronal function, which then manifest in the appearance of clinical symptoms [43, 113, 114]. The progression of gliovascular dysfunction and subsequent neurodegeneration

observed in EAE is hypothesized to model the progression of MS emphasizing the therapeutic value of understanding ECM mediated regulation of the BBB.

Figure I-1. Cellular components of the blood-brain barrier.

(A) The BBB is formed by the integration of numerous cellular components within the CNS including endothelial cells, pericytes, astrocytes and an extensive ECM that is assembled into a basement membrane. Endothelial cells of the CNS are sealed by tight junctions that form a primary physical barrier of the BBB. Endothelial cells are meshwork by a layer of ECM that forms a basement membrane in which pericytes are embedded. Pericytes form direct contacts to endothelial cells through peg-socket junctions, which facilitate intracellular crosstalk and stabilization of both cell types. Astrocytes form processes that encircle the abluminal portion of endothelial cells, nearly covering the entire surface. Adapted from Obermeier et al. 2013 [5]. (B) Molecular components of endothelial tight junctions of the BBB. Transmembrane proteins such as Occludin, the Claudin family, Junctional Adhesion Molecule-1 (JAM-1) and Zonula Occludens (ZO-1) form physical barriers to seal the paracellular space. Vascular Endothelial (VE) Adherens junctions contribute to the stability of the endothelial cells and restrict permeability of the cerebrovasculature. Adapted from Förster et al. 2008 [9].

A)

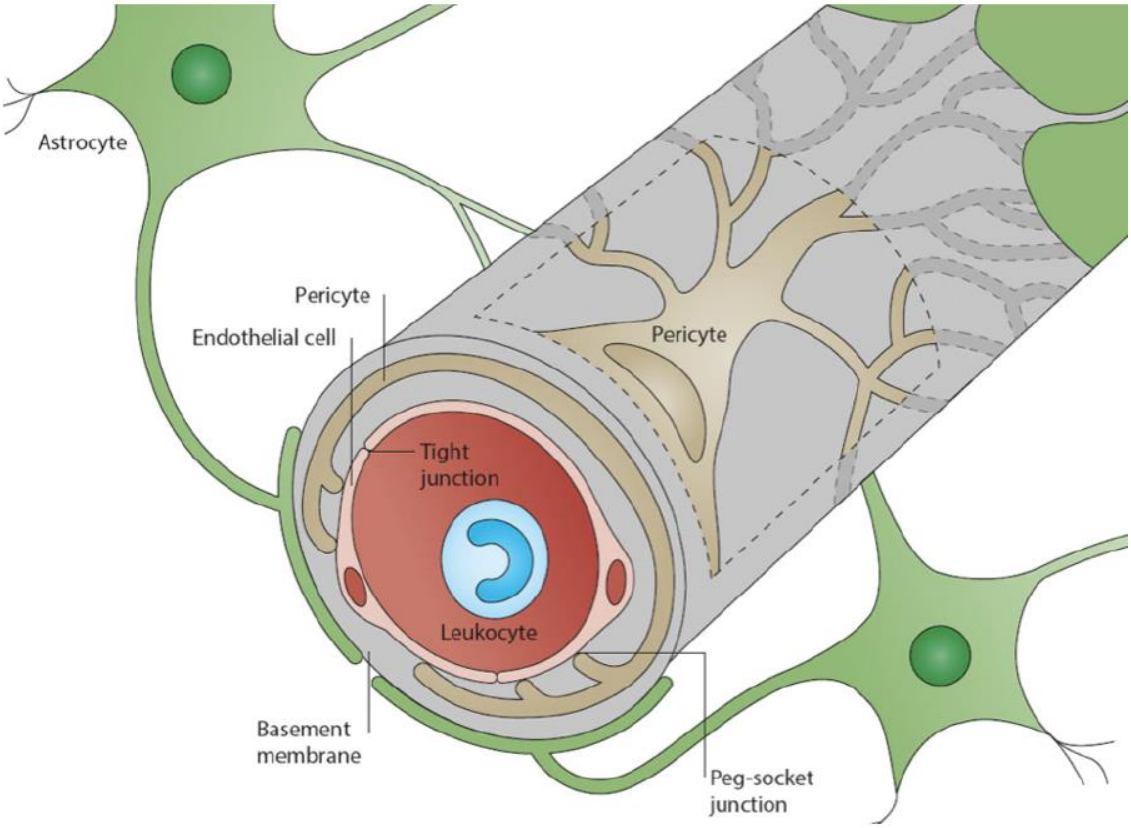
Astrocyte
Pericyte
Endothelial cell
Pericyte
Tight junction
Leukocyte
Basement membrane
Peg-socket junction

B)

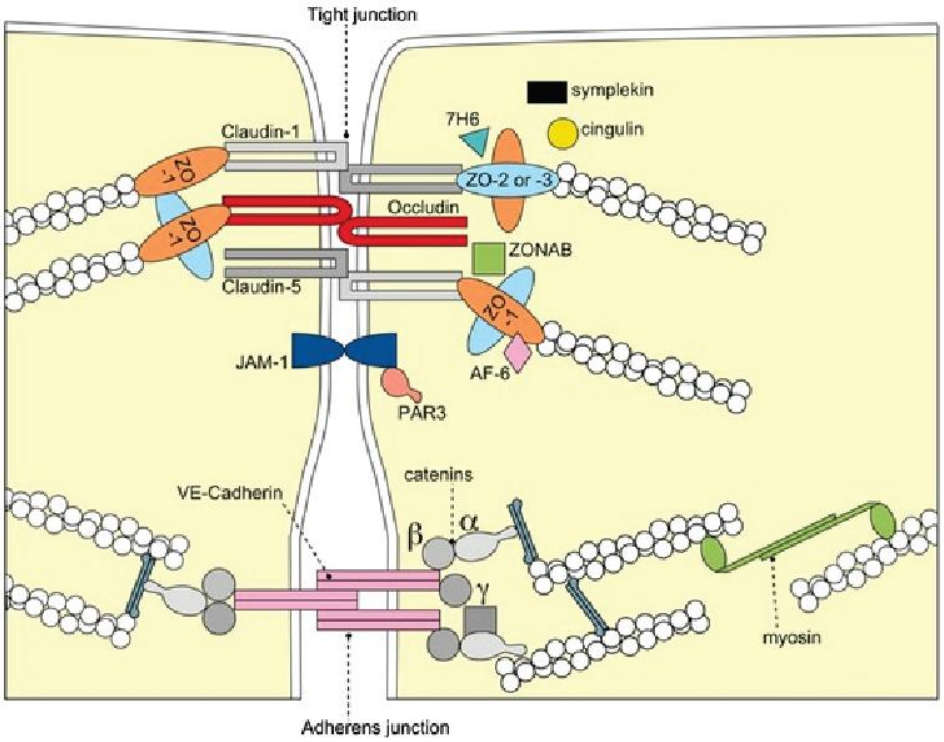
Tight junction
symplekin
7H6
cingulin
Claudin-1
ZO-1
ZO-2 or -3
Occludin
ZO-1
ZONAB
Claudin-5
ZO-1
JAM-1
AF-6
PAR3
catenins
VE-Cadherin
β
α
γ
myosin
Adherens junction

Figure I-2. Laminin chains and heterodimer structure.

(A) Laminin molecules that have been identified form heterotrimers composed of three different gene products: one alpha (α), one beta (β) and one gamma (γ) subunit. Laminin chains contain globular and rod domains. The α chains contain five globular domains (LG1-5) at the C terminus. Laminin α3, α4, and α5, LG4-5 domains can be cleaved, however all LG domains of laminin α1 and α2 remain attached. The LG domains of each laminin chain bind specific adhesion receptors (labeled in figure). The N-terminal of all laminin chains contains epidermal growth factor-like (LE) repeats and (LN) globular domains. Adapted from Domogatskaya et al. 2012 [50]. (B) Representative schematics of laminin heterotrimers found at the gliovascular interface. Depicted Left to Right: Laminin 111 (α1β1γ1, orange), 211 (α2β1γ1, red), 411 (α4β1γ1, yellow) and 511 (α5β1γ1, green). Several α globular LG domains at the C-terminus provide binding sites to adhesion receptors such as integrins and dystroglycan. At the N-terminal LN globular domains at the short arms of the heterotrimers α, β, and γ chains facilitate laminin molecule self-assembly and polymerization. Adapted from Yousif et al. 2013 [61].

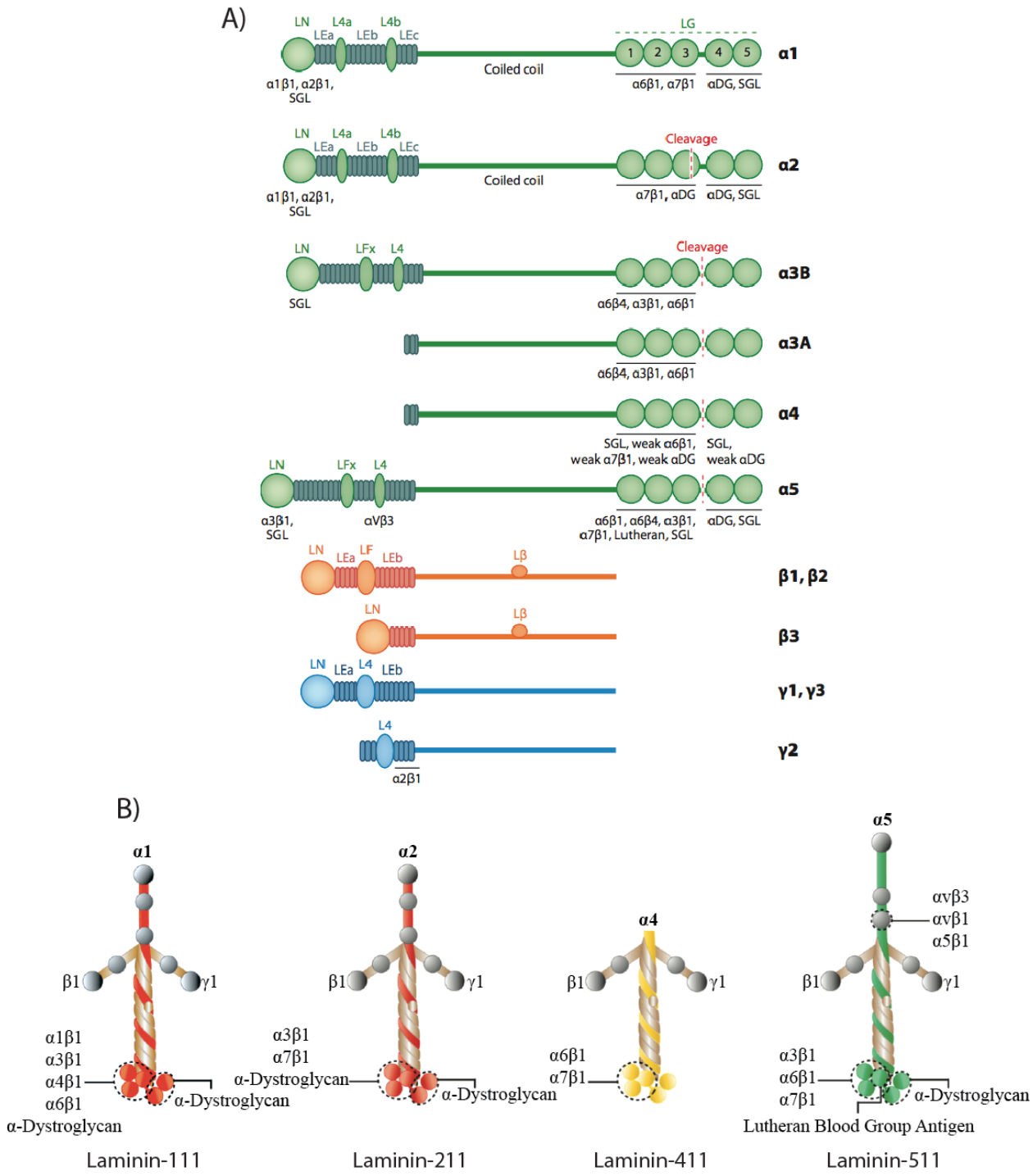
A)
LN
L4a
L4b
LEa
LEb
LEc
LG
1
2
3
4
5
α1
Coiled coil
α1β1, α2β1, SGL
α6β1, α7β1
αDG, SGL
Cleavage
α2
α7β1, αDG
LFx
L4
α3B
SGL
α6β4, α3β1, α6β1
α3A
α4
SGL, weak α6β1, weak α7β1, weak αDG
SGL, weak αDG
α5
α3β1, SGL
αVβ3
α6β1, α6β4, α3β1, α7β1, Lutheran, SGL
LF
Lβ
β1, β2
β3
γ1, γ3
γ2
α2β1
B)
α1
α2
α4
α5
β1
γ1
α1β1
α3β1
α4β1
α6β1
α-Dystroglycan
α3β1
α7β1
α6β1
α7β1
αvβ3
αvβ1
α5β1
Lutheran Blood Group Antigen
Laminin-111
Laminin-211
Laminin-411
Laminin-511

Figure I-3. Basal lamina formation and distribution of laminin at the gliovascular interface.

(A) Basal lamina formation is a complex multistep process directed by laminin. Laminins bind cell surface associated receptors such as sulfated glycolipids (SGLs), integrins and α-dystroglycan through laminin LG domains. Laminins form extensive sheet configurations through polymerization facilitated by laminin LN domain interactions. LG domains bind SGLs and integrins so that laminin self-assembly occurs selectively anchored to cell surfaces. Laminin polymerization is further stabilized by the binding of nidogen and collagen-IV to laminin to form a three-dimension network. An additional layer of complexity arises from agrin and perlecan, which bind the network of laminin-nidogen and cell surface receptors. Adapted from Yurchenco 2011 [51]. (B) Laminin chains are heterogeneously distributed throughout the gliovascular interface. The endothelial basal lamina of blood vessels contains laminin 411 and 511 (containing α4 and α5, respectively). The parenchymal basal lamina, largely derived from astrocytes, contains laminin-111 and -211 (containing α1 and α2, respectively). Pericytes cover the abluminal interface of the cerebral vasculature and are believed to contribute laminin 211 to the perivascular space between the endothelial and parenchymal basal lamina. Adapted from Masocha et al. 2004 [115].

A)

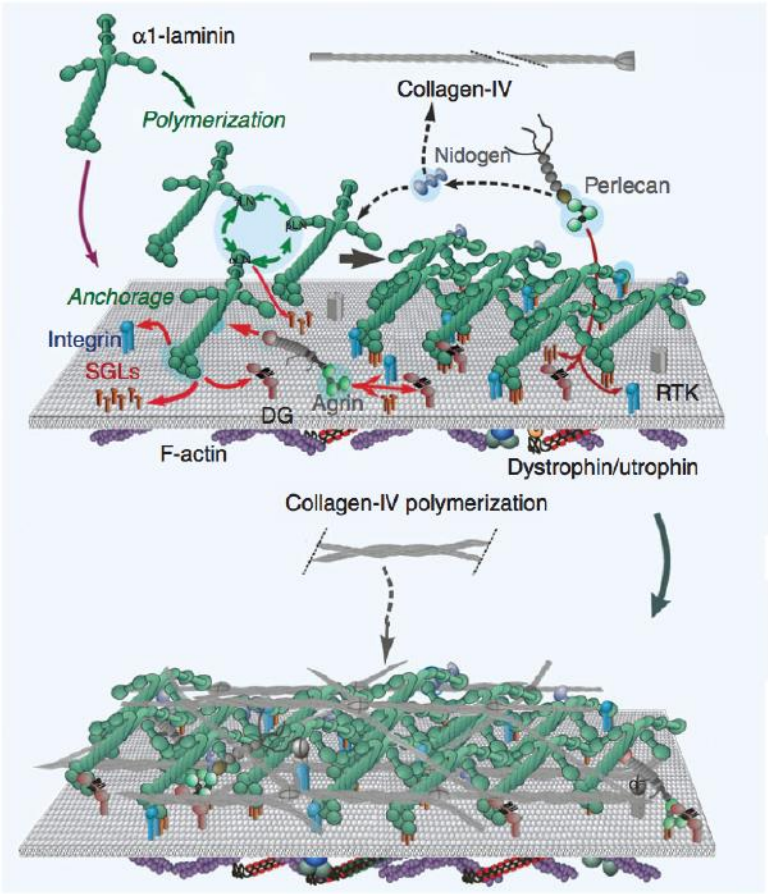
α1-laminin
Polymerization
Collagen-IV
Nidogen
Perlecan
Anchorage
Integrin
SGLs
DG
Agrin
RTK
F-actin
Dystrophin/utrophin
Collagen-IV polymerization

B)

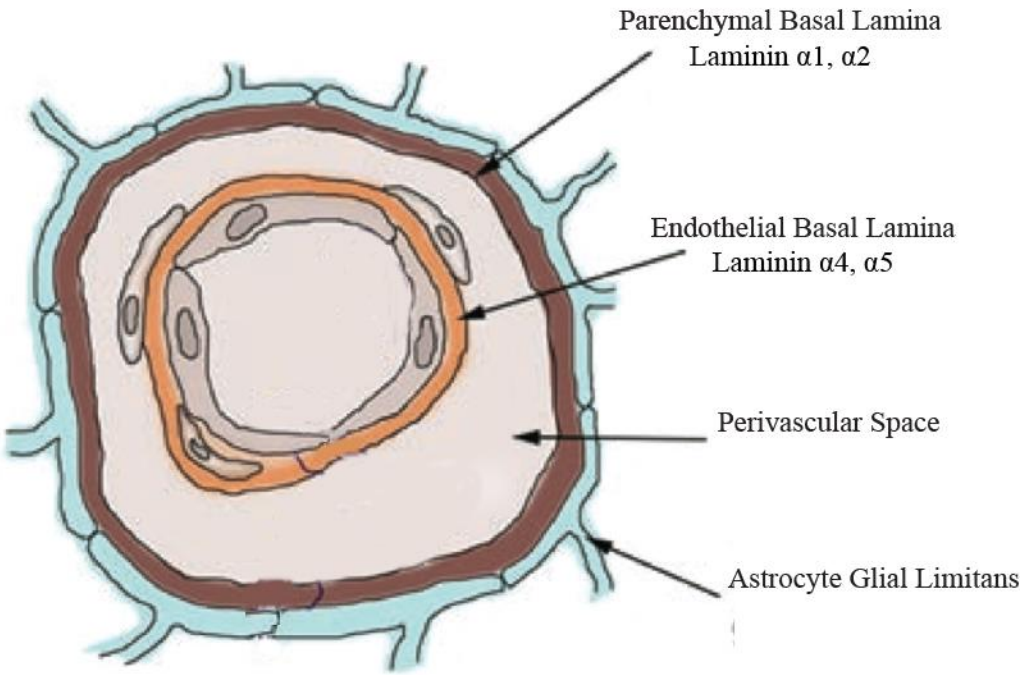
Parenchymal Basal Lamina
Laminin α1, α2
Endothelial Basal Lamina
Laminin α4, α5
Perivascular Space
Astrocyte Glial Limitans

Figure I-4. Dystroglycan is a central component of the Dystrophin-associated Glycoprotein Complex (DGC).

(A) Adhesion of astrocyte end feet at the gliovascular interface is facilitated through dystroglycan, an adhesion receptor that physically links the ECM to the actin cytoskeleton through interactions with extracellular ligands expressed in the basal lamina, such as laminins. (B) Dystroglycan binds to laminin globular (LG) domains through the heavily glycosylated extracellular α-dystroglycan subunit, which physically anchors the intracellular components associated with the transmembrane β-dystroglycan subunit. Dystroglycan is a central component of the dystrophin-associated glycoprotein complex (DGC) at astrocyte endfeet, which physically links astrocyte endfeet to the vasculature of the CNS and polarizes channels to the vascular interface such as Aquaporin-4 (AQP4) and Kir4.1 (Not shown). Adapted from Waite et al. 2012 [79].

A)

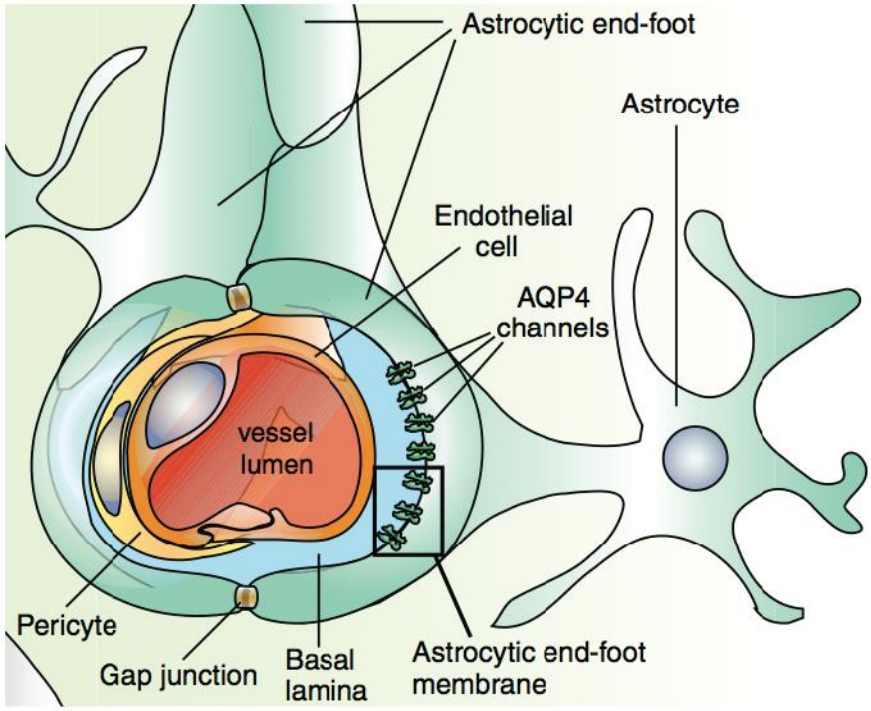
Astrocytic end-foot
Astrocyte
Endothelial cell
AQP4 channels
vessel lumen
Pericyte
Gap junction
Basal lamina
Astrocytic end-foot membrane

B)

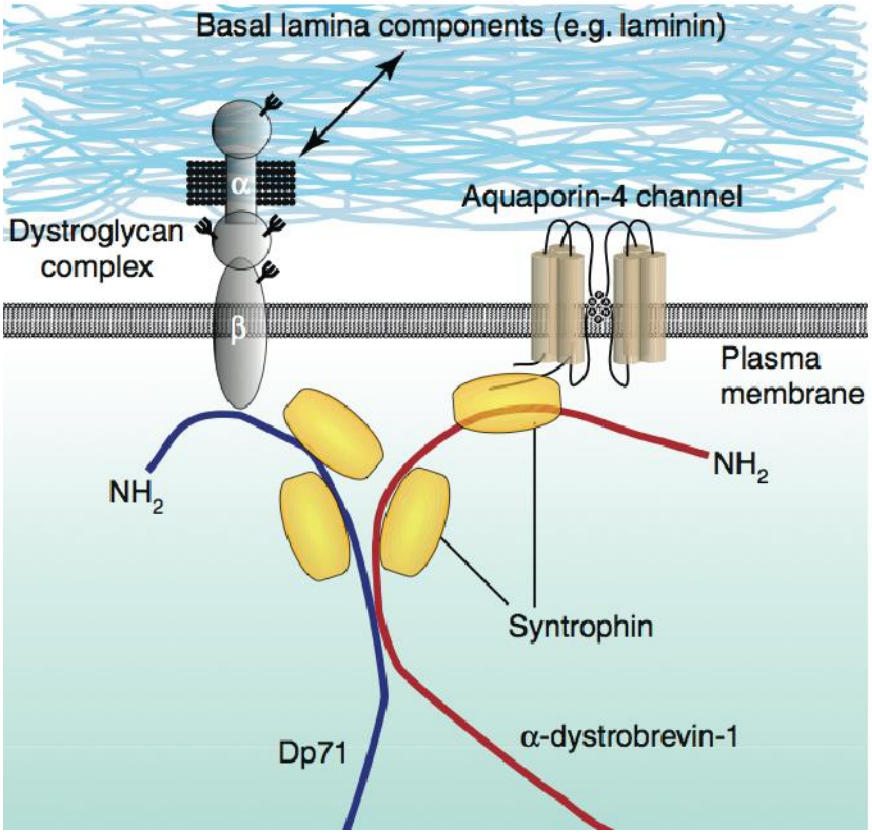
Basal lamina components (e.g. laminin)
α
Aquaporin-4 channel
Dystroglycan complex
β
Plasma membrane
NH2
NH2
Syntrophin
Dp71
α-dystrobrevin-1

CHAPTER II: THE ROLE OF LAMININ ALPHA 2 IN THE DEVELOPMENT AND FUNCTION OF THE BLOOD-BRAIN BARRIER

Laminins are major constituents of the gliovascular basal lamina (BL) of the blood-brain barrier (BBB), however, the role of laminins in BBB development remains unclear. Here we report that LAMA2-/- mice, lacking expression of the laminin α2 subunit of the laminin-211 heterotrimer expressed by astrocytes and pericytes, have a defective BBB in which systemically-circulated tracer leaks into the brain parenchyma. The LAMA2-/- vascular endothelium had significant abnormalities including altered integrity and composition of the endothelial BL, inappropriate expression of embryonic vascular endothelial protein MECA32, substantially reduced pericyte coverage, and tight junction abnormalities. Additionally, astrocytic endfeet were hypertrophic and lacked appropriately polarized aquaporin4 channels. Laminin-211 appears to mediate these effects at least in part by through dystroglycan receptor interactions, as preventing dystroglycan expression in neural cells led to a similar set of BBB abnormalities and gliovascular disturbances, which additionally included perturbed vascular endothelial Glut1 localization. These findings provide insight into the cell and molecular changes that occur in congenital muscular dystrophies caused by LAMA2 mutations or inappropriate dystroglycan post-translational modifications, which have accompanying brain abnormalities including seizures. Our results indicate a novel role for laminin-dystroglycan interactions in the cooperative integration of astrocytes, endothelial cells and pericytes in regulating the BBB.

Introduction

The blood-brain barrier (BBB) is comprised of physical barriers and transport mechanisms that critically regulate CNS homeostasis. Brain endothelial cells (BECs), together with astrocytes, pericytes and vascular smooth muscle cells (VSMCs), comprise the gliovascular unit. Complex cellular interactions within the gliovascular unit regulate the development of unique BEC properties including specialized tight-junctions, suppressed vesicular transport, and barrier-specific transport proteins [31, 116-118]. In addition to cell-cell interactions, cell-extracellular matrix (ECM) interactions are also proposed to regulate BBB properties, as an extensive ECM network resides between perivascular astrocytic endfeet and BECs. This gliovascular basal lamina (BL) exists either as two distinct BLs, an astrocyte-produced parenchymal BL and a BEC-produced endothelial BL, or, as a fusion of the two BL, creating a composite BL [62]. Pericytes, which also critically regulate barrier properties, reside within this composite gliovascular BL, having an interface with both astrocytes and BECs [31, 102, 117]. While the gliovascular BL comprises a key "outer barrier" of the mature BBB, the role of specific cell-ECM interactions in the maturation and function of the BBB remains unclear.

The laminins are major components of the gliovascular BL, serving as ligands for receptors such as integrins [62, 64, 65], and dystroglycan [67]. Laminins are heterotrimers, with each laminin having a designation reflecting its subunit composition, e.g. laminini-111 is composed of laminin $\alpha 1$, $\beta 1$, and $\gamma 1$ subunits [46, 119]. Individual laminins are distributed differentially throughout the composite gliovascular BL, with the parenchymal BL containing laminins-111 and -211 produced by astrocytes, and the endothelial BL containing laminins-411 and -511 produced by endothelial cells [62]. Laminins-211, -411, and -511 are similar to laminin-111 but in place of $\alpha 1$ contain a2, a4, or a5, respectively. Endothelial laminins are

essential for brain vascular development, as mice that lack laminin α4 have vascular BL defects, vessel dilation and decreased vessel integrity [68]. Interestingly, laminin α4 deficient mice upregulate laminin α5, which inhibits T-cell extravasation across the BBB during brain inflammation, thus providing resistance to Experimental Autoimmune encephalomyelitis [69].

In contrast to endothelial laminins, the roles of astrocytic laminins are less clear. Initially, ultrastructural analysis in dy/dy mice, which laminin α2 is deficient but not absent) revealed no obvious defects [70]. However, mutations in *LAMA2*, which encodes laminin α2, or in genes that encode enzymes needed for dystroglycan post-translational modifications, cause congenital muscular dystrophies with accompanying brain abnormalities, including seizures, perturbed cortical development and MRI white matter hypointensities [67, 71-75], with MRI abnormalities hypothesized to reflect, at least in part, BBB defects [76]. Recently, mice that lack laminin γ1 expression selectively (removing laminins-111 and -211) in astrocytes were reported to have impaired VSMC function and hemorrhagic stroke [27]. However the best understood role for astrocytic laminins at the gliovascular interface is as a ligand for dystroglycan, a component of the dystrophin-glycoprotein-complex (DGC) localized at perivascular astrocytic endfeet [65, 78]. Disruption of components of the DGC, e.g. α-dystrobrevin or dystrophin, results in altered AQP4 distribution at glial endfeet and increased vascular permeability [80, 81]. And, in cultured astrocytes, laminin binding to dystroglycan facilitates AQP4 polarization [78, 82-84]. In addition, pericytes themselves reportedly express laminin α2 [31]. Intriguingly, in mice with an engineered pericyte deficiency, areas of the vasculature devoid of pericyte coverage coincide with laminin α2 loss at astrocyte endfeet, suggesting that α2–containing laminins may also regulate pericyte-gliovascular interactions [31].

To gain insight into how ECM interactions at the gliovascular interface contribute to BBB development, we inactivated the *LAMA2* gene to selectively eliminate laminin-211 from all cells of the developing brain. We identified laminin-211 as a novel regulator of the selective permeability of the BBB, both contributing to the acquisition of cerebrovascular pericyte coverage in the developing brain and multiple aspects of gliovascular cell-cell and cell-ECM interactions, including glial endfeet architecture. Our findings suggest that laminin-dystroglycan interactions at the gliovascular interface regulate the maturation and function of the BBB, and that BBB dysregulation may contribute to CNS abnormalities observed in CMD.

Results

The development of the cerebral vasculature in the absence of laminin alpha2

The distribution of laminins has been well characterized in the vasculature of the adult cerebral cortex, where a composite basal lamina (BL) is derived from endothelial and parenchymal (astrocytes and meninges) sources. The endothelial laminin heterotrimers (laminins-411 and -511) contain laminin α4 and α5, respectively, whereas the parenchymal laminin heterotrimers (laminins-111 and -211) contain laminin α1 and α2, respectively [61]. The loss of laminin a2 expression in people causes developmental brain abnormalities of which the underlying cellular disturbances remain unclear [120]. To determine whether laminin-211 influences the development and function of the cerebral vasculature, we analyzed LAMA2 -/- mice relative to their wild type littermates. LAMA2-/- mice die at approximately 4 weeks of age so vascular development was evaluated at 3 weeks of age, reflecting a late juvenile / young adult stage of development.

To confirm the lack of laminin α2 protein in LAMA2 -/- brains, we conducted laminin α2 immunohistochemistry (Fig. II-1 A and B). As expected, wild-type mice had laminin α2 protein most prominently in the BLs of the pia and vasculature (Fig. II-1A), with higher magnifications revealing laminin α2 protein enrichment at the interface between astrocytic endfeet and vascular endothelial cells (Fig. II-1B). In matched regions obtained from LAMA2 -/- littermate mice, no laminin α2 protein was observed in any region (Fig. II-1 A and B).

Next, to determine if the absence of laminin α2 influenced the development of the cerebral vasculature, several key cell types were assessed. We evaluated the morphology of astrocytes and their processes to elucidate potential changes in the gliovascular interface by conducting glial fibrillary acidic protein (GFAP) immunohistochemistry (Fig. II-2A) at postnatal day 21. Overall, LAMA2 -/- mice had increased GFAP immunoreactivity suggestive of reactive

gliosis, which was particularly apparent in astrocytic processes lining the vasculature of the cerebral cortex and included robust hypertrophied processes enveloping the vasculature. We quantified the area of GFAP immunoreactivity relative to the number of GFAP+ cells. LAMA2 -/- mice had significantly increased GFAP area relative to the total number of GFAP+ cells (Fig. II-2B) in the cortex (21,827.14 ± 1426.28 μm^2 in LAMA2 -/- versus 7,192.65 ± 882.17 μm^2 in wild type; n=3; P< .0001). However, in LAMA2 -/- mice the total number of cortical GFAP+ cells (Fig. II-2C) was not significantly different relative to wild-type littermate controls (323.24 ± 7.6 cells/mm^2 in LAMA2 -/- versus 326.56 ± 23.21 cells/mm^2 in wild type; n=3; P= 0.91). We further quantified GFAP levels by western immunoblotting and found that at postnatal day 21 protein levels of GFAP were significantly higher in LAMA2 -/- cerebral cortices than in wild type littermate cerebral cortices (Fig. II-2D; 0.505 ± 0.031 in LAMA2 -/- versus 0.344 ± 0.008 in wild type, n=6, P< 0.001).

We next evaluated the gross morphology of the vasculature in the cerebral cortex by performing immunohistochemistry to detect the endothelial cell protein CD31 (Fig. II-3A) followed by morphometric analysis of vascular density and complexity. In LAMA2 -/- mice cortical vascular density (Fig. II-3B) was not significantly different (4.619 ±0.35 in LAMA2 -/- versus 5.587 ±0.20 in wild type, n=3, P= 0.08). However, cortical vascular complexity (Fig. II-3C), measured as branch points per 100 μm segments, was significantly lower in LAMA2-/- cerebral cortices relative to that in wild-type littermate controls (0.929 ±0.12 in LAMA2 -/- versus 1.374 ±0.14 in wild type, n=3, P= 0.006). To visualize vascular smooth muscle cells (VSMCs) that are associated with larger caliber blood vessels, we conducted α-smooth muscle actin (α-SMA) immunohistochemistry (Fig. II-4A). The blood vessels that were positive for α-SMA in LAMA2 -/- mice had a decreased intensity of immunoreactivity, suggestive of reduced

levels of α-SMA protein, which would be indicative of decreased VSMCs contractility. Next, α-SMA coverage along blood vessels was quantified at postnatal day 21. LAMA2 -/- mice had significantly reduced (51.5% reduction) α-SMA immunoreactivity relative to blood vessel area (Fig. II-4B; 0.278 ±0.028 in LAMA2 -/- versus 0.573 ± 0.044 in wild type; n=3; P= 0.005). We further quantified α-SMA at postnatal day 21 by western immunoblotting and found that α-SMA protein levels in LAMA2 -/- mice were significantly lower relative to those in wild-type littermates (Fig. II-4C; 0.124 ± 0.019 in LAMA2 -/- versus 0.215 ± 0.033 in wild type; n=6; P=0.01). Together these data confirm that laminin α2 is absent in LAMA2 -/- mice and that all major cell types in the glial-vascular unit that contribute to the barrier properties are present in LAMA2 -/- mice. However, LAMA2 -/- brains have hallmarks of reactive gliosis, altered gliovascular morphology, and reduced α-SMA-positive blood vessels, suggestive of blood-brain barrier dysfunction and/or immaturity.

Laminin regulates the permeability of the blood-brain barrier

To investigate the impact of laminin α2 on the functional integrity of the BBB we assessed several indicators. First, an acute 30 minute circulation of the azo-dye Evans Blue was performed at postnatal day 21. Evans Blue dye functions by binding protein components of the circulating blood such as serum albumin, which can then cross into the brain parenchyma in pathological situations where the BBB is compromised. Using identical acquisition parameters, large amounts of Evans Blue was observed in the parenchymal space in the cortex, striatum, hippocampus, and cerebellum of LAMA2 -/- mice relative to that in wild type littermates (Fig. II-5A). Furthermore, extraction of Evans Blue dye from the whole cerebral cortex followed by a reading of optical density at 620 nm (Fig. II-5B) indicated a statistically significant difference in

the level of Evans Blue in LAMA2 -/- cortices relative to that in wild type littermates (3.013 ± 0.571 in LAMA2 -/- versus 0.978 ± 0.057 in wild type; n=3; P=0.024). To further investigate the possibility of a compromised BBB, we assessed the presence of leukocytes, which should not enter the cerebral parenchyma under normal physiological conditions. We performed immunohistochemistry against the common leukocyte antigen CD45, and against laminin-111 to visualize the basal lamina of blood vessels (Fig. II-6A, left panel). In LAMA2 -/- brains, CD45+ cells can be detected outside of the vasculature in the parenchymal space. Since CD45 can be expressed by activated microglial under some circumstances, we further assessed potential leukocyte infiltration by performing immunohistochemistry against the ε chain of the T-cell receptor associated CD3 complex, to detect leukocytes within the parenchymal space, in conjunction with laminin-111 immunohistochemistry to visualize the basal lamina of blood vessels. In LAMA2 -/- brains, CD3+ cells can be detected outside of the vasculature in the parenchymal space (Fig. II-6A, right panels), further confirming leukocyte transmigration. A leaky BBB with accompanying leukocyte infiltration would be predicted to elicit an innate immune response within the brain. We therefore analyzed microglial activation using immunohistochemistry against the monocyte specific protein iba-1 in the striatum of postnatal day 21 mice (Fig. II-6B). In LAMA2 -/- brains, iba-1 positive microglia are more plentiful and have an amoeboid morphology, characteristic of activated microglia, whereas iba-1 positive microglia in wild type mice have long branch like processes characteristic of resting microglia (Fig. II-6B, far right panel) and are less numerous (Fig. II-6C; 445.91 ± 13.57 cells/mm^2 in LAMA2 -/- versus 223.78 ± 9.95 cells/mm^2 in wild type; n=3; P< 0.001). Together, these data indicate that the BBB in LAMA2-/- mice has compromised selective permeability characteristics, leading to activation of resident immune cells within the CNS.

Impaired maturation of the blood-brain barrier in LAMA2-/- mice

To determine whether laminins influenced the maturation of the BBB, we evaluated features of the cerebral vasculature that are known to be regulated by the induction and maturation of barrier features. We conducted immunohistochemistry against glucose transporter 1 (Glut-1), a transporter that regulates the metabolic environment of the cerebral parenchyma and whose expression normally coincides with the BBB maturation. Relative to that in wild type littermates, however, we observed no significant change in Glut-1 immunoreactivity in LAMA2-/- mice at post-natal day 21 (Fig. II-7A; 0.561 ± 0.067 in LAMA2 -/- versus 0.536 ± 0.026 in wild type, n=3, P=0.74). Protein analysis by western immunoblotting also indicated no significant changes in Glut-1 levels at postnatal days 1, 8, 15 and 21 (Fig. II-7B). Relative Glut-1 protein levels at postnatal day 1 (P1) were 6.878 ± 1.42 in LAMA2 -/- cerebral cortices versus 8.303 ± 2.54 in wild-type cortices, n=3, P= 0.650; at P8 were 9.163 ± 0.81 in LAMA2 -/- versus 11.077 ± 2.48 in wild-type, n=3, P= 0.504; at P15 were 1.501 ± 0.25in LAMA2 -/- versus 1.062 ± 0.16 in wild-type, n=3, P= 0.211; and at P21 were 1.179 ± 0.12 in LAMA2 -/- versus 0.912 ± 0.08 in wild-type, n=3, P= 0.136. These data suggest that laminin α2 does not significantly affect overall Glut-1 protein levels or localization at the gliovascular interface.

To further evaluate BBB development, we conducted immunohistochemistry against MECA32 (i.e., plasmalemma vesicle-associated protein, Plvap), which is expressed in the peripheral vasculature throughout development but ceases to be expressed in the cerebrovasculature during embryonic development (corresponding with the establishment of barrier properties). MECA32/Plvap is involved in vesicular transport in endothelial cells and is highly expressed in permeable vessels of peripheral tissues [117, 121, 122]. In the postnatal CNS, however, MECA32 expression is limited to circumventricular organs, which reside outside

of the confines of the BBB [123]. However, re-expression of MECA32 has been observed in pathological conditions where CNS inflammation is prominent such as experimental autoimmune encephalitis (EAE) and other models of neuroinflammation [124-126]. Immunoreactivity for MECA32 was observed in a subset of large vessels distributed throughout the cortex, striatum and hippocampus of postnatal day 21 LAMA2 -/- mice, whereas no MECA32 immunoreactivity was detected in wild type mice outside of the circumventricular organs (Fig. II-8A). We further characterized MECA32 vascular coverage at postnatal day 21 and found that LAMA2 -/- mice had significantly increased levels of MECA32 relative to blood vessel area (Fig. II-8C; 0.282 ± 0.035 in LAMA2 -/- versus 0.103 ± 0.021 in wild type; n=3; P= 0.012). We also performed MECA32 immunohistochemistry on brain sections from mice that had been injected with Evans Blue dye and found that MECA32 immunoreactive large blood vessels were *always* associated with Evans Blue leakage into the brain parenchyma (Fig. II-8B). It should be noted that in Fig. II-8B, we substantially increased the brightness of the Evans Blue signal in order to visualize all blood vessels in the field, therefore the Evans Blue difference between wild-type and knockout is no longer apparent in these images. Finally, we analyzed MECA32 by western immunoblotting and found that MECA32 protein levels were significantly higher in LAMA2-/- cerebral cortices at postnatal day 21 than in wild type littermate cerebral cortices (Fig. II-8D; 3.041 ± 0.21 in LAMA2 -/- versus 0.677 ± 0.1 in wild-type, n=3, P= 0.029).

To evaluate the development of inter-endothelial tight junctions, which act as physical barriers against passage through vascular fenestrations, we conducted immunohistochemistry against tight junction components Zonula Occludens 1 (ZO-1), Claudin-5 and Occludin, Although the formation of tight junctions was apparent in LAMA2 -/- mice and wild type controls at postnatal day 21, differences in morphology were observed in high magnification

confocal images in LAMA2 -/- mutants (Fig. II-9A). ZO-1 immunoreactivity was distributed in a pattern consistent with continuous adherens complexes in both LAMA2 -/- and wild-type however, LAMA2 -/- mice displayed morphological abnormities including regions of increased junctional hypertrophy and undulation. In addition, we observed decreased immunoreactivity of claudin-5 and occludin in LAMA2 -/- mice relative to wild-type littermates (Fig. II-9A). Additionally, we quantified overall protein levels of tight junction components by western immunoblotting. Quantification of ZO-1 protein levels by western immunoblotting indicated that ZO-1 levels (Fig. II-9B) did not significantly differ between LAMA2 -/- mice and wild-type littermate controls (0.971 ± 0.233 in LAMA2-/- versus 1.001 ±0.167 in wildtype (1.02 fold of wildtype ± 0.3), n=3, P= 0.92), indicating that ZO-1 morphology, but not production, differs in LAMA2-/- mice. We further quantified the protein levels of the adherens junction components, VE-cadherin, claudin-5 and occludin. Western blots indicated that VE-cadherin levels were significantly lower in LAMA2-/- mice relative to those in wildtype littermates at postnatal day 21 (Fig. II-9B; 2.198 ± 0.51 in LAMA2-/- versus 5.976 ± 0.881 in wildtype (0.37 fold of wild-type ± 0.08), n=3, P= 0.021). Claudin-5 levels were also significantly lower in LAMA2-/- mice relative to those in wildtype littermate control mice (Fig. II-9B; 0.153 ± 0.025 in LAMA2-/- versus 0.379 ± 0.065 in wildtype (0.42 fold of wildtype ± 0.06), n=6, P= 0.005). Additionally, western blots indicated that occludin levels were significantly lower in LAMA2-/- mice relative to those in wild-type littermates (Fig. II-9B; 0.576 ± 0.142 in LAMA2-/- versus 0.995 ± 0.139 in wild-type (0.57 fold of wild-type ± 0.13), n=6, P= 0.01).

Inappropriate MECA32 expression in the postnatal CNS vasculature and significant decreases in the adherens junction components VE-cadherin, claudin-5 and occludin, with additional morphological differences in ZO-1 immunoreactive tight junctions, together indicate

that the absence of laminin α2 impacts BBB maturation, and further suggests that perturbed vascular endothelial maturation or homeostasis may contribute to increased BBB permeability.

Laminin regulates cerebral vasculature pericyte coverage

The cerebral vasculature is extensively covered by pericytes, which express high levels of the platelet-derived growth factor receptor-β (PDGFR-β), a necessary signaling receptor for pericyte recruitment [36]. The absence or loss of vascular pericyte coverage is highly correlated with vascular leakage at the BBB [31]. To assess pericyte coverage throughout different regions of the CNS, we utilized PDGFR-β and collagen IV immunohistochemistry to visualize pericytes and the basal lamina of the cerebral vasculature, respectively. First, we performed laminin α2, PDGFR-β and collagen IV immunohistochemistry to assess whether laminin α2 is colocalized with pericytes along the vasculature in wild type mice (Fig. II-10A). We observed a high level of colocalization of laminin α2 and PDGFR-β, which suggests a close association of laminin α2 with pericytes and furthermore supports the possibility that pericytes themselves may express laminin α2 *in vivo*. Next, we sought to quantify pericyte coverage along the cerebral vasculature in the cerebral cortex, striatum and hippocampus of LAMA2-/- and wild type mice. Pericyte coverage along blood vessels, visualized in confocal three-dimensional reconstructions of PDGR-β/collagen IV immunohistochemistry, appeared profoundly lower in LAMA2-/- cerebral cortices then that in wild type littermates (Fig. II-10B). Next, pericyte coverage along blood vessels was quantified in mice at postnatal day 21. LAMA2-/- mice had significantly reduced pericyte coverage relative to blood vessel area in all regions evaluated (Fig. II-10C): in the cortex, a 60.47% reduction (0.17 ± 0.011 in LAMA2-/- versus 0.43 ± 0.014 in wild type; n=3; P= 0.007); in the striatum, a 33.34% reduction (0.08 ± 0.007 in LAMA2-/- versus 0.25 ± 0.003 in wild type; n=3; P= 0.001); and in the hippocampus, a 56.52% reduction (0.20 ± 0.014 in

LAMA2-/- versus 0.46 ± 0.023 in wild-type; n=3; P= 0.001) relative to wild type littermates. We further quantified PDGFRβ at postnatal day 21 by western immunoblotting and found that PDGFRβ protein levels in LAMA2-/- mice were significantly lower relative to those in wild-type littermates (Fig. II-10D; 0.255 ± 0.035 in LAMA2-/- versus 0.345 ± 0.027 in wild type; n=6; P=0.04). We then compared pericyte coverage of the cerebral vasculature in developing littermates at postnatal days 1, 8, 15 and 21 to determine whether changes in pericytes coverage in the vasculature of LAMA2 -/- mice occurred earlier in postnatal development (Fig. II-10E). Throughout postnatal development the vasculature of LAMA2-/- cerebral cortices had decreased pericyte coverage when compared to that in wild-type littermates. At postnatal day 1, LAMA2-/- mice already had significantly reduced pericyte coverage in the cortical vasculature relative to wildtype littermates (0.103 ± 0.016 in LAMA2-/- versus 0.278 ± 0.06 in wild type; n=3; P= 0.048). Together, these data indicate that the absence of laminin α2 significantly perturbs the ability of pericytes to interact with the cerebrovasculature during postnatal development. The fact that pericyte coverage appears to be disturbed in numerous brain regions, and is apparent from birth, furthermore supports our observations that BBB leakage is widespread and not confined to particular regions as a localized "damage response", but instead is a developmental abnormality.

Channel localization at astrocytic endfeet is altered in LAMA2-/- mice

Astrocytic endfeet use the dystrophin-associated glycoprotein complex (DGC) to facilitate the localization of homeostatic channels such as AQP4 to the gliovascular interface. The laminin receptor dystroglycan acts as a central component of the DGC, physically linking AQP4 through intracellular adaptor proteins such as α-dystrobrevin. Previous studies have

provided evidence that physical interactions with α-dystrobrevin are required to maintain polarized distributions of AQP4 at astrocytic endfeet [80]. To investigate the role of laminin α2 in localizing channels at astrocytic endfeet, we conducted immunohistochemistry against AQP4 in conjunction with GFAP to visualize circumferential astrocytic processes at the gliovascular interface. We observed decreased immunoreactivity of AQP4 (Fig. II-11A) at astrocytic endfeet in LAMA2 -/- cerebral cortices relative to that in wild type littermates at postnatal day 21. LAMA2 -/- mice had significantly decreased levels of AQP4 immunoreactivity distributed at vascular-associated astrocytic endfeet (Fig. II-11B; 3.628 ± 0.97 in LAMA2 -/- versus 14.213 ±1.21 in wild type; n=3; P= 0.002). However, relative protein levels of AQP4 were not significantly different between groups at postnatal day 21 (Fig. II-11C; 1.847 ± 0.31 in LAMA2 -/- versus 1.99 ± 0.23 in wild type; n=3; P= 0.730). These data indicate that AQP4 protein levels do not significantly differ, but that AQP4 localization, and perhaps clustering, is perturbed. To address whether AQP4 function was compromised we evaluated brain water content, which we found to be significantly elevated in LAMA2 -/- mice compared to that in wild type littermates (Fig. II-11D; 80.15 ± 0.380 in LAMA2 -/- versus 78.32 ±. 0.654 in wild type; n=9; P= 0.028). These data suggest that laminin α2 is required for both maintaining the polarization of AQP4 channels at astrocytic endfeet and facilitating the function of AQP4 to regulate cerebral osmotic homeostasis

Next, we sought to characterize the adhesion receptors that are known to interact with laminin α2 at the gliovascular interface by conducting β-dystroglycan and β1-integrin immunohistochemistry (Fig. II-12 A and C). In LAMA2-/- mice at postnatal day 21 there was no change in β-dystroglycan immunoreactivity associated with astrocytic endfeet (Fig. II-12A), whereas a decrease in β1-integrin vascular coverage was observed (Fig. II-12C). Furthermore,

protein lysates prepared from cerebral cortices at postnatal day 21 were evaluated by western blot and no significant differences in total β-dystroglycan protein levels were observed in LAMA2-/- mice (Fig. II-12B; 90.723 ±11.0527 in LAMA2 -/- versus 92.097 ±4.704in wild type; n=3; P= 0.915). Increased levels of cleaved 30 kDa dystroglycan, mediated by MMPs 2 and 9, are observed during periods of disturbed BBB function in Experimental Autoimmune Encephalomyelitis (EAE) [43], and we noted that there was a slight increase in the relative amount of the cleaved 30 kD β-dystroglycan fragment in LAMA2-/- cerebral cortices, although not significantly so (13.74 ±0.29% in LAMA2 -/- versus 9.53 ±2.23% in wild type; n=3; P= 0.135). To investigate whether the absence of LAMA2 influenced the degree to which astrocyte endfeet were associated with β-dystroglycan, we quantified astrocytic endfeet processes in association with β-dystroglycan immunoreactivity at the gliovascular interface. We found a significant decrease in the percentage of β-dystroglycan positive astrocytes in association with blood vessels in LAMA2 -/- mice relative to those in wild type littermates (45.035% ±6.377 in LAMA2 -/- versus 53.613% ± 2.208 in wild type; n=3; P= 0.031). These results suggest that disturbed adhesive interactions at astrocytic endfeet may contribute to the dysfunction of the neurovascular unit of LAMA2 -/- mice.

To further investigate potential changes in β1-integrins in LAMA2-/- brains, we quantified β1-integrin vascular coverage. LAMA2 -/- mice had significantly reduced (a 27.45% reduction) β1-integrin vascular-associated immunoreactivity relative to blood vessel area at postnatal day 21 (Fig. II-12D; 0.259 ± 0.018 in LAMA2-/- versus 0.357 ± 0.019 in wild type; n=3; P= 0.02). We further quantified overall levels of β1-integrin in the cerebral cortex at postnatal day 21 by western immunoblotting and found no significant differences (Fig. II-12E; 1.39 ±0.13 in LAMA2 -/- versus 1.92 ±0.34 in wild type; n=6; P=0.128). It should be noted

that β1 integrin is expressed in astrocytic endfeet, but is also expressed in pericytes, oligodendrocytes, microglia, neural stem cells, and vascular endothelial cells, thus changes in β1 integrin localized to the BBB is not likely to be reflected in whole cortex lysates. These data suggest that laminin α2 is required both for the correct localization of AQP4 at astrocyte endfeet and contributes to the ability of β1-integrins to localize along the vasculature, presumably also in astrocytes but perhaps additionally through changes in pericyte and/or endothelial cell integrin distribution. In contrast, β-dystroglycan localization at the gliovascular interface may be compensated for by other ECM components such as α1-subunit containing laminins.

LAMA2-/- mice have breaches in the gliovascular basal lamina

The gliovascular basal lamina acts to physically separate the resident cells of the perivascular environment while also creating a continuous matrix that links each cell type together. To investigate the role of laminin α2 on the structure and composition of the gliovascular basal lamina, we utilized two strategies: (1) Ultrastructure analysis via transmission electron microscopy (TEM), and (2) immunohistochemistry against known components of the gliovascular basal lamina. We observed no obvious differences in the basal lamina or gross vascular defects in capillary ultrastructure of LAMA2-/- mice (Fig. II-13A) compared to wildtype mice. However, we observed perturbed tight junction morphology in blood vessels of LAMA2-/- mice in contrast to those wildtype littermates (Fig. II-13B, tight junction's colorized green). In LAMA2 -/- mice, many tight junctions appeared to be narrow and undulating, extending throughout the endothelia lumen. Moreover, large caliber vessels of LAMA2-/- mice had more endocytic vesicles than typical, indicative of transport dysfunction (Fig. II-13B, red arrows). In addition, detachment and/or discontinuity of both the parenchymal and the

endothelial basal lamina were readily observed in large vessels of LAMA2-/- mice (Fig. II-13C, white asterisks; parenchymal BL, blue; endothelial BL, red). LAMA2 -/- mice had discontinuous regions in the gliovascular BL (182 breaches were found upon inspection of 109,030.13 nm of BL in LAMA2 -/- whereas 0 breaches were found upon inspection of 106,145.12 nm of BL in wildtype; Mann-Whitney U-Statistic= 0.00; T=10.00; n=4; P=0.029).

Next, we conducted immunohistochemistry to detect α1, α4, α5 and γ1 laminin subunits, in conjunction with GFAP immunohistochemistry, to determine whether the levels of other laminins were altered in LAMA2-/- brains at postnatal day 21 (Fig. II-14A). In order to characterize endothelial cell laminins, we quantified vascular coverage of α4, α5 and γ1 containing laminins. LAMA2-/- mice had no significant changes in laminin α4 vascular coverage relative to that in wildtype littermates (0.94 ± 0.02 in LAMA2-/- versus 0.963 ± 0.005 in wildtype; n=3; P=0.443). In contrast, LAMA2-/- mice had significantly reduced laminin α5 vascular coverage relative to that in wildtype littermates (0.664 ± 0.033 in LAMA2-/- versus 0.966 ± 0.014 in wildtype; n=3; P=<0.001). Since laminin-511 production by vascular endothelial cells usually increases postnatally during BBB maturation [61], a deficit in laminin-511 levels could reflect the lack of BBB maturity in LAMA2-/- brains. LAMA2 -/- mice also had significantly reduced laminin γ1 vascular coverage relative to that in wildtype littermates (0.442 ± 0.027 in LAMA2-/- versus 0.936 ±0.013 in wild type; n=3; P= <0.001). We also observed a modest increase in laminin α1 immunoreactivity in LAMA2 -/- mice relative to that in wildtype littermates (not shown), suggesting that the loss of laminin-211 led to an increase in laminin-111, possibly as a means to compensate. No change in collagen IV immunoreactivity was observed in LAMA2 -/- mice relative to controls. These data suggest that laminin α2 is required for the

proper formation and/or maintenance of the parenchymal and endothelial basal lamina within the cerebrovasculature of LAMA2-/- mice.

Laminin-dystroglycan interactions potentiate the ability of astrocytes to cluster AQP4

To investigate the ability of laminins to facilitate the polarization of homeostatic channels such as AQP4, we utilized an astrocyte-based assay to test the ability of substrates to aggregate channels in the plasma membrane. We prepared primary astrocytes from LAMA2-/- and wild type littermate brains to test the ability of endogenous astrocytic laminin α2 to organize AQP4. When cultured over several days, astrocytes organized AQP4 into mesh-like networks and clusters at the interface between the cell and the plastic, this clustering ability was enhanced by growing the astrocytes on slides coated with laminin (Figure II-15A, left panels). It should be noted that astrocytes grown on PDL substrates express endogenous laminins-111 and -211, which contribute to the "baseline" of clusters in this long-term culture. In contrast, astrocytes from LAMA2-/- neonates had a marked deficit in AQP4 clusters when grown on PDL (Figure II-15A, right panels, *PDL*). However, the ability of LAMA2-/- astrocytes to cluster AQP4 was rescued by growing the cells on laminin-211 (Figure II-15A, right panels, *laminin*). To quantify changes in the ability of LAMA2-/- astrocytes to cluster AQP4, we conducted AQP4 and GFAP immunohistochemistry and then uniformly applied intensity thresh-holding to determine cluster areas, i.e. areas of intense AQP4 immunoreactivity. AQP4 cluster area relative to total GFAP-positive cell coverage area was then calculated per field. When astrocytes were grown on PDL, we observed significantly decreased relative AQP4 clusters in astrocytes derived from LAMA2 -/- mice compared to wild-type astrocytes (Figure II-15B; 0.063 ± 0.025 in LAMA2-/- versus 0.126 ± 0.038 in wildtype (0.45 fold of wild-type, ± 0.07); n=5; P= 0.01). In contrast, the ability

of LAMA2 -/- astrocytes to cluster AQP4 on laminin substrate was similar to wild type astrocytes grown on a laminin substrate (Figure II-15B; 0.386 ±0.075 in LAMA2 -/- versus 0.491 ±0.061 in wild-type (0.79 fold of wild-type, ±0.14); n=5; P=0.312). Together, these data suggest that laminin interactions with dystroglycan and, to a lesser extent, β1-integrins, potentiate the ability of astrocytes to aggregate AQP4 channels into clusters. The ability of laminin substrates to rescue AQP4 clustering in LAMA2 -/- astrocytes furthermore indicates that LAMA2-/- have appropriate levels of functional laminin receptors that are responsive to the exogenously applied laminin.

Discussion

ECM proteins are thought to contribute to BBB function by generating the physical barrier of the gliovascular BL. Here we report that α2-subunit containing laminins not only have an important contribution to the physical integrity of the gliovascular BL, but also promote BBB maturation by increasing pericyte interactions with the vascular endothelium. The failure to produce α2-containing laminins results in a leaky BBB with characteristics of immaturity: expression of embryonic vascular proteins such as MECA32, limited pericyte coverage, and poorly polarized channel distribution in astrocytes. And, while vascular endothelial tight junctions are present in LAMA2-/- brains, some observations suggest tight junction immaturity including reduced levels of VE-cadherin, Occludin, and Claudin-5, a thinner and undulating tight junction appearance by TEM, differences in junctional protein immunoreactive morphology, and inappropriate appearance of endocytic vesicles.

Laminins, pericytes, and BBB maturation

In the current study we provide evidence that LAMA2-/- mice have profound alterations in BBB development and function. For example, Evans Blue dye from the circulatory system quickly crosses into the brain parenchyma in LAMA2/- mice, with all regions of the CNS examined thus far (the frontal cortex, striatum, hippocampus, and cerebellum) exhibiting the "leaky brain" phenotype. However, decreased pericyte coverage along the vasculature may underlie this increased BBB permeability, rather than a failure of vascular endothelial cells to form tight junctions. However, tight junctions in the LAMA2-/- vasculature, while present, may be functionally compromised to some degree as they have various morphological abnormalities and decreased levels of VE-cadherin, occludin, and claudin-5.

Perturbed pericyte coverage in LAMA2-/- mice appears to be a developmental defect, as it was observed from birth onwards until early adulthood. α-SMA levels were also lower in LAMA2-/- brains, suggesting that laminins normally contribute to VSMC maturation, which is in agreement with a recent finding that astrocyte-derived laminins promote VSMC maturation [27]. A conditional knockout of β1-containing integrins in both pericytes and VSMCs using PDGFRβ-Cre resulted in decreased VSMC differentiation, providing further support for a role for laminin receptor interactions in promoting VSMC maturation [64]. However, a separate more recent study using the mice that lack laminin expression selectively in astrocytes, reported increased levels of α-SMA immunoreactivity associated with the cerebral vasculature, suggesting that laminins can also suppress VSMC maturation [77]. The mechanism by which laminins could either decrease or increase VSMCs maturation remains unclear, however these studies clearly highlight laminins as key regulators of VSMCs.

In the cerebral cortex of adult LAMA2 -/- mice we observed inappropriate expression of MECA32 (i.e., Plvap), which normally associates with caveolae and regulates endothelial vesicular trafficking [127]. MECA32 is found postnatal development in various tissues with fenestrated endothelium but in the brain MECA32 expression is strictly embryonic, with MECA32 loss coinciding with BBB maturation [128]. Coinciding with inappropriate MECA32 expression, we also detected an overabundance of endocytotic vesicles in the vasculature endothelial cells of LAMA2-/- mice. Pericytes have the ability to suppress Plvap expression [117], indicating that the decreased pericyte coverage in LAMA2-/- mice may result in dysregulation of vascular endothelial cell transport mechanisms. Together these findings indicate a novel role for laminin α2 in the regulation of pericytes. In addition, the loss of pericyte coverage in dystroglycan conditional knockout mice closely mirrors that in LAMA2-/- mice,

suggesting that pericyte defects observed in LAMA2-/- mice at least in part are a result of losing key gliovascular laminin-dystroglycan interactions.

Laminin α2, as part of the laminin-211 heterotrimer, contributes to the parenchymal and composite BLs of large caliber blood vessels and capillaries, respectively [62]. Laminin α2 is produced by astrocytes and can be localized to astrocytic endfeet that run along cerebral vessels, and thus is often referred to as an astrocytic laminin. However, in the complete absence of laminin-211 expression from astrocytes in laminin γ1 conditional knockouts, laminin α2 protein is still observed in protein lysates from the cerebral cortex, albeit at lower levels than normal, suggesting that other cell types besides astrocytes contribute laminin α2 [27]. Indeed, purified pericytes from the CNS have been observed to express several ECM proteins in culture, including laminin α2 [29] and, intriguingly, *in vivo* studies suggest that in the absence of pericytes, laminin α2 protein levels at the gliovascular interface are substantially lower [31, 70]. And, loss of laminin γ1 gene expression from astrocytes did not significantly impact PDGFR-β immunoreactivity along the vasculature of the CNS [27], in contrast to what was observed in our study with a global loss of LAMA2 expression from all brain cells. Additionally, an astrocyte-specific conditional β1- integrin knockout resulted in a profound loss of astrocytic laminin-111 and -211 expression, however these β1-integrin astrocyte knockout mice had no change in BBB permeability (although pericyte coverage per se was not addressed) [98]. Thus, it is worth considering in future studies whether the pericyte abnormalities observed in LAMA2-/- brains reflects failed autocrine interactions between pericytes and *pericyte-secreted laminins*, and whether disturbances in brain vascular endothelial cells, at least in part, result from a loss of laminin from pericytes.

Laminin regulates gliovascular ECM composition

An extensive network of ECM contacts all of the resident cell types of the gliovascular interface facilitating both BBB structural integrity and cellular communication. In the current study we observed structural defects, i.e. areas of discontinuous or breached BL, in the parenchymal and endothelial BLs of large caliber blood vessels of LAMA2-/- brains . However it remains unclear whether these breaches reflect a failure in BL development or reflect a failure in BL maintenance. Furthermore, the relative contribution of various laminin subunits appeared to be altered in the LAMA2 -/- gliovascular interface, indicating that the observed phenotypes could be quite complex and in some instances may reflect changes in *other* laminin subunits that arise as a secondary consequence of changes in laminin α2 expression. Most strikingly in the LAMA2-/- cerebral vasculature we observed decreased immunoreactivity of laminin α5. The laminin α5 subunit is a key component of laminin-511, which along with laminin-411 comprises the brain vascular endothelial laminins [62]. Unlike laminin-411 expression, which is present in embryonic brain vascular endothelial cells, laminin-511 expression appears later and can be found concentrated in areas of high pericyte recruitment [62]. It remains unclear whether the dysregulation of laminin-511 levels in LAMA2-/- brains is related specifically to the poor pericyte coverage or simply may reflect the more global failure of brain vascular endothelial maturity. Overall these data support a role for α2-containing laminins, i.e. laminin-211, in orchestrating the integrity and composition of BLs, including the endothelial BL, at the gliovascular interface.

Laminin and CNS immune surveillance

The CNS vasculature is a dynamic yet highly controlled system that helps regulate the brain parenchyma. Normally, the vasculature BL acts as a physical barrier to transendothelial migration of leukocytes. In LAMA2-/- mice, however, we observed leukocytes in the brain parenchyma, indicating that peripheral immune cells were inappropriately crossing the BBB. Laminin α5 has been shown to negatively regulate the ability of T-cells to extravasate into the brain parenchyma during Experimental Autoimmune Encephalomyelitis (EAE) [69], suggesting that the relatively low level of laminin α5 seen in the LAMA2-/- brain vasculature may contribute to inappropriate T cell infiltration. The proteolytic cleavage of β-dystroglycan by MMPs during EAE has also been shown to facilitate transendothelial migration of leukocytes [43]. In the current study we observed an increased level of cleaved β-dystroglycan in LAMA2-/- brains, suggesting that inappropriate dystroglycan cleavage may contribute to the observed increased T-cell extravasation. On the other had, an increase in dystroglycan cleavage may also result as a *consequence* of BBB breakdown and the subsequent innate immune activation, as activated microglia are known to secrete MMPs responsible for dystroglycan cleavage [43]. Additionally, immune cell migration has been observed at sites devoid of pericyte coverage, suggesting that the decreased pericyte coverage in LAMA2 -/- mice contributes to T-cell migration into the brain parenchyma [129, 130].

When the BBB is compromised microglia, the resident immune cells of the CNS, encounter "foreign" substances, which result in microglial process contraction and activation. LAMA2-/- brains had more iba1+ microglia, with many more of them displaying an activated morphology indicating that microglia had been activated by the presence of infiltrating immune cells. As stated previously, MECA32, usually confined to embryonic brain vascular endothelial

cells, was observed in LAMA2 -/- brain vasculature at postnatal day 21 and even as late as postnatal day 28 (not shown). In pathological conditions such as Alzheimer's disease and EAE, inflammation is known to trigger reexpression of MECA32 in the compromised vasculature of the CNS [124-126, 131]. Thus inflammatory changes, e.g. increased microglial cell activation, may contribute to re-expression of MECA32 in LAMA2-/- brains.

Laminin-dystroglycan interactions regulate astrocytic endfeet architecture

Components of the DGC contribute to the establishment and maintenance of appropriate astrocytic endfoot architecture with polarized localization of homeostatic channels. In LAMA2 mutants we observed disturbances in the polarized localization of AQP4, indicating that laminin binding to dystroglycan is required to regulate AQP4 polarization. Additionally, in longer-term cultures, with the absence of *endogenously* produced laminin α2, astrocytes derived from LAMA2-/- brains were defective in their ability to form AQP4 aggregates and clusters (but were rescued by exogenous laminin). Finally, while AQP4 distribution was clearly different in LAMA2-/- brains, we did not observe changes in overall AQP4 protein levels, consistent with our hypothesis that laminins influence AQP4 distribution *but not* AQP4 protein production or stability. These findings support existing reports that other components of the DGC, e.g. dystrophin, syntrophins, and dystrobrevin, also regulate glial endfeet channel polarity, such that osmotic regulation and neuronal metabolism is disturbed in their absence [80, 84, 103, 132, 133]. In the current study we also found that brain water content is increased in LAMA2-/- mice, providing further support for the hypothesis that loss of AQP4 polarity contributes to osmotic disturbances.

In summary, we identified new roles for laminin at the CNS gliovascular interface, where laminin-dystroglycan interactions regulate BBB development, structure and function, at least in part by regulating pericyte coverage of brain vascular endothelial cells. We furthermore provide the first report of a specific role for α2-containing laminins (laminin-211) in gliovascular BL structure and function, with implications for the CNS pathologies that result from LAMA2 mutations in congenital muscular dystrophies (MDC1A). We conclude that laminin-mediated signals from non-endothelial cells such as astrocytes and pericytes, underlie successful BBB development/function, a finding that has implications for understanding the connection between BBB breakdown and conditions with neurodegenerative pathology including stroke, Alzheimer's disease, and Multiple Sclerosis. Future studies will be of interest to determine whether laminins act as extrinsic organizers of the spatial arrangement of the gliovascular interface or directly modulate cellular phenotypes through signaling mechanisms downstream of adhesion receptors such as dystroglycan.

Figure II-1. Verification of LAMA2 gene deletion.

(A) Laminin α2 (Lm α2) immunoreactivity (red) was observed in the pial basal lamina and in the vasculature basal lamina in wild-type (WT) cerebral cortices, but was absent in LAMA2-/- cerebral cortices. (B) Laminin α2 immunoreactivity (Lm α2; red) was detected along blood vessels at the gliovascular interface of astrocytic endfeet (GFAP, green) of WT at P21, but not in LAMA2-/- mice. Scale bars: 50 μm. Figure adapted from Menezes et al. 2014 [28].

A)

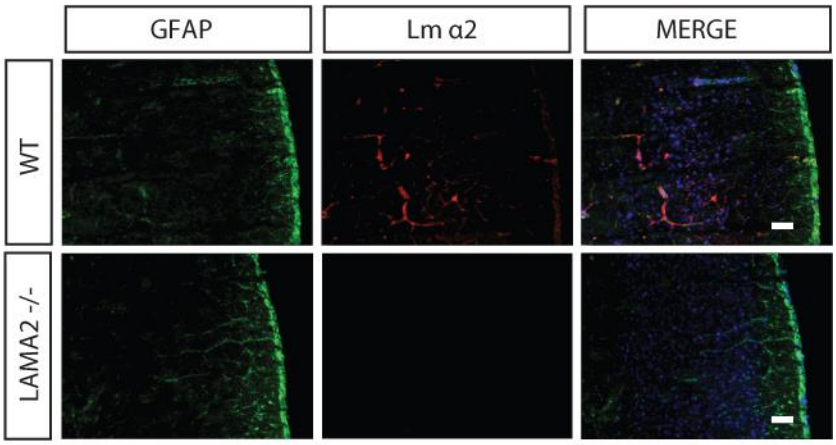

B)

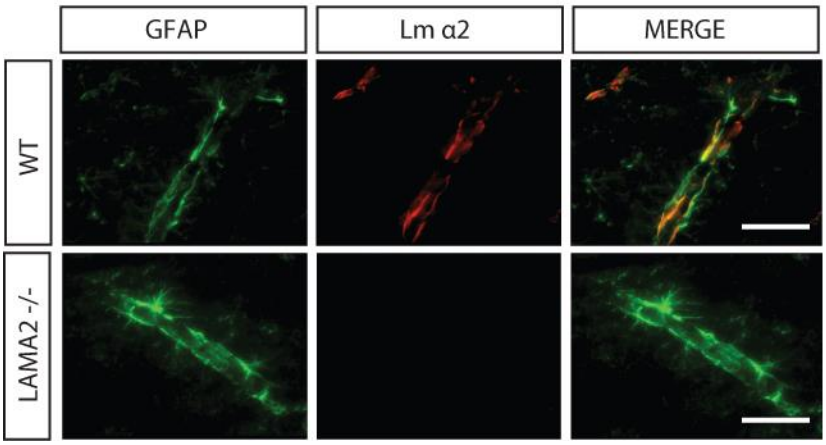

Figure II-2. Astrocyte development in LAMA2 mutant mice.

(A) Immunohistochemistry to detect astrocytes (GFAP) in the cerebral cortices of LAMA2-/- mice or wild type (WT) littermates at postnatal day 21. (A) In LAMA2-/- mice, astrocytic processes (GFAP, green) appear to be hypertrophic, characteristic of reactive gliosis. (B) GFAP immunoreactive area was increased in LAMA2-/- cortices relative to that in WT cortices. (C) The density of GFAP positive cells did not significantly differ between LAMA2-/- and wild type (WT) littermate cerebral cortices at postnatal day 21. (D) Western immunoblotting for GFAP and p115 (protein loading control) in lysates from P21 LAMA2-/- and WT cerebral cortices. Protein levels of GFAP were significantly elevated in LAMA2 -/- mice. ***$p<0.001$, Student's t-test; error bars, SEM; Scale bars: 50 μm. Figure adapted from Menezes et al. 2014 [28].

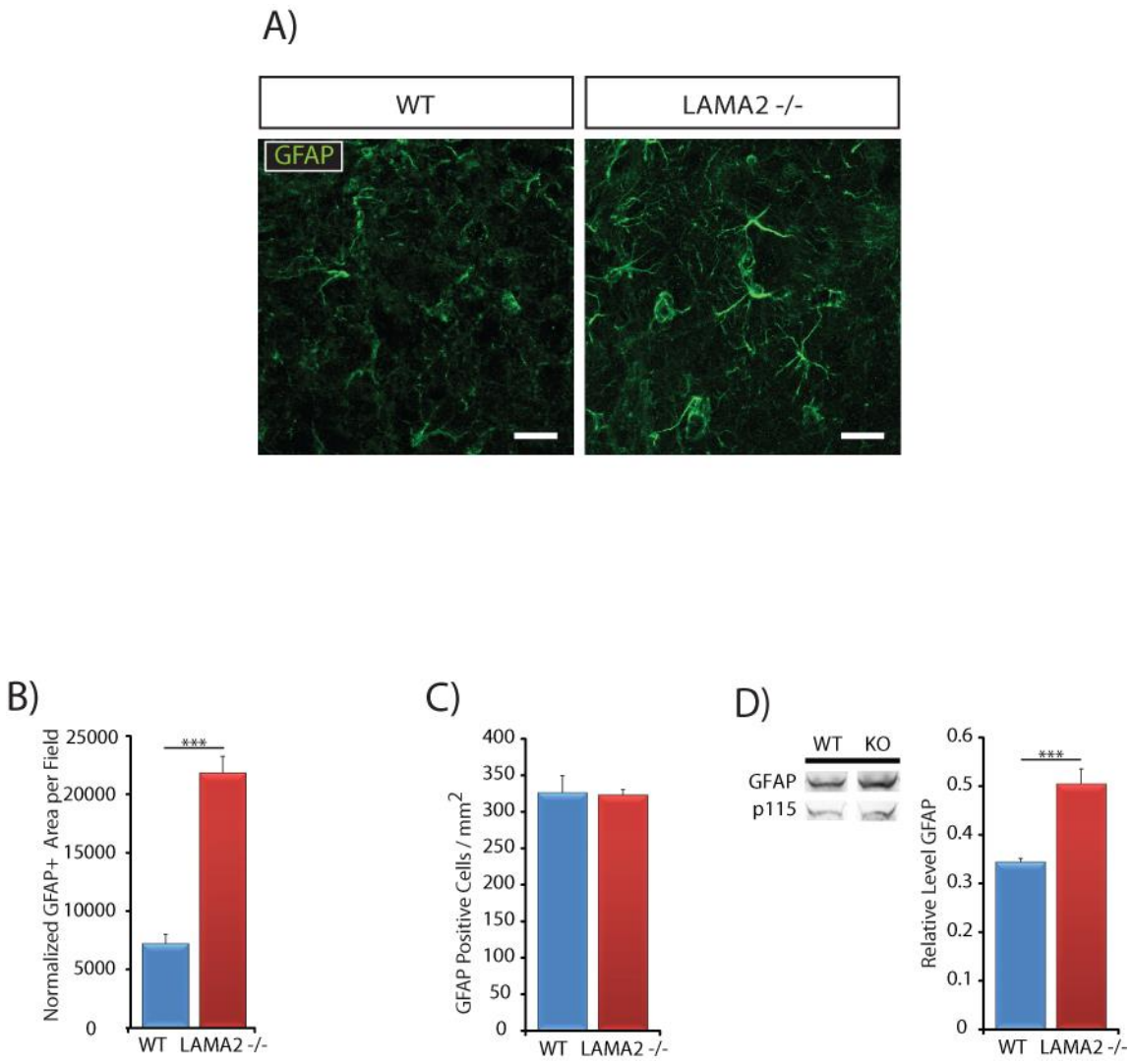
A)
WT
LAMA2 -/-
GFAP
B)
Normalized GFAP+ Area per Field
25000
20000
15000
10000
5000
0
***
WT
LAMA2 -/-
C)
GFAP Positive Cells / mm2
400
350
300
250
200
150
100
50
0
WT
LAMA2 -/-
D)
WT
KO
GFAP
p115
Relative Level GFAP
0.6
0.5
0.4
0.3
0.2
0.1
0
***
WT
LAMA2 -/-

Figure II-3. Vascular development in LAMA2 mutant cortices.

(A) Immunohistochemistry to detect endothelial cells (CD31) in the cerebral cortices of LAMA2-/- mice or wild type (WT) littermates at postnatal day 21. (B) In LAMA2-/- mice, vascular endothelial cell density (CD31, red) is grossly normal, with decreased branching complexity (C). **$p \leq 0.01$, Student's t-test; error bars, SEM; Scale bars: 50 μm. Figure adapted from Menezes et al. 2014 [28].

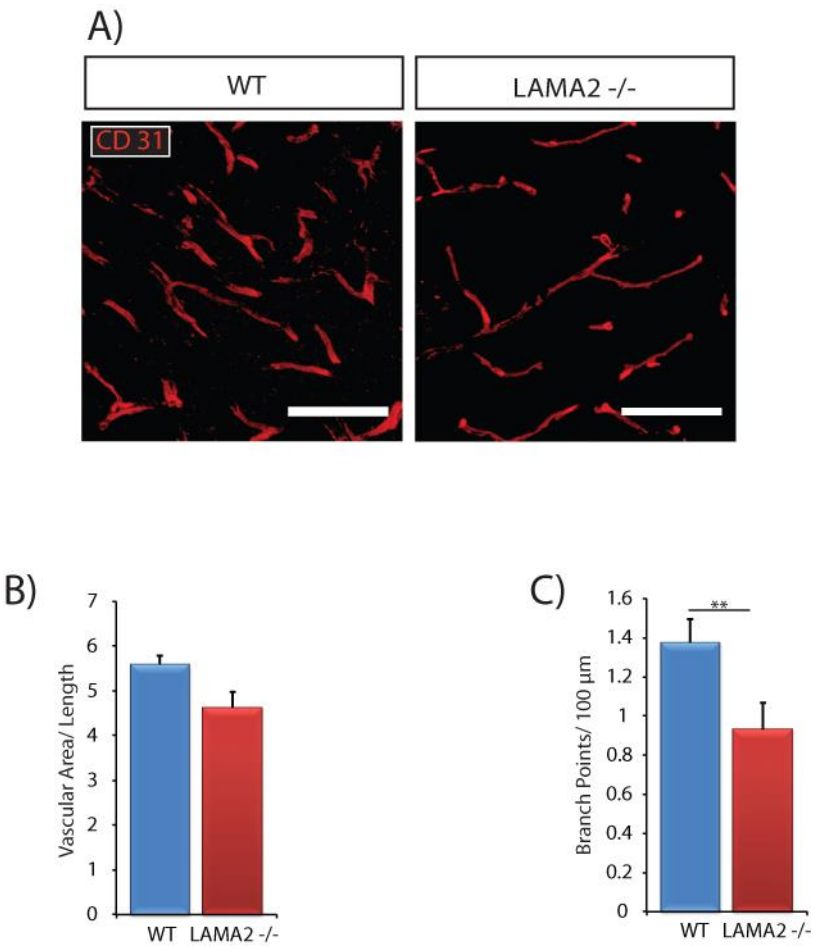
A)
WT
LAMA2 -/-
CD 31
B)
Vascular Area/ Length
0
1
2
3
4
5
6
7
WT
LAMA2 -/-
C)
Branch Points/ 100 µm
0
0.2
0.4
0.6
0.8
1
1.2
1.4
1.6
**
WT
LAMA2 -/-

Figure II-4. Vascular smooth muscle cell (VSMC) development is perturbed in in the absence of LAMA2.

(A) Immunohistochemistry to detect α-smooth muscle actin (α-SMA) in vascular smooth muscle cells in the cerebral cortices of LAMA2-/- mice or wild type (WT) littermates at postnatal day 21. (A) α-SMA immunoreactivity (green) in LAMA2 -/- mice appears to be decreased compared to that in WT littermates. (B) Quantification of area of α-SMA immunoreactivity coverage relative to laminin-111 (pan-laminin immunoreactivity as vasculature area) in LAMA2-/- and WT at postnatal day 21. Coverage of α-SMA was reduced in LAMA2-/- mice. (C) Quantification of α-SMA by western blot; α-SMA protein levels in LAMA2-/- cerebral cortical lysates are significantly reduced relative to those from wild type littermates. **$p \leq 0.01$, Student's t-test; error bars, SEM; Scale bars: 50 μm. Figure adapted from Menezes et al. 2014 [28].

A)

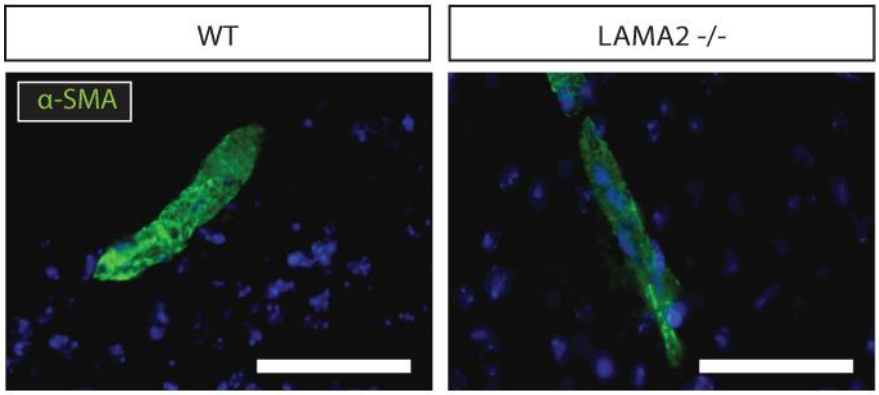
WT
LAMA2 -/-
α-SMA

B)

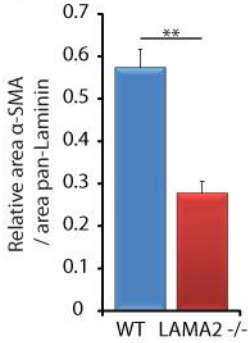
Relative area α-SMA / area pan-Laminin
0.7
0.6
0.5
0.4
0.3
0.2
0.1
0
**
WT
LAMA2 -/-

C)

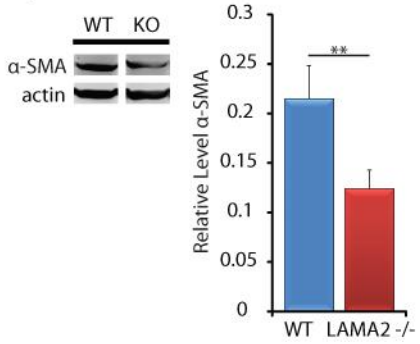
WT
KO
α-SMA
actin
Relative Level α-SMA
0.3
0.25
0.2
0.15
0.1
0.05
0
**
WT
LAMA2 -/-

Figure II-5. LAMA2 regulates BBB permeability.

(A) Extravasation of Evans Blue dye (red) is seen in the parenchymal space in coronal sections taken from the cerebral cortex, striatum, hippocampus and cerebellum in LAMA2-/- and WT littermate mice at P21. Residual signal in WT was restricted to endothelial lumen. (B) Quantification of Evans Blue dye extracted from LAMA2-/- and WT cerebral cortices at P21. The level of Blue in LAMA2 -/- cortices was significantly elevated compared to that in WT littermates. *$p<0.05$, Student's t-test; n=3. Scale bars: 50 μm. Figure adapted from Menezes et al. 2014 [28].

A)

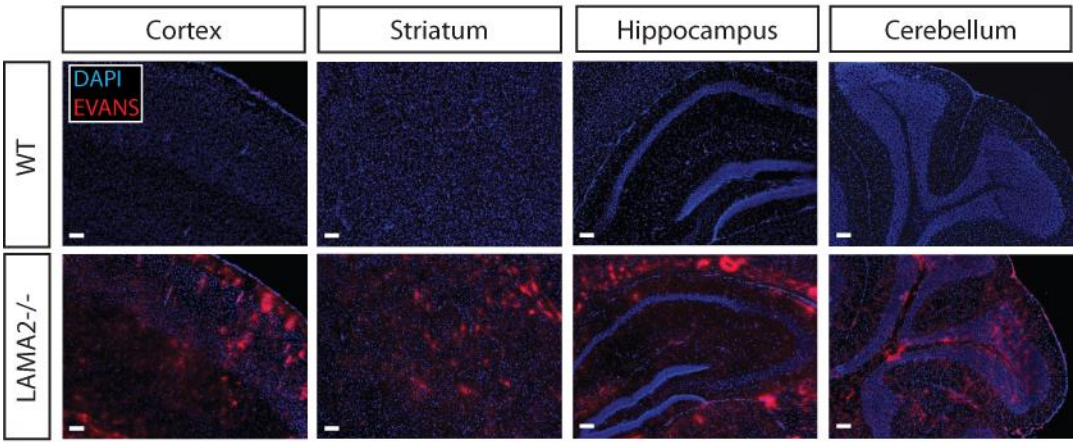
Cortex
Striatum
Hippocampus
Cerebellum
WT
LAMA2-/-
DAPI
EVANS

B)

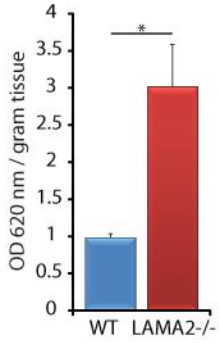
OD 620 nm / gram tissue
4
3.5
3
2.5
2
1.5
1
0.5
0
*
WT
LAMA2-/-

Figure II-6. Microglial/ macrophage activation and leukocyte accumulation in the parenchyma of LAMA2 mutants.

(A) Immunohistochemistry to detect laminin-111 ("pan-lm" as antibody detects laminin α1, β1, and γ1 subunits, green), CD45 (red, left panel) and CD3 (red, right panels) in LAMA2-/- and WT mice at postnatal day 21. CD45+ and CD3+ cells were observed in the cerebral parenchyma of LAMA2-/- but not WT mice. (B) Immunohistochemistry to detect microglia/ macrophages (iba-1, green) in the striatum of LAMA2-/- and WT mice at postnatal day 21. The striatum of LAMA2-/- mice had more microglia with the amoeboid morphology characteristic of activated microglia (right panel) relative to those in WT littermates. (C) Quantification of iba1+ cells (microglia/ macrophages) in the striatum of LAMA2-/- and WT mice at postnatal day 21. Iba1+ cells per area in the striatum of LAMA2-/- mice were significantly elevated compared to those in WT littermates. ***$p<0.001$, Student's t-test; n=3. Scale bars: 50 μm. Figure adapted from Menezes et al. 2014 [28].

A)

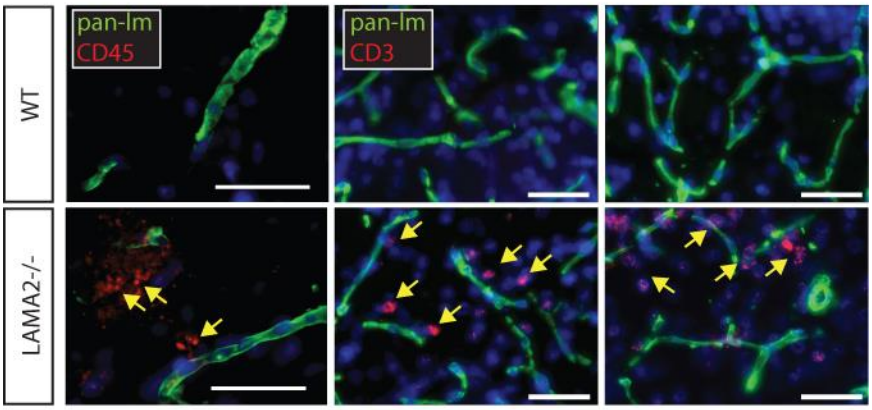
WT
LAMA2-/-
pan-lm
CD45
pan-lm
CD3

B)

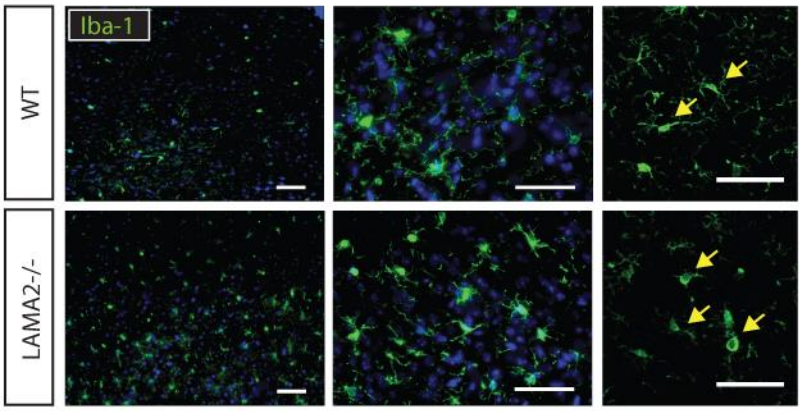
WT
LAMA2-/-
Iba-1

C)

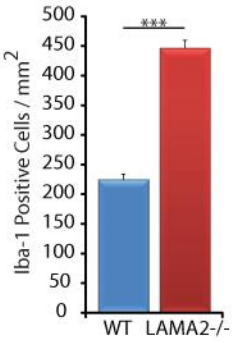
***
Iba-1 Positive Cells / mm2
500
450
400
350
300
250
200
150
100
50
0
WT
LAMA2-/-

Figure II-7. BBB metabolic transporters develop in LAMA2 mutants.

(A) Immunohistochemistry to detect Glut-1 and any subunit of laminin-111 ((laminin α1, β1, or γ1 subunits; i.e., pan-laminin) in the vascular endothelial cells in coronal sections at postnatal day 21 in LAMA2-/- and WT cerebral cortices. Glut-1 immunoreactivity in LAMA2-/- mice appears to be comparable to that in WT control littermates. (B) Western immunoblotting for Glut-1 at postnatal day 1 (P1), P8, P15 and P21 using lysates from LAMA2-/- and WT cerebral cortices. No changes in Glut-1 levels were observed. p115 blots are shown as loading controls. Figure adapted from Menezes et al. 2014 [28].

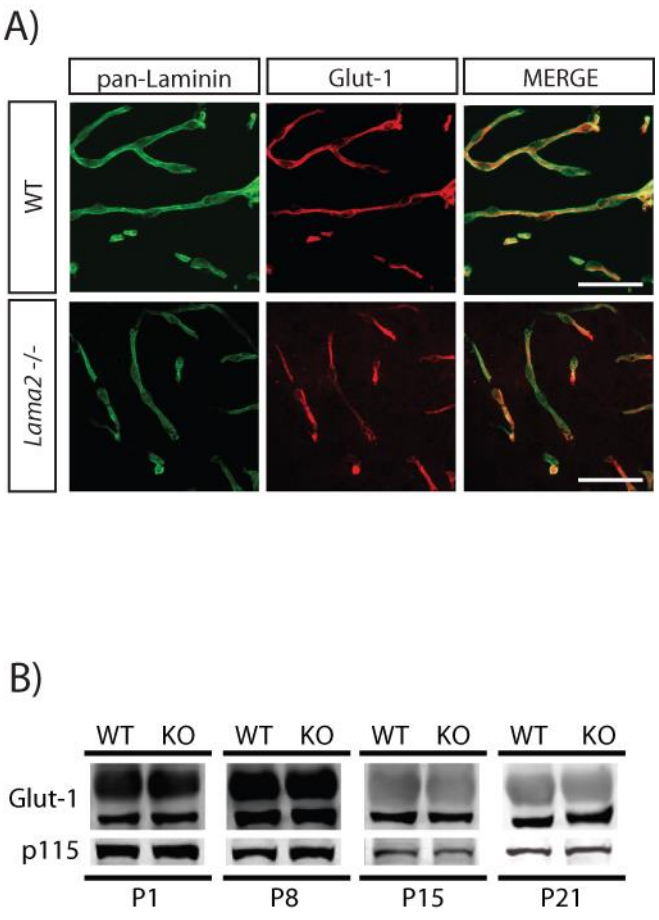
A)
pan-Laminin
Glut-1
MERGE
WT
Lama2 -/-
B)
WT KO WT KO WT KO WT KO
Glut-1
p115
P1
P8
P15
P21

Figure II-8. Impaired vascular maturation in LAMA2-/- mice.

(A) Immunohistochemistry to detect any subunit of laminin-111 and MECA-32 in the vascular endothelial cells in coronal sections from postnatal day 21 LAMA2-/- and WT mice. MECA-32 immunoreactivity was detected in LAMA2-/- brain vascular endothelial cells but not in WT. (B) Extravasation of Evans Blue dye (red) in the parenchymal space is associated with MECA32 immunoreactivity (green) in LAMA2-/- cerebral cortices but not in WT. (C) Quantification of area of MECA32 immunoreactivity coverage relative to laminin-111 coverage (pan-laminin, to indicate total vasculature area) in LAMA2-/- and WT cerebral cortices at postnatal day 21. Coverage of MECA32 was increased in LAMA2-/- mice. (D) Western immunoblotting for MECA-32 and p115 (protein loading control) in lysates from P21 LAMA2 -/- and WT cerebral cortices. MECA-32 levels were significantly elevated in LAMA2-/- cerebral cortices compared to those in WT controls. *$p<0.05$, Student's t-test; error bars, SEM; n=3. Scale bars: 50 μm. Figure adapted from Menezes et al. 2014 [28].

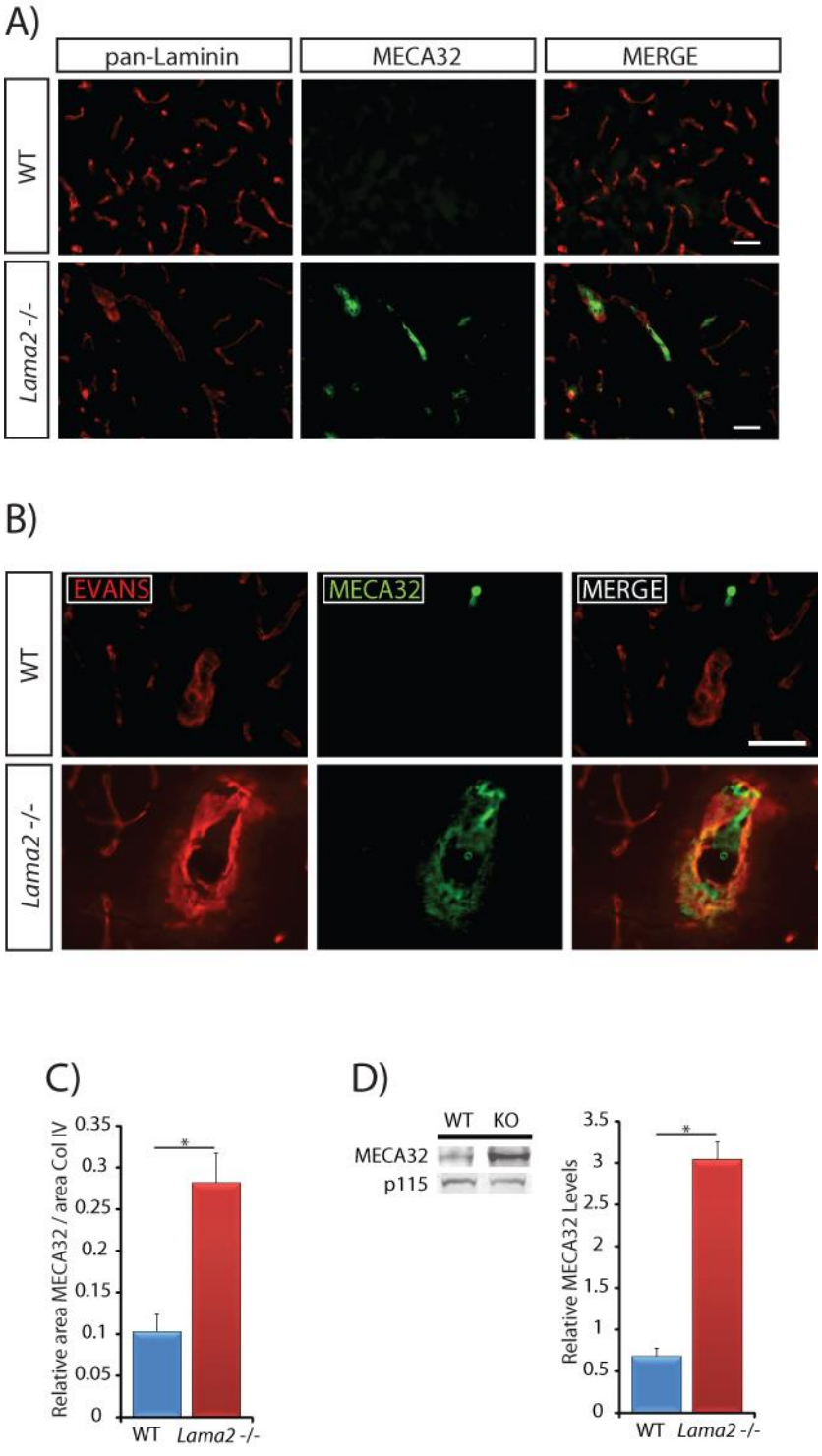
A)
pan-Laminin
MECA32
MERGE
WT
Lama2 -/-
B)
EVANS
MECA32
MERGE
WT
Lama2 -/-
C)
Relative area MECA32 / area Col IV
0.35
0.3
0.25
0.2
0.15
0.1
0.05
0
*
WT
Lama2 -/-
D)
WT
KO
MECA32
p115
Relative MECA32 Levels
3.5
3
2.5
2
1.5
1
0.5
0
*
WT
Lama2 -/-

Figure II-9. Tight junction morphology and levels are perturbed in LAMA2 mutants.

(A) Immunohistochemistry to detect the interendothelial tight junction proteins; ZO-1 (red), Claudin-5 (green), and Occludin (magenta) in LAMA2-/- and WT cerebral cortices at postnatal day 21. High magnification confocal imaging reveals ZO-1 morphology is altered in LAMA2 -/- , however protein levels were not significantly decreased. In contrast, immunoreactivity for Claudin-5 and Occludin are significantly reduced in LAMA2 -/- mice (white dashed line depicts the path of the blood vessel). (B) Representative western immunoblots for ZO-1, VE-Cadherin, Claudin-5, and Occludin (p115 and β-actin, protein loading controls) at P21 in lysates from LAMA2 -/- and WT cerebral cortices. VE-Cadherin, Claudin-5, and Occludin levels were significantly decreased in LAMA2-/- cerebral cortices. *$p< 0.05$, **$p<.01$, Student's t-test; error bars, SEM; n=6. Scale bars: 10 μm. Figure adapted from Menezes et al. 2014 [28].

A)

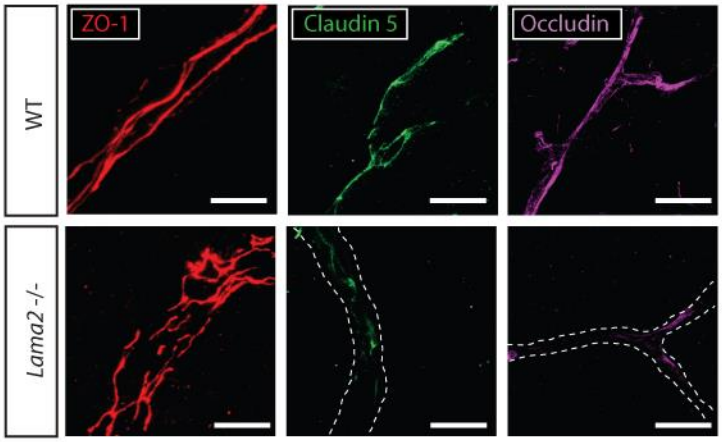
ZO-1
Claudin 5
Occludin
WT
Lama2 -/-

B)

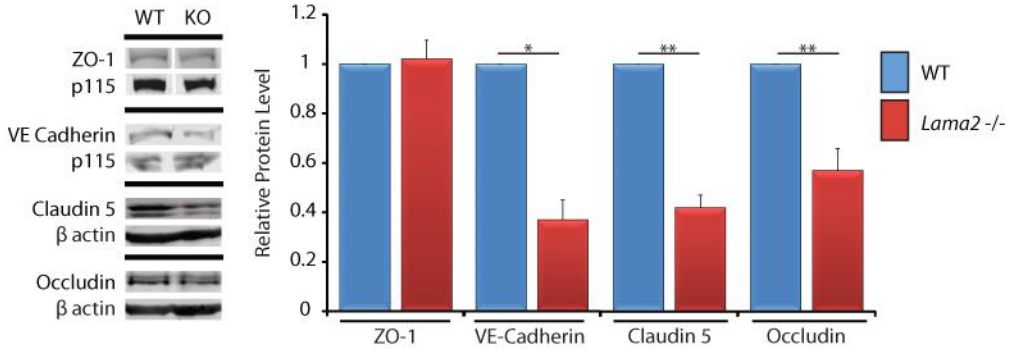
WT
KO
ZO-1
p115
VE Cadherin
p115
Claudin 5
β actin
Occludin
β actin
Relative Protein Level
1.2
1
0.8
0.6
0.4
0.2
0
*
**
**
ZO-1
VE-Cadherin
Claudin 5
Occludin
WT
Lama2 -/-

Figure II-10. Decreased pericyte coverage of the vasculature in LAMA2 -/- brains.

(A) Immunohistochemistry to detect laminin α2 (Lm α2, green), collagen type IV (Col IV, purple) and pericytes (PDGFRβ, red) in wild type brains. Lm α2 colocalizes with the pericyte marker PDGFRβ along the basal lamina of brain vascular endothelial cells. (B) Immunohistochemistry to detect PDGFRβ (green) and Col IV (red) associated with the vasculature in LAMA2-/- and WT brains at postnatal day 21. LAMA2-/- mice have decreased PDGFRβ immunoreactivity along the brain vasculature. (C) Quantification of area of PDGFRβ coverage relative to Col IV area (vasculature area) in LAMA2-/- and WT brains at postnatal day 21. Pericyte coverage was reduced in the cerebral cortex, striatum and hippocampus of LAMA2-/- mice. (D) Western immunoblotting for PDGFR-β and β–Actin (protein loading control) in lysates from postnatal day 21 LAMA2-/- and WT cerebral cortices. The protein level of PDGFR-β was found to be significantly lower in LAMA2-/- cortical lysates relative to WT controls. (E) Immunohistochemistry to detect PDGFRβ (green) and Col IV (red) associated with the vasculature in LAMA2-/- and WT brains through development (postnatal days 1, 8, 15 and 21). LAMA2-/- mice have decreased PDGFRβ immunoreactivity along the vasculature from birth throughout postnatal development. **$p<0.01$, ***$p<0.001$, Student's t-test; error bars, SEM; n=3 (C), n=6 (D). Scale bars: 20 μm (A), 50 μm (B,E). Figure adapted from Menezes et al. 2014 [28].

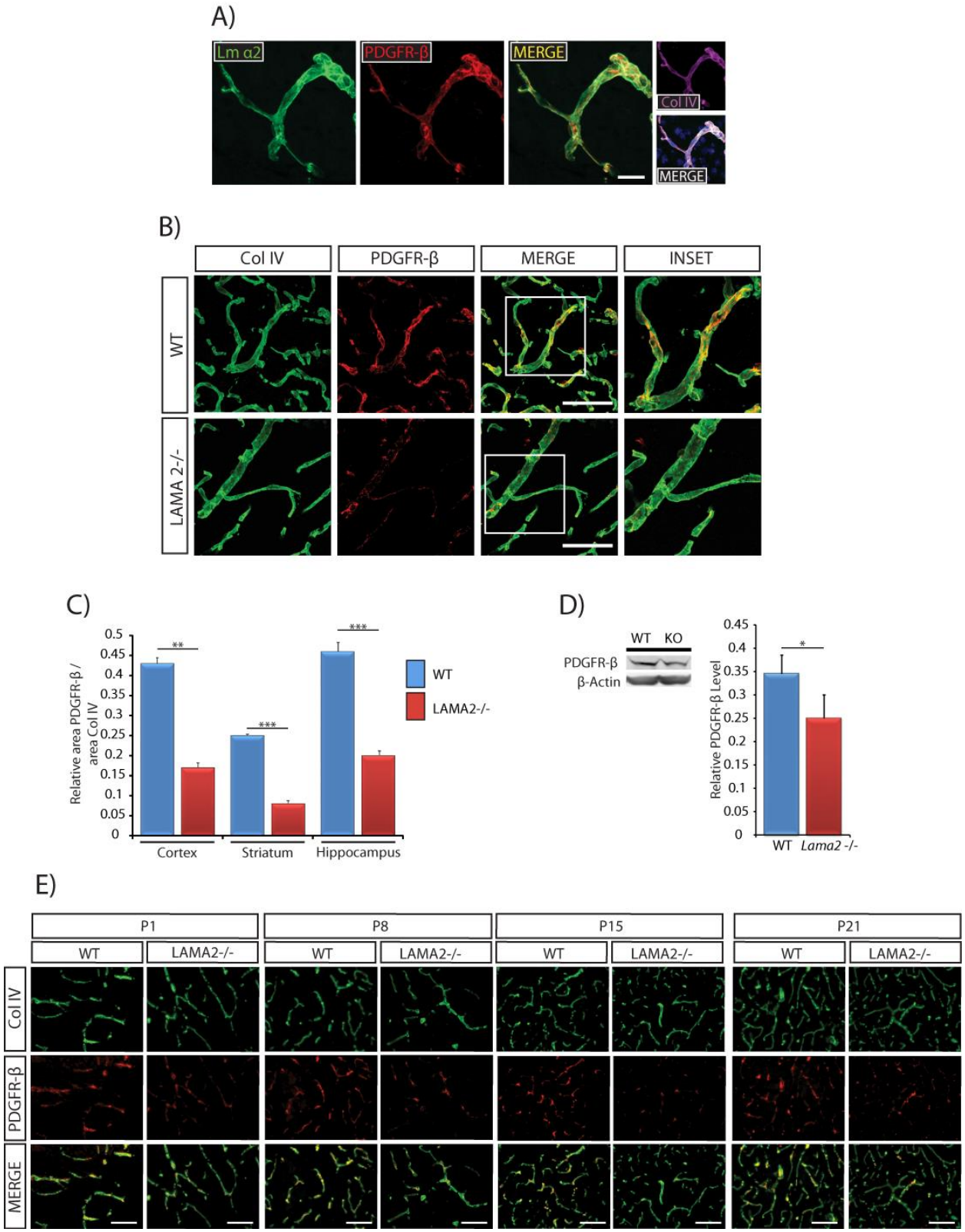
A)
Lm α2
PDGFR-β
MERGE
Col IV
MERGE
B)
Col IV
PDGFR-β
MERGE
INSET
WT
LAMA 2-/-
C)
Relative area PDGFR-β / area Col IV
0.5
0.45
0.4
0.35
0.3
0.25
0.2
0.15
0.1
0.05
0
**
***
***
WT
LAMA2-/-
Cortex
Striatum
Hippocampus
D)
WT KO
PDGFR-β
β-Actin
Relative PDGFR-β Level
0.45
0.4
0.35
0.3
0.25
0.2
0.15
0.1
0.05
0
*
WT
Lama2 -/-
E)
P1
P8
P15
P21
WT
LAMA2-/-
WT
LAMA2-/-
WT
LAMA2-/-
WT
LAMA2-/-
Col IV
PDGFR-β
MERGE

Figure II-11. Channel localization at endfeet is altered in the absence of LAMA2.

(A) Immunohistochemistry to detect AQP4 (red) and GFAP (green) in LAMA2 -/- and wild type astrocytic endfeet. AQP4 immunoreactivity was decreased in LAMA2 -/- mice. **(**B) Quantification of AQP4 immunoreactivity along astrocytic endfeet relative to vessel length. AQP4 coverage along astrocytic endfeet was significantly reduced in LAMA2-/- mice relative to littermate controls. **p< 0.01, Student's t-test; error bars, SEM; n=3. (C) Western immunoblotting for AQP4 and p115 (protein loading control) in lysates from postnatal day 21 LAMA2 -/- and WT cerebral cortices. No significant differences in protein levels were observed. (D) Quantification of brain water content in cortices isolated from LAMA2 -/- and wild type mice. Brain water content was elevated in LAMA2 -/- mice relative to littermate controls. *p<0.05, **p<0.01, Student's t-test; error bars, SEM; n=9. Scale bars: 20 μm. Figure adapted from Menezes et al. 2014 [28].

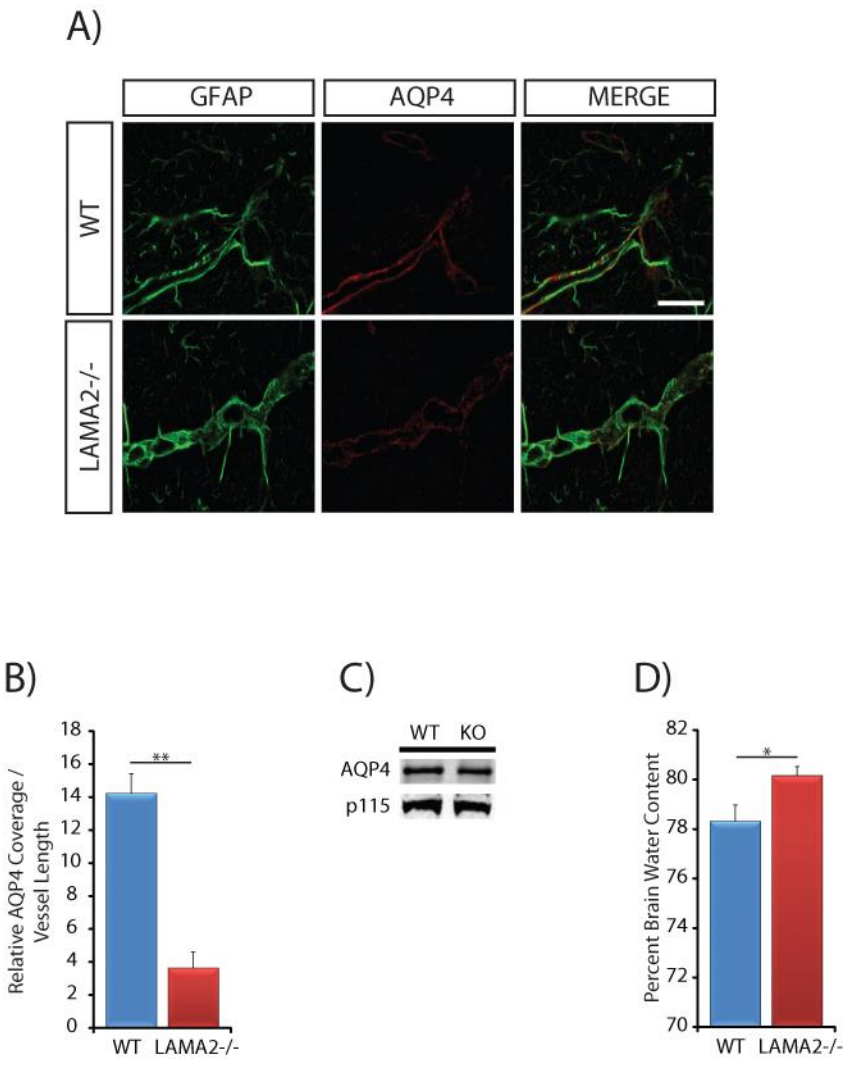
A)
GFAP
AQP4
MERGE
WT
LAMA2-/-
B)
Relative AQP4 Coverage / Vessel Length
18
16
14
12
10
8
6
4
2
0
**
WT
LAMA2-/-
C)
WT
KO
AQP4
p115
D)
Percent Brain Water Content
82
80
78
76
74
72
70
*
WT
LAMA2-/-

Figure II-12. Adhesion receptors of the gliovascular interface.

(A) Immunohistochemistry to detect β-dystroglycan (red) and GFAP (green) in LAMA2-/- and WT astrocytic endfeet. (B) Western immunoblotting for β-dystroglycan and p115 (protein loading control) in lysates from postnatal day 21 LAMA2-/- and WT cerebral cortices. No significant differences in protein levels were observed. (C) Immunohistochemistry to detect β1-integrin (red) and collagen IV (Col IV, vasculature, green) in LAMA2-/- and WT along astrocytic endfeet and vasculature. (D) Quantification of area of β1-integrin immunoreactivity coverage relative to collagen IV immunoreactivity (collagen IV to indicate total vasculature area) in LAMA2-/- and WT cerebral cortices at postnatal day 21. Vascular coverage of β1-integrin was reduced in LAMA2-/- mice. (E) Western immunoblotting for β1-integrin and p115 (protein loading control) in lysates from postnatal day 21 LAMA2-/- and WT cerebral cortices. No significant differences in protein levels were observed. *$p<0.05$, Student's t-test; error bars, SEM; n=3. Scale bars: 50 μm. Figure adapted from Menezes et al. 2014 [9, 28].

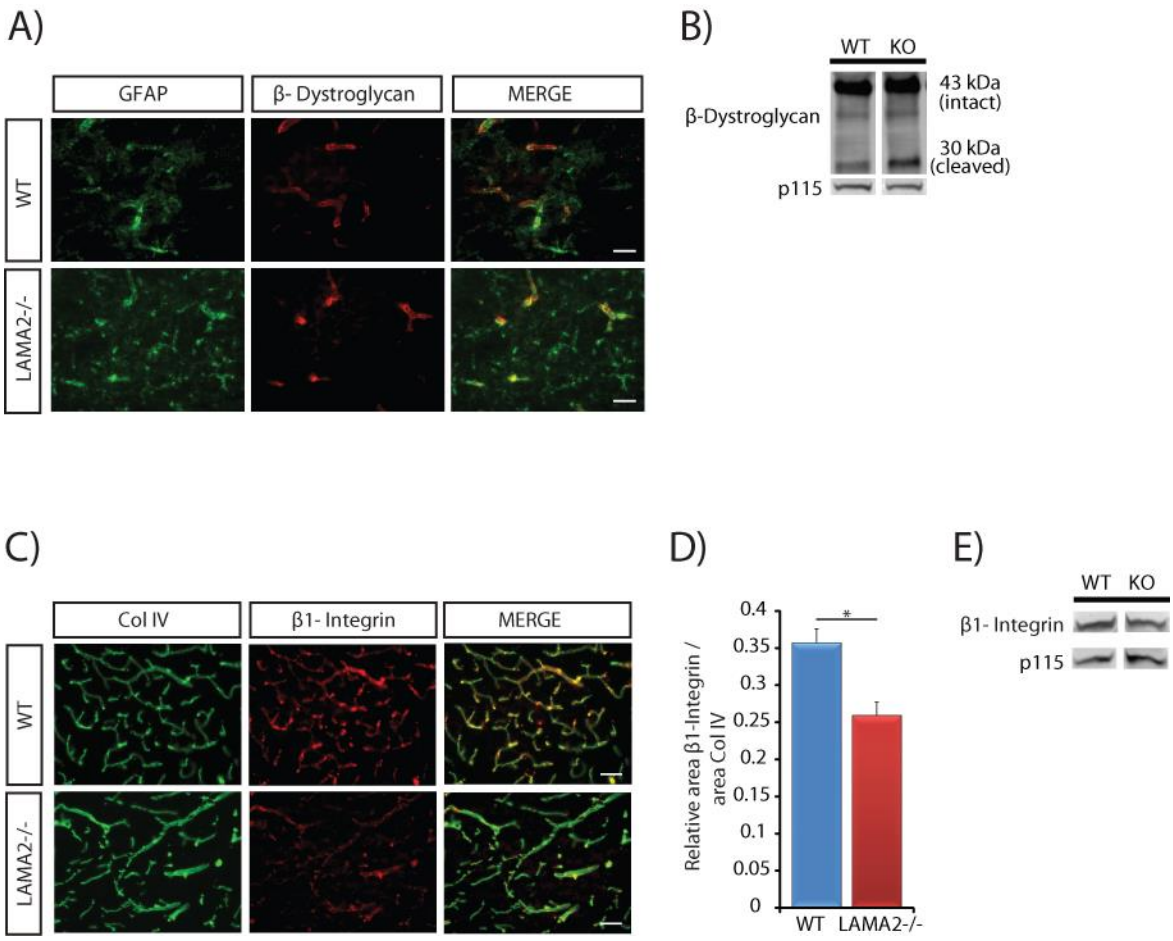
A)
GFAP
β- Dystroglycan
MERGE
WT
LAMA2-/-
B)
WT
KO
β-Dystroglycan
43 kDa
(intact)
30 kDa
(cleaved)
p115
C)
Col IV
β1- Integrin
MERGE
WT
LAMA2-/-
D)
Relative area β1-Integrin / area Col IV
0.4
0.35
0.3
0.25
0.2
0.15
0.1
0.05
0
*
WT
LAMA2-/-
E)
WT
KO
β1- Integrin
p115

Figure II-13. Altered structure of the BBB basal lamina in LAMA2 mutants.

(A-C) Transmission electron micrographs to evaluate the ultrastructure of the gliovascular interface in LAMA2-/- and wild type littermate brains at postnatal day 21. (A) No obvious defects were apparent in the brain capillary basal lamina (BL) of LAMA2-/- mice. (B) Tight junction morphology (green) in LAMA2-/- vascular endothelial cells morphology is abnormal in contrast to that observed in wild type littermates. LAMA2-/- tight junctions appear to be elongated with long, spindly regions traversing the endothelium. Additionally, endocytic vesicles (red arrows) were observed in LAMA2-/- vascular endothelial cells. (C) Regions of the parenchymal BL (blue) and endothelial BL (red) are discontinuous (white asterisk) in large caliber blood vessels of LAMA2-/- mice. Scale bars: 500 nm (A,B) and 100 nm (C). Figure adapted from Menezes et al. 2014 [28].

A)

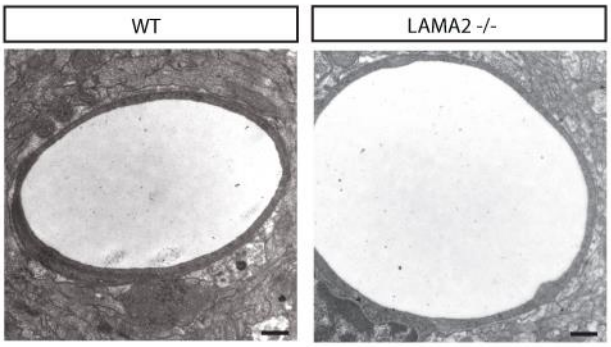

B)

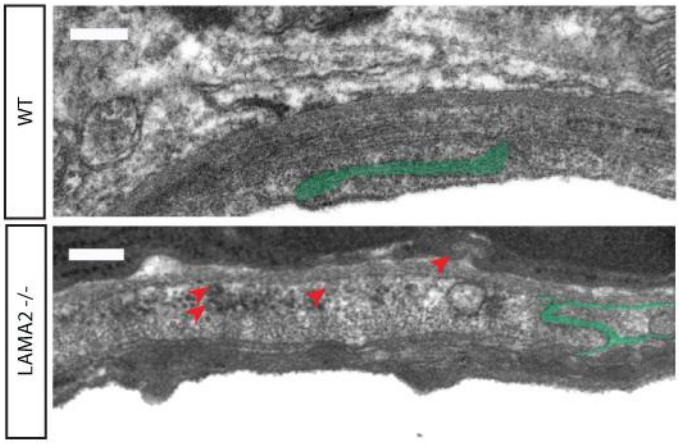

C)

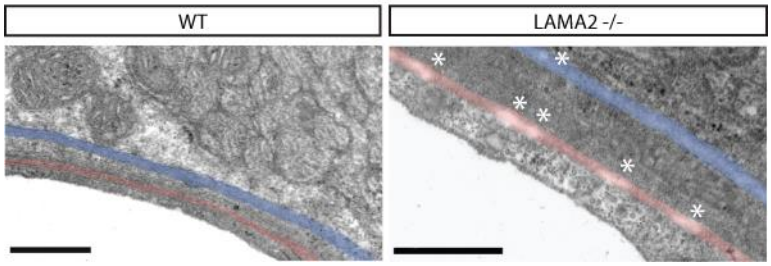

Figure II-14. Deletion of LAMA2 results in altered gliovascular laminin composition.

(A) Immunohistochemistry to detect components of the BL in conjunction with GFAP in the cerebral cortices of *Lama2*$^{-/-}$ and WT mice at postnatal day 21. Laminin α1, α4, α5, γ1, laminin-111 (a polyclonal antibody that recognizes laminin α1, β1, and γ1 subunits), and collagen IV (col IV) were detected in the gliovascular BL of *Lama2*$^{-/-}$ and WT brains. Laminin α5 immunoreactivity was reduced in *Lama2*$^{-/-}$ mice. Scale bars: 50 μm. Figure adapted from Menezes et al. 2014 [28].

A)

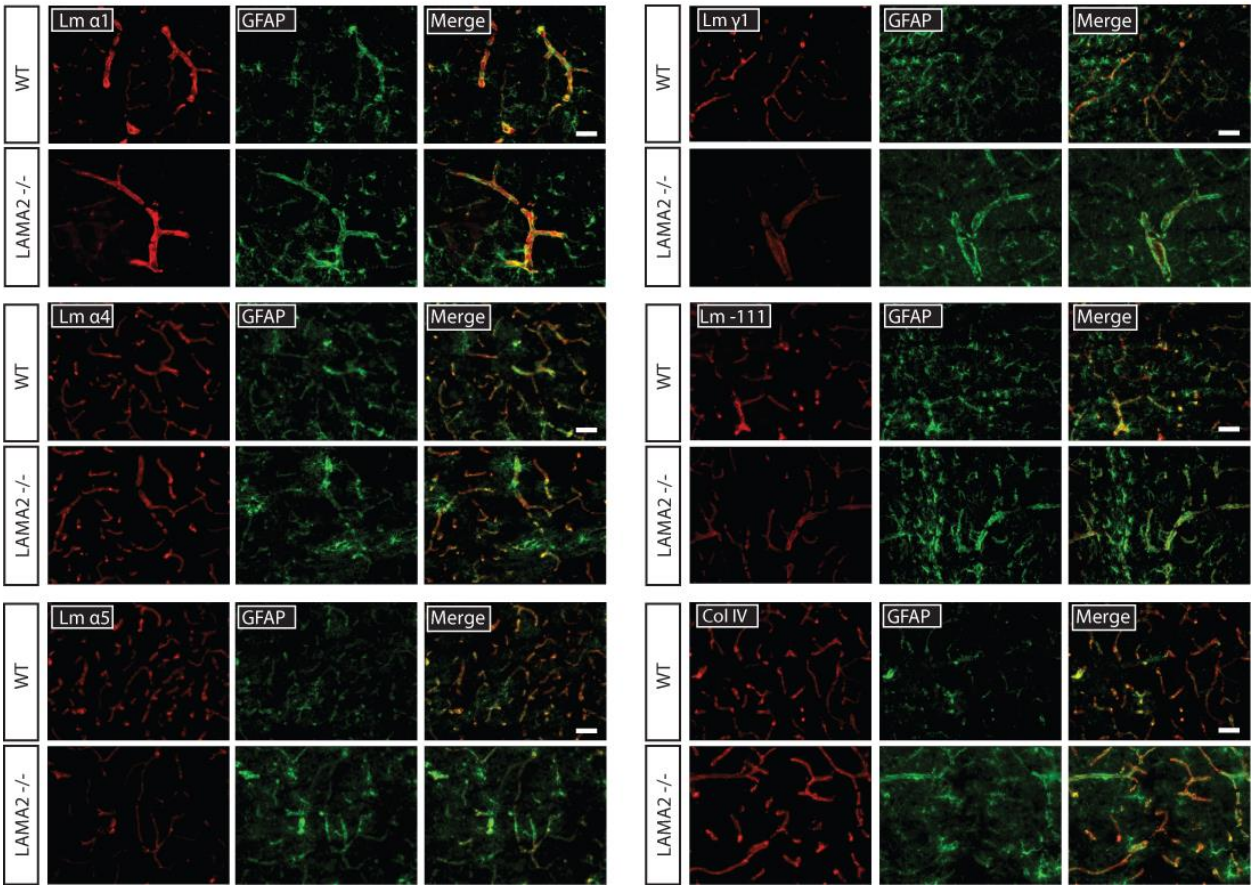

Figure II-15. Laminin substrate potentiates channel clustering in LAMA2 null astrocytes. (A) Immunohistochemistry to detect GFAP (red) and AQP4 (green) in astrocytes derived from LAMA2-/- and WT mice. LAMA2-/- astrocytes were deficient in their ability to assemble AQP4 clusters in long term cultures, however growth on purified laminin-211 substrate rescued the ability of LAMA2-/- astrocytes to form AQP4 clusters. Colorized AQP4 clusters (bottom panel, red) depicts regions where AQP4 immunoreactivity intensity was above threshold value. (B) Quantification of relative coverage by AQP4 clusters in astrocytes derived from LAMA2-/- and WT mice on poly-D-lysine or purified laminin-211 substrates. Relative coverage by AQP4 clusters was significantly reduced in LAMA2-/- grown on PDL relative to WT astrocytes. **$p \leq 0.01$, Student's t-test; error bars, SEM; n=5. The ability of LAMA2-/- astrocytes to form AQP4 clusters was rescued by laminin-211 substrate. Scale Bars: 25 μm. Figure adapted from Menezes et al. 2014 [28].

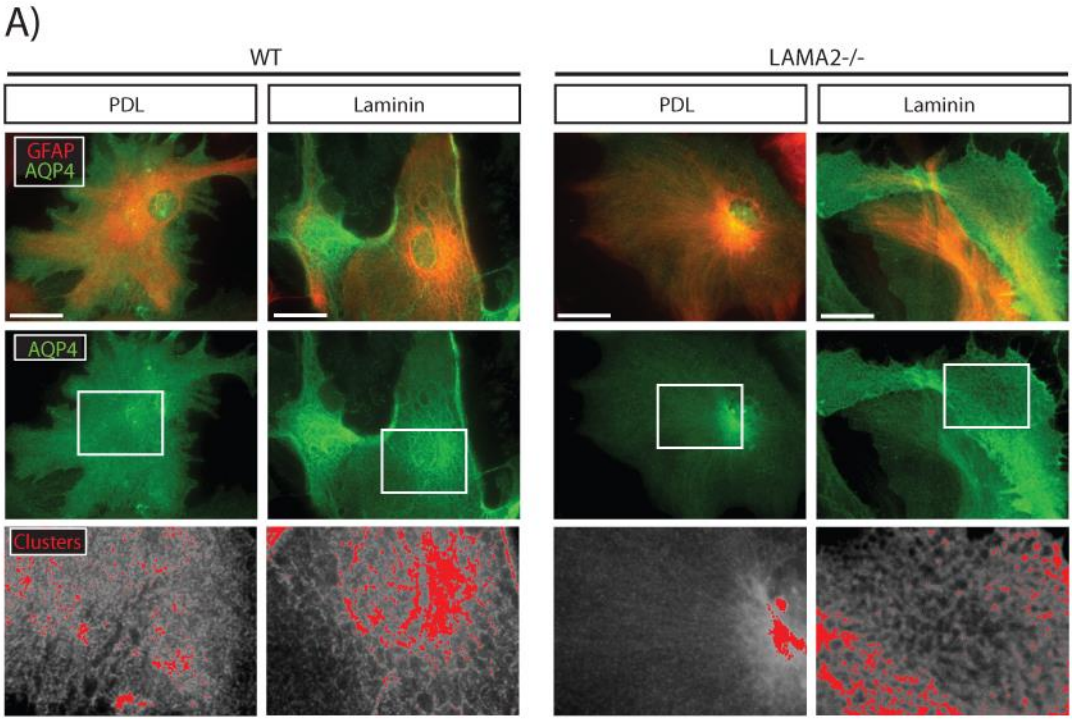
A)
WT
LAMA2-/-
PDL
Laminin
PDL
Laminin
GFAP
AQP4
AQP4
Clusters

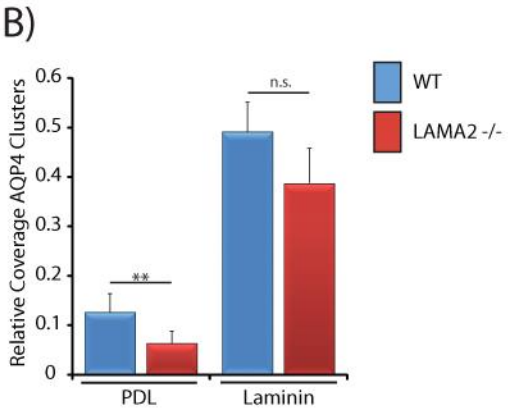
B)
Relative Coverage AQP4 Clusters
0.6
0.5
0.4
0.3
0.2
0.1
0
**
n.s.
WT
LAMA2 -/-
PDL
Laminin

Figure II-16. Overview of cellular and molecular changes in the BBB that occur in the absence of LAMA2.

(A) Pericyte (red) coverage of the brain vasculature (green) is decreased in LAMA2-/- mice. (B) Laminin a2 is produced by astrocytes (purple) and, possibly, pericytes (red) at the gliovascular interface. In the absence of laminin a2 expression (LAMA2-/-) both parenchymal (pBL) and endothelial (eBL) are present but contain breaches. Vascular endothelial cells in LAMA2-/- brains have elevated levels of endocytic vesicles, indicative of transcytosis and BBB immaturity, as well as altered tight junction composition and morphology. Astrocytic processes appear hypertrophic in LAMA2-/- brains, with astrocytic endfeet lacking the appropriate polarization of aquaporin4 (AQP4) channels (blue ovals). Figure adapted from Menezes et al. 2014 [28].

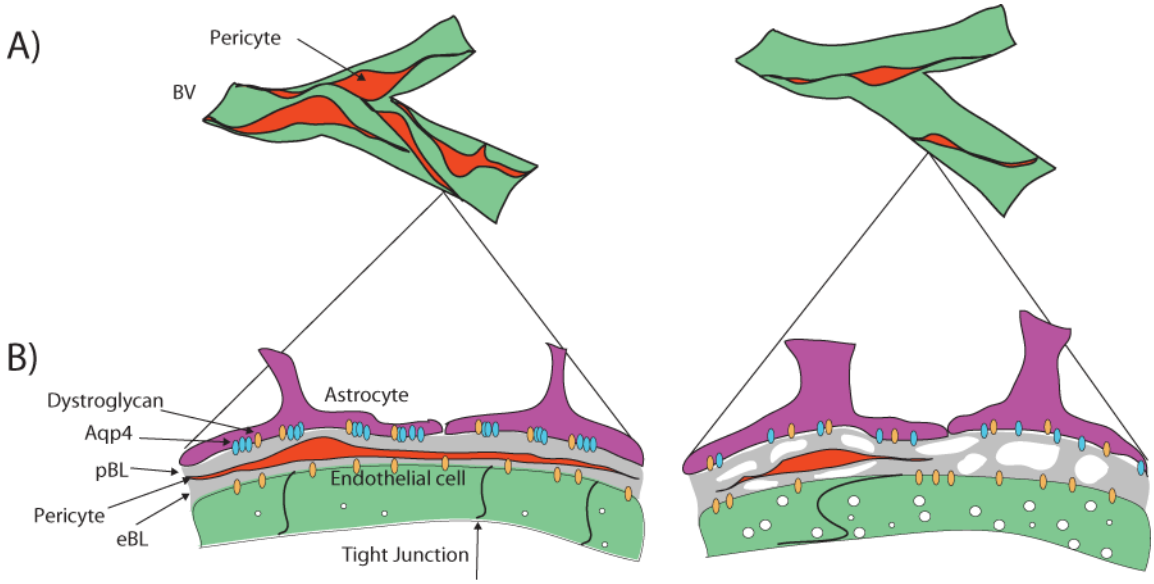

Wild Type

LAMA2 -/-

CHAPTER III: THE ROLE OF DYSTROGLYCAN THE DEVELOPMENT AND FUNCTION OF THE BLOOD-BRAIN BARRIER

The adhesion receptor dystroglycan is highly expressed along perivascular astrocyte endfeet, forming extensive contacts with the gliovascular lamina BL of the BBB. However, the role of dystroglycan in BBB development remains unclear. Here we report that DAG1 CKO mice, lacking expression of dystroglycan in neural lineage cells including astrocytes and neurons, have a defective BBB in which systemically-circulated Evans Blue tracer bound to serum albumin accumulated in the brain parenchyma. We found the cerebral vasculature of DAG1 CKO mice had significant abnormalities including altered integrity of the endothelial BL, substantially reduced pericyte coverage, tight junction abnormalities and perturbed Glut1 transporter localization. Additionally, DAG1 CKO astrocytic endfeet were hypertrophic and lacked polarized aquaporin 4 channels. Dystroglycan appears to mediate these effects at least in part through association with Laminin-211 at the gliovascular interface, as removing Laminin-211 expression led to a similar set of BBB abnormalities and gliovascular disturbances. These findings provide further mechanistic insight into the cellular and molecular changes that occur in congenital muscular dystrophies caused by LAMA2 mutations or inappropriate DAG1 post-translational modifications, both of which have accompanying brain abnormalities including seizures. Our results indicate a novel role for laminin-dystroglycan interactions in the cooperative integration of cellular components of the gliovascular interface, including astrocytes, endothelial cells and pericytes in regulating the BBB.

Introduction

The complex interplay between the cellular components of the BBB, in part mediated by the ECM of the gliovascular interface is critical for barrier development and function. Cell-matrix interactions are facilitated through matrix adhesion receptors expressed along the gliovascular interface, including members of the integrin family and dystroglycan [2]. The function of integrins expressed in ECs [87-90], pericytes [64, 91, 92], and astrocytes [65, 87, 90, 93] have been well characterized in the dynamic regulation of signaling pathways critical for barrier formation and function in postnatal development, as well as trauma to the BBB such as focal ischemia and hypoxia. In contrast the role of dystroglycan in the development and function of the BBB is poorly understood [90]. However, in pathological conditions that result in the disruption of the BBB, such as focal cerebral ischemia and Experimentally Autoimmune Encephalomyelitis (EAE), dystroglycan expression at endfeet interface is reduced, suggesting a critical role in maintaining BBB integrity and dystroglycan's potential value in the development of novel therapeutic strategies [43, 101].

At the gliovascular interface, dystroglycan is most well known as the central component of the dystrophin-associated glycoprotein complex (DGC) that lines astrocytic endfeet processes along the cerebrovasculature [78, 102]. At the DGC dystroglycan binds matrix ligands, forming a physical linkage between the enfeet and the network of ECM at the gliovascular interface. The DGC links intracellular actin cytoskeleton via dystrophin and aggregates channels along astrocytic endfeet via α-dystrobrevin, which physically links aquaporin (AQP4) channels to the complex. Inactivation of the genes that encode either dystrophin or α-syntrophin results in delayed onset edema, altered AQP4 distribution at glial endfeet, altered tight junction levels and morphology, increased cerebrovascular permeability [80, 81, 103-107]. However, the deletion

of AQP4 itself does not impact barrier development, suggesting the DGC itself must contribute to additional interactions that facilitate BBB integrity [108]. Perturbed barrier function and regulation of cerebral homeostasis in the absence of dystrophin and α-dystrobrevin warrants further inquiry to elucidate mechanistic insight of how the DGC regulates the cellular development and function of the BBB.

To gain insight into how laminin- dystroglycan interactions at the gliovascular interface contribute to BBB development we inactivated the DAG1 gene that encodes dystroglycan in neural lineage cells. We identified neural lineage dystroglycan, expressed along circumferential astrocyte endfeet and neurons, as a novel regulator of cerebrovascular pericyte coverage acquisition during barrier development, functional tight junction morphology, adherens junction composition, and multiple aspects of gliovascular cell-cell and cell-ECM interactions, including glial endfeet architecture. Our findings suggest that laminin-dystroglycan interactions at the gliovascular interface regulate the maturation and function of the BBB. These findings also provide insight into the cell and molecular changes that occur as a consequence of congenital muscular dystrophies caused by LAMA2 mutations or inappropriate dystroglycan post-translational modifications, which have accompanying brain abnormalities including seizures. Our results indicate a novel role for laminin-dystroglycan interactions in the cooperative integration of endothelial cells, astrocytes, and pericytes in regulating the BBB.

Results

Dystroglycan regulates the integrity of the blood-brain barrier

To investigate the role of the adhesion receptor dystroglycan in the formation and function of the BBB in vivo, we used a conditional knockout strategy to eliminate dystroglycan expression from all neural lineage cells, including astrocytes. Permeability of the BBB was assessed using Evans Blue dye circulated through the vasculature. In the absence of neural lineage dystroglycan, extravasation of Evans blue into the brain parenchyma was apparent in sections obtained from the frontal cortex, striatum and hippocampus (Fig. III-1A). Furthermore, a statistically significant increase in the level of Evans Blue in extracts from cerebral cortices was found in dystroglycan conditional knockouts relative to that in wild type littermates (Fig. III-B; 2.493 ± 0.109 in DAG1 CKO versus 1.164 ± 0.143 in wild type; n=4; P< 0.001).

Dystroglycan regulates cerebrovascular pericyte coverage

Considering the altered pericyte coverage observed in LAMA2-/- mice, we next sought to elucidate whether laminin-dystroglycan interactions regulate vascular pericyte cell coverage. We performed PDGFRβ and collagen IV immunohistochemistry in matched cortical sections from dystroglycan conditional knockouts and wild type littermates at postnatal day 23 (Fig. III-2A) and found decreased PDGFRβ immunoreactivity along blood vessels in dystroglycan conditional mutants relative to the robust coverage observed in wild type mice (Fig. III-2A). Quantification revealed significantly reduced (~50.0% reduction) pericyte coverage along blood vessels in dystroglycan conditional mutants relative to that in wild-type littermates (Fig. III-2B; 0.235 ± 0.036 in DAG1 CKO versus 0.47 ± 0.018 in wild type; n=4; P=0.001). We further quantified PDGFRβ at postnatal day 21 by western immunoblotting and found that PDGFRβ protein levels in DAG1 CKO mice were significantly lower relative to those in wild-type littermates (Fig. III-2C; 0.29 ± 0.04 in DAG1 versus 0.215 ± 0.02 in wild type; n=5; P=0.04).

Dystroglycan regulates BBB specific transporter distribution

To elucidate whether dystroglycan regulates the induction of transporters associated with barrier development, we next conducted Glut-1 immunohistochemistry (Fig. III-3A). We observed a decrease in Glut-1 immunoreactivity in dystroglycan conditional knockout brains relative to that in wild type littermates (a 38.83% reduction), suggesting a developmental delay or deficit in BBB maturation (Fig. III-3B; 0.323 ± 0.022 in DAG1 CKO versus 0.528 ± 0.055 in wild type; n=3; P= 0.026).

Dystroglycan regulates tight junction morphology and adherens junction expression

To evaluate the development of inter-endothelial tight junctions, we conducted immunohistochemistry against ZO-1, Claudin-5, and Occludin. Although the formation of tight junctions was apparent in DAG1 CKO mice at postnatal day 21, the junctional morphology in DAG1 CKO mutants appeared to be discontinuous with regions of focal hypertrophy and undulation observed in high magnification confocal images (Fig. III-4A). We also quantified the levels of junctional proteins by western immunoblotting (Fig. III-4B). ZO-1 protein levels did not significantly differ between dystroglycan knockout mice and wild-type littermates (Fig. III-4B; 0.641 ±0.15 in DAG1 CKO versus 0.728 ± 0.07 in wild type (0.86 fold of wild-type ± 0.14), n=3, P= 0.404). Claudin-5 protein levels did not significantly differ between dystroglycan knockout mice and wildtype littermates (Fig. III-4B; 1.503 ± 0.227 in DAG1 CKO versus 1.581 ± 0.22 in wild type (0.97 fold of wild-type ± 0.13), n=5, P=0.67). Occludin protein levels did not significantly differ between dystroglycan knockout mice and wild-type littermate controls (Fig. III-4B; 2.16 ± 0.057 in DAG1 CKO versus 2.54 ± 0.42 in wild type (0.94 fold of wild-type ± 0.19), n=5, P=0.43). However, the protein level of VE-Cadherin was significantly reduced in

DAG1 CKO mutants (Fig. III-4B; 0.584 ± 0.089 in DAG1 CKO versus 0.81 ± 0.035 in wild type (0.72 fold of wild type ± 0.13), n=5, P=0.04).

Dystroglycan regulates astrocytic endfeet polarization

To determine whether dystroglycan is necessary to maintain the polarized organization of astrocytic endfeet *in vivo* we conducted AQP4 immunohistochemistry in conjunction with GFAP immunohistochemistry (Fig. III-5A). We observed decreased immunoreactivity of AQP4 in dystroglycan conditional knockout brains at postnatal day 21, whereas in wild type littermates AQP4 channels were highly enriched at GFAP positive processes that line the vasculature (Fig. III-5A). It should also be noted that in dystroglycan conditional knockout brains, perivascular GFAP immunoreactivity was increased, characteristic of reactive gliosis and swollen astrocytic endfeet. To characterize the spatial distribution of AQP4, we quantified AQP4 along astrocyte endfeet at postnatal day 21 and found that dystroglycan conditional knockout mice had significantly decreased AQP4 distributed along astrocytic endfeet relative to that in wild-type littermates (Fig. III-5B; 2.406 ± 1.203 in DAG1 CKO versus 8.295 ± 0.878 in wild type; n=3; P=0.017).

Laminin-dystroglycan interactions potentiate the ability of astrocytes to cluster AQP4

To investigate the ability of laminins to facilitate the polarization of homeostatic channels such as AQP4, via binding integrin and dystroglycan receptors we utilized an *in vitro* astrocyte based assay. Utilizing primary astrocytes isolated from rat neonates to test the effects of blocking dystroglycan and/or β1-containing integrins with blocking antibodies (IIH6 and Ha2/5, respectively) prior to the acute administration of soluble laminin, which normally induces clusters of AQP4 [134]. We conducted AQP4 and GFAP immunohistochemistry (Fig. III-6A)

and then uniformly applied intensity thresh-holding to determine cluster areas, i.e. areas of intense AQP4 immunoreactivity. AQP4 cluster area relative to total GFAP-positive cell coverage area was then calculated per field. After 7 hours of laminin incubation, we observed a significant increase in AQP4 clusters in control cells, as has been reported previously (Fig. III-6B; 0.100 ± 0.009 in control plus laminin-111 versus 0.023 ± 0.003 in control alone, n=3, $P< 0.001$). In the presence of dystroglycan-blocking antibodies (IIH6) there was a substantial decrease in laminin-induced AQP4 clusters (Fig. III-6B; 0.0233 ± 0.003 IIH6 versus 0.100 ± 0.009 in control plus laminin-111, n=3, $P< 0.001$). Blocking the β1-integrin subunit also resulted in a significant decrease in laminin-induced AQP4 clusters, although not as large a decrease as was observed by blocking dystroglycan (Fig. III-6B; 0.051 ± 0.007 Ha2/5 versus 0.100 ± 0.009 in control plus laminin-111, n=3, $P< 0.001$). The largest decrease in laminin-induced AQP4 clusters, however, resulted from blocking both dystroglycan and β1-integrins concurrently (Fig. III-6B; 0.015 ± 0.002 dual versus 0.100 ± 0.009 in control plus laminin-111, n=3, $P< 0.001$).

Discussion

The removal of dystroglycan expression in neural cells leads to increased BBB permeability in conjunction with a similar set of gliovascular cellular disturbances we observed in LAMA2-/- brains, laminin-dystroglycan interactions are likely to be mediating a significant portion of α2-containing laminins at the gliovascular interface. Interestingly dystroglycan-deficient brains may even be more profoundly compromised than laminin-deficient brains, as Glut-1 transporter distribution, while normal in LAMA2-/- cerebral vasculature, is perturbed in DAG1 CKO mice. Vascular pericyte coverage is decreased in both LAMA2-/- and DAG1 CKO supporting the concept that pericyte and VSMC cell development requires extrinsic cues from ECM, facilitated through laminin-α2 and dystroglycan.

Together, these data indicate that dystroglycan expressed in neural lineage cells, such as astrocyte endfeet, is required to develop functional barrier properties, as well to localize homeostatic channel proteins and metabolic transporters at the gliovascular interface. In addition, although interendothelial junctional proteins such as Claudin-5, Occludin and ZO-1 were present at normal levels, VE-cadherin levels were decreased and morphological abnormalities in junctional protein localization were observed. The abnormalities in tight junction morphology, and decreased VE-Cadherins levels are likely to contribute to the observed changes in vascular permeability. Our findings furthermore indicate that dystroglycan-mediated ECM interactions, likely with laminin-211, promote pericyte coverage along the cerebral cortical vasculature (Figure III-7A).

In summary, we identified new roles for dystroglycan and laminin at the gliovascular interface, where laminin-dystroglycan interactions regulate BBB development, structure and function, at least in part by regulating pericyte coverage of brain vascular endothelial cells. We

furthermore provide the first report of a specific role for dystroglycan in regulating barrier development and function, with implications for the CNS pathologies that result from DAG1 mutations in CMD. We conclude that dystroglycan functions to facilitate ECM interactions from laminin produced in endothelial cells, and cellular components of the BBB such as astrocytes and pericyte to promote BBB development and function. Our findings have implications for understanding the connection between BBB breakdown and conditions with neurodegenerative pathology including stroke, Alzheimer's disease, and Multiple Sclerosis. Future studies, discussed in Chapter IV, will explore whether laminin-dystroglycan interactions facilitate barrier repair following stroke and function in the removal of waste from the CNS via AQP4, thereby preventing neurodegeneration through metabolite accumulation.

Figure III-1. Dystroglycan regulates the function of the blood-brain barrier.

(A) Evans Blue dye (red) in the parenchymal space is apparent in coronal sections taken from cerebral cortex, striatum and hippocampus in DAG1 CKO and WT mice at postnatal day 23. Residual signal in WT littermate control mice was restricted to the endothelial lumen. (B) Quantification of Evans Blue dye extracted from DAG1 CKO and WT cerebral cortices at postnatal day 21. The level of Evans Blue in DAG1 cortices was significantly elevated compared to that in WT littermates. ***$p < 0.001$, Student's t-test; error bars, SEM; n=4. Figure adapted from Menezes et al. 2014 [28].

A)

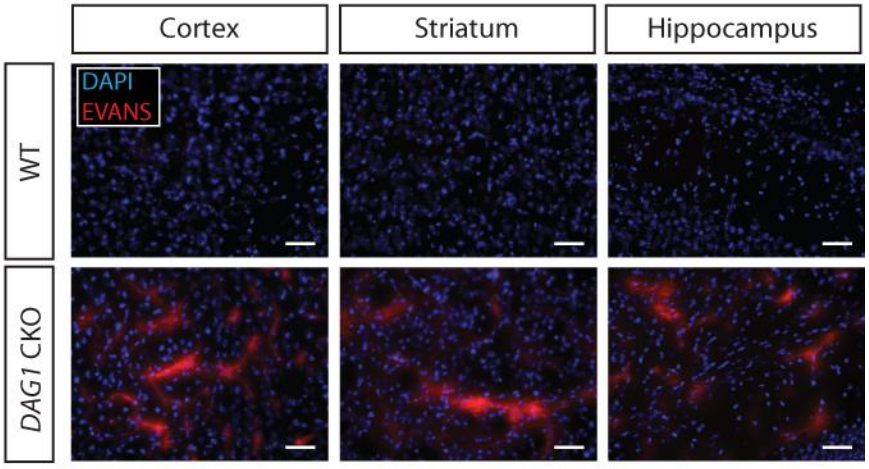
Cortex
Striatum
Hippocampus
DAPI
EVANS
WT
DAG1 CKO

B)

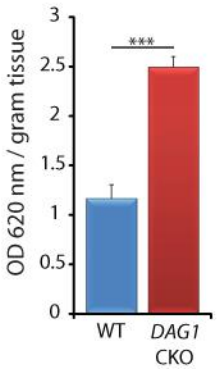
***
OD 620 nm / gram tissue
3
2.5
2
1.5
1
0.5
0
WT
DAG1 CKO

Figure III-2. Dystroglycan regulates cerebrovascular pericyte coverage.

(A) PDGFRβ immunohistochemistry to detect pericytes (red) and collagen IV immunohistochemistry (col IV, green) to visualize the endothelial basal lamina associated with the vasculature of DAG1 CKO and WT cerebral cortices at postnatal day 23. In DAG1 CKO mice PDGFRβ immunoreactivity was notably decreased. (B) Quantification of area of PDGFRβ coverage relative to collagen IV area (total vasculature area) in DAG1 and WT brains at postnatal day 21. Pericyte coverage was reduced in the cerebral cortex of DAG1 CKO mice. (C) Western immunoblotting for PDGFR-β and β–Actin (protein loading control) in lysates from postnatal day 21 DAG1 CKO and WT cerebral cortices. The protein level of PDGFR-β was found to be significantly lower in DAG1 CKO cortical lysates relative to WT controls. *$p < 0.05$, ***$p < 0.001$, Student's t-test; error bars, SEM; n=4 (B), n=5 (C). Figure adapted from Menezes et al. 2014 [28].

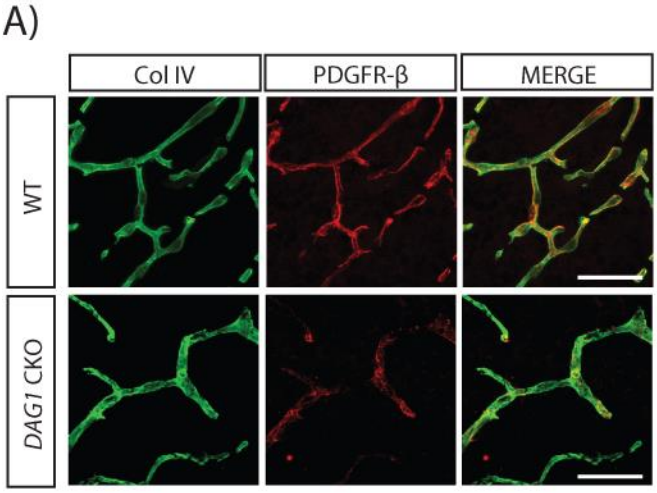
A)
Col IV
PDGFR-β
MERGE
WT
DAG1 CKO

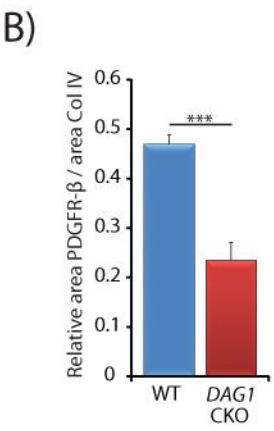
B)
Relative area PDGFR-β / area Col IV
0.6
0.5
0.4
0.3
0.2
0.1
0
***
WT
DAG1 CKO

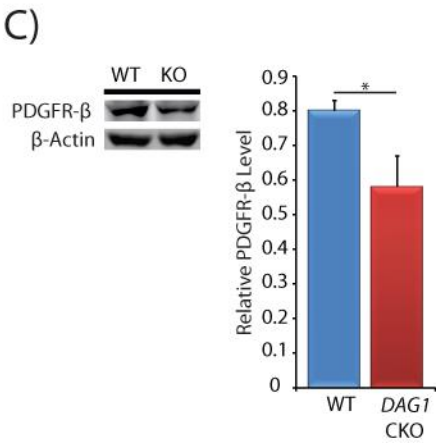
C)
WT
KO
PDGFR-β
β-Actin
Relative PDGFR-β Level
0.9
0.8
0.7
0.6
0.5
0.4
0.3
0.2
0.1
0
*
WT
DAG1 CKO

Figure III-3. Dystroglycan regulates cerebrovascular Glut-1 coverage.

(A) Immunohistochemistry to detect Glut-1 (green) and laminin-111 (pan-Laminin) in vascular endothelial cells in the cerebral cortex from DAG1 CKO and wild type littermates. Glut-1 immunoreactivity appeared to be less intense in DAG1 CKO brain vascular endothelial cells than in WT controls. (B) Quantification of area of Glut-1 immunoreactivity coverage relative to laminin-111 (pan-Laminin, vasculature area) in DAG1 and WT at postnatal day 21. Vascular coverage of Glut-1 was decreased in DAG1 CKO mice. *$p<0.05$, Student's t-test; error bars, SEM; n=3. Scale bars: 50 μm. Figure adapted from Menezes et al. 2014 [28].

A)

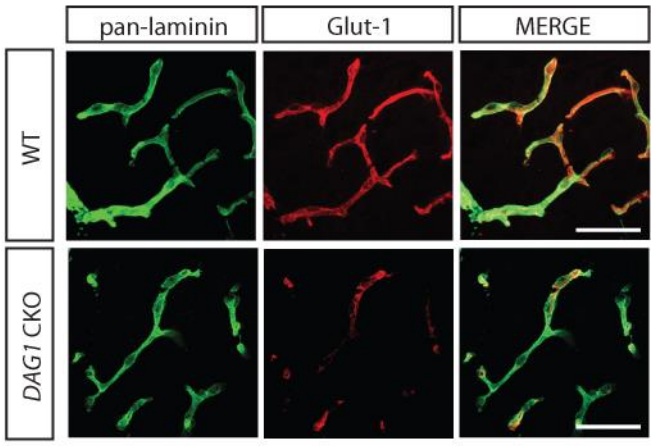
pan-laminin
Glut-1
MERGE
WT
DAG1 CKO

B)

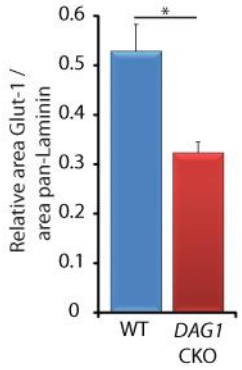
*
0.6
0.5
0.4
0.3
0.2
0.1
0
Relative area Glut-1 / area pan-Laminin
WT
DAG1 CKO

Figure III-4. Dystroglycan regulates tight-junction morphology and VE-Cadherin expression.

(A) Immunohistochemistry to detect the interendothelial tight junction proteins; ZO-1 (red), Claudin-5 (green), and Occludin (magenta) in DAG1 CKO and WT cerebral cortices at postnatal day 21. High magnification confocal imaging to reveal differences in ZO-1, Claudin-5 and Occludin morphology relative to wild-type. (B) Representative western immunoblots for ZO-1, VE-Cadherin, Claudin-5, and Occludin (p115 and β-actin, protein loading controls) at postnatal day 21 in lysates from DAG1 and WT cerebral cortices. No significant changes in ZO-1, Claudin-5 or Occludin protein levels were observed, however VE-Cadherin levels were significantly reduced in DAG1 CKO mice. *$p<0.05$, Student's t-test; error bars, SEM; n=5. Scale bars: 20 μm. Figure adapted from Menezes et al. 2014 [28].

A)

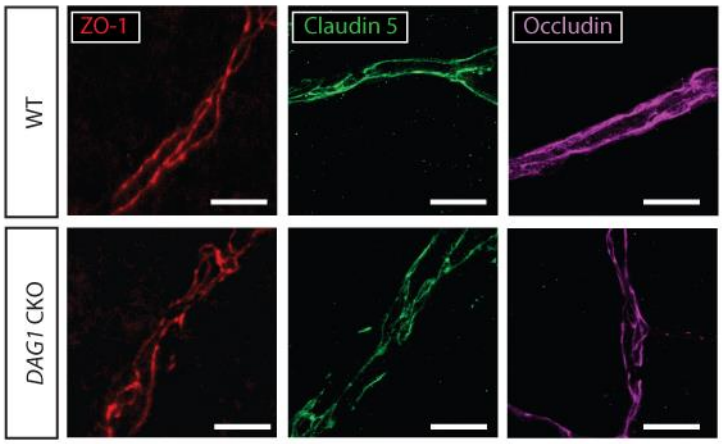
ZO-1
Claudin 5
Occludin
WT
DAG1 CKO

B)

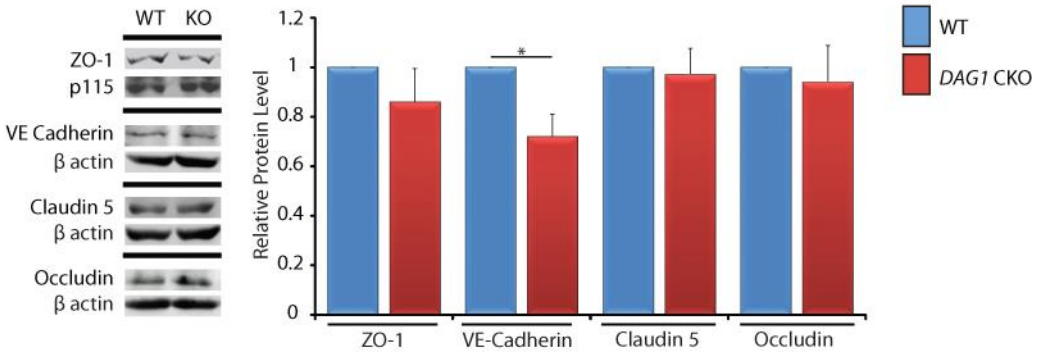
WT
KO
ZO-1
p115
VE Cadherin
β actin
Claudin 5
β actin
Occludin
β actin
Relative Protein Level
1.2
1
0.8
0.6
0.4
0.2
0
*
ZO-1
VE-Cadherin
Claudin 5
Occludin
WT
DAG1 CKO

Figure III-5. Dystroglycan regulates AQP4 channel polarization.

(A) Immunohistochemistry to detect GFAP (green) and AQP4 (red) in the cerebral cortices of DAG1 CKO and WT mice. DAG1 CKO mice have decreased AQP4 immunoreactivity and increased GFAP immunoreactivity. (B) Quantification of AQP4 coverage along astrocytic endfeet relative to vessel length. AQP4 coverage along astrocytic endfeet was significantly reduced in DAG1 CKO mice relative to wild-type controls. *$p<0.05$, Student's t-test; error bars, SEM; n=3. Scale bars: 50 μm. Figure adapted from Menezes et al. 2014 [28].

A)

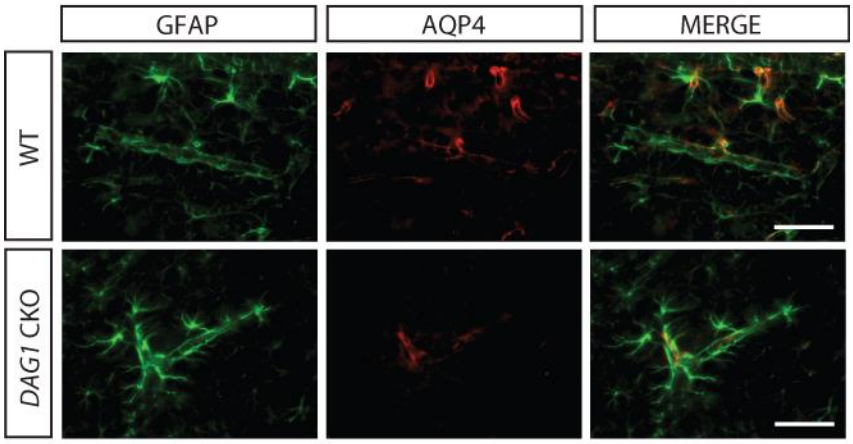
GFAP
AQP4
MERGE
WT
DAG1 CKO

B)

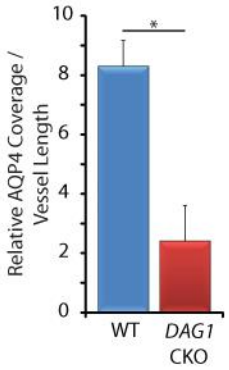
Relative AQP4 Coverage / Vessel Length
10
8
6
4
2
0
*
WT
DAG1 CKO

Figure III-6. Dystroglycan regulates AQP4 channel polarization.

(A) Immunohistochemistry to detect GFAP (red) and AQP4 (green) on primary astrocytes treated either laminin-111 alone or in conjunction with prior addition of blocking antibodies to Dystroglycan (IIH6) or β Integrins (Ha2/5). Colorized AQP4 clusters (bottom panel, red) depicts regions where AQP4 immunoreactivity intensity was above threshold value (i.e., cluster region). (B) Quantification of relative coverage by AQP4 clusters after no treatment, treatment with laminin alone, or with laminin in conjunction blocking antibody pre-treatments. Dystroglycan blocking antibodies, and, to a lesser extent, integrin blocking antibodies, reduce the ability of laminin to induce AQP4 clusters. **p< 0.01, ***p< 0.001, Holm-Sidak ANOVA; error bars, SEM; n=3. Figure adapted from Menezes et al. 2014 [28].

A)

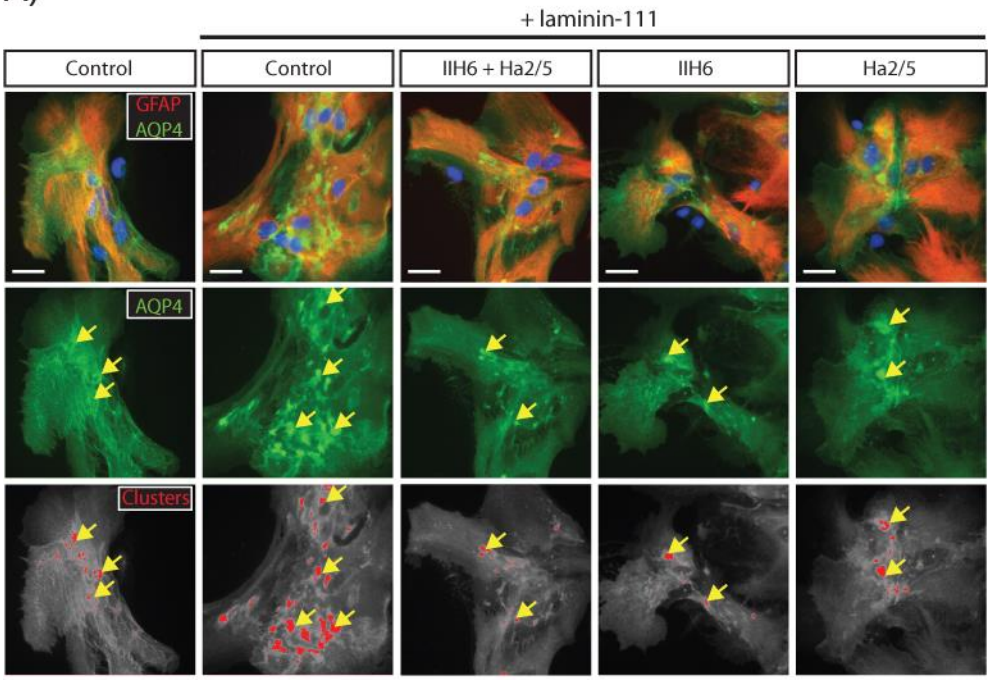
+ laminin-111
Control
Control
IIH6 + Ha2/5
IIH6
Ha2/5
GFAP
AQP4
AQP4
Clusters

B)

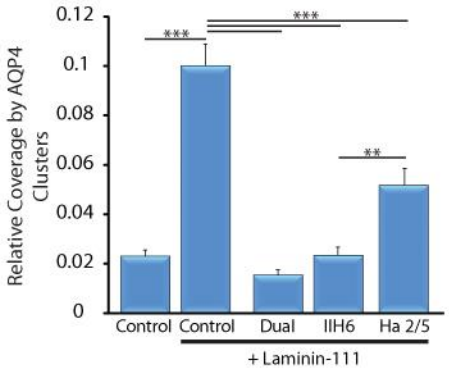
Relative Coverage by AQP4 Clusters
0.12
0.1
0.08
0.06
0.04
0.02
0
***
***
**
Control
Control
Dual
IIH6
Ha 2/5
+ Laminin-111

Figure III-7. Overview of cellular and molecular changes in the BBB that occur in the absence of neural lineage DAG1.

(A) Pericyte (red) coverage of the brain vasculature (green) is decreased in DAG1 CKO mice. (B) Laminin α2 is produced by astrocytes (purple) and, possibly, pericytes (red) at the gliovascular interface, which binds the adhesion receptor dystroglycan (orange). In the absence of neural lineage DAG1 expression (DAG1 CKO) vascular endothelial cells have reduced pericyte coverage, as well as perturbed tight junction composition and undulated morphology. Astrocytic processes appear hypertrophic in DAG1 CKO brains, with astrocytic endfeet lacking the appropriate polarization of aquaporin4 (AQP4) channels (blue ovals). Elements of Figure III-7 have been adapted from Menezes et al. 2014 [28].

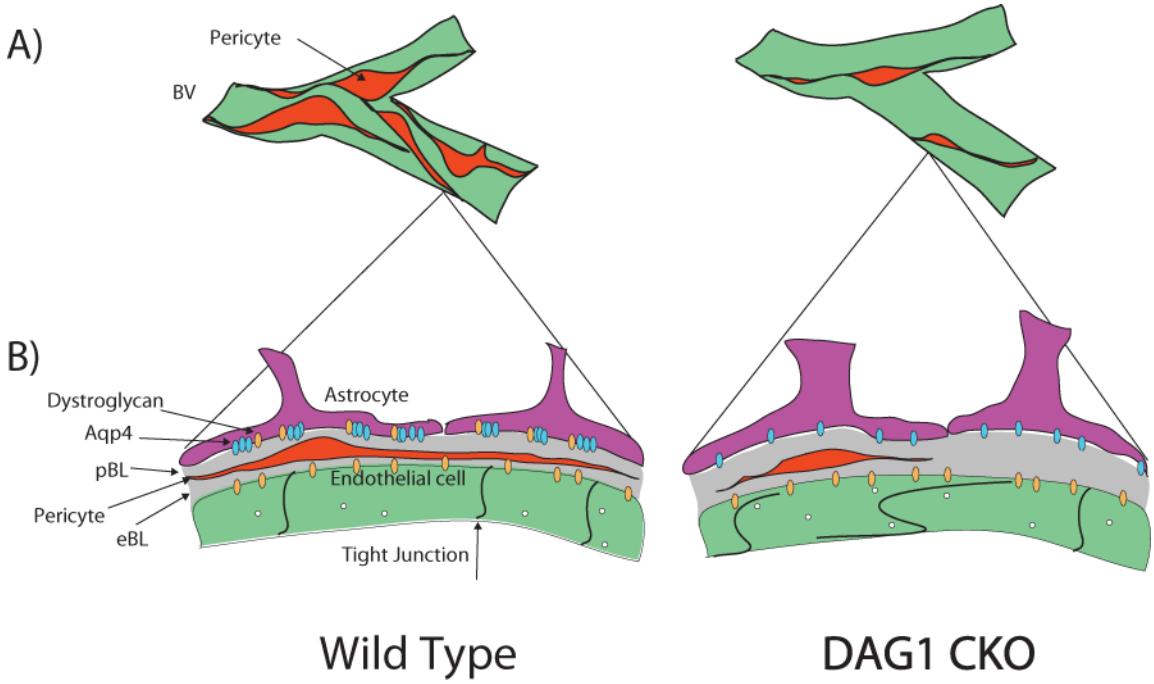
A)
Pericyte
BV
B)
Dystroglycan
Aqp4
pBL
Pericyte
eBL
Astrocyte
Endothelial cell
Tight Junction
Wild Type
DAG1 CKO

CHAPTER IV: CONCLUSIONS AND FUTURE CONSIDERATIONS

In this work, the development and function of the BBB facilitated through the ECM protein laminin α2 and its adhesion receptor dystroglycan were examined. Using the dy^{3k}/dy^{3k} LAMA2 knockout and Nestin Cre-lox DAG1 conditional knockout (CKO) mice we identified that laminin α2 and dystroglycan are regulators of BBB integrity. In LAMA2 and DAG1 mutants the permeability of the BBB was significantly increased, resulting in accumulation of systemically circulated tracer within the cerebral parenchyma. Increased BBB permeability in LAMA2 and DAG1 mutants was associated with decreased pericyte coverage, as well as dysregulation of TJs and adherens junctions. Further, the architecture of perivascular endfeet in LAMA2 and DAG1 mutants was perturbed, resulting in diffuse AQP4 distribution along the cerebral vasculature.

In LAMA2 knockouts we found that TJ component levels were decreased and morphology was abnormal. Further, BEC development in LAMA2 mutants was perturbed, as the immature EC cell marker MECA32 persisted through postnatal development. The gliovascular ECM composition of LAMA2 mutants was altered, with decreased laminin α5 levels, as well as discontinuous regions of the endothelial and parenchymal BL ultrastructure. In DAG1 CKO mice we found that the adherens junction, VE-Cadherin was down regulated and that while TJ levels were preserved, TJ morphology was abnormal.

In the following sections experiments to explore the role of dystroglycan in novel contexts, such as understanding BBB repair mechanism following stroke, and facilitation of paravascular transport along the gliovascular interface, are described. The experiments proposed

as future directions build on the knowledge gained through our study of LAMA2 and DAG1 mutants, to aid in the design of therapeutic strategies and ultimately to alleviate the of suffering of those afflicted with BBB related pathologies.

Future considerations

Interactions among BECs, astrocytes, pericytes, and vascular smooth muscle cells are thought to be essential for developing the BBB [2-5]. Cell-ECM interactions are also proposed to regulate BBB properties, as an extensive ECM resides between perivascular astrocytic endfeet and BECs. This gliovascular basal lamina (BL) exists either as separate astrocyte-derived parenchymal BLs and BEC-derived endothelial BLs, or as a composite BL with astrocytic and endothelial components [6]. Pericytes, critical for normal barrier properties, reside within the composite BL and interface with both astrocytes and BECS [3, 4, 7]. While the gliovascular BL comprises a key physical barrier of the mature BBB, it remains unclear if cell-ECM interactions regulate maturation through development and repair following barrier disruption.

Laminins are major components of the gliovascular BL, and serve as ligands for adhesion receptors such as β1-integrins and dystroglycan expressed on the major cellular components of the BBB [62, 64, 65]. The parenchymal BL contains astrocyte-derived laminins-111 and -211, whereas the endothelial BL contains endothelial-derived laminins-411 and -511 [62]. Endothelial laminins contribute to vascular development, as mice without laminin-411 have perturbed capillary development, vascular BL defects, and decreased vessel integrity [68], but upregulate laminin-511, which inhibits T-cell BBB extravasation during inflammation, thus conferring resistance to experimental autoimmune encephalomyelitis (EAE) [69]. In contrast to endothelial laminins, the role of astrocyte laminins is less clear, as mice with reduced, but not ablated,

laminin-211 expression have no apparent brain vasculature defects [70], yet transgenic mice that lack astrocytic expression of both laminins-111 and -211 suffer hemorrhagic stroke from impaired VSMC [27]. However, laminin-211 may not be exclusively astrocytic, as pericyte expression of laminin-211 has been reported [31] and pericyte loss and accompanying BBB maturation defects coincide with laminin-α2 loss at the gliovascular interface [31]. Interesting, following human and experimentally stroke induced by middle cerebral artery occlusion (MCAO), where the BBB has been compromised, pericyte coverage is significantly decreased while matrix components such as laminin α2 and γ1 are significantly increased [135, 136]. These observations suggest a relationship between ECM modulation and endogenous repair mechanisms to address damage sustained by the cerebral vasculature.

To gain insight into laminin-dystroglycan interactions at the gliovascular interface, we evaluated BBB maturation in LAMA2 mutants, in which laminin-211 has been removed from all cells, or in mice that lack dystroglycan expression selectively in neural lineage cells. We identified laminin-211 as a novel regulator of cerebrovascular pericytes in the developing brain, with a key role in determining the permeability of the BBB, as well as contributing to the development of normal glial endfeet architecture. These observations warrant further investigation of laminin and dystroglycan in the context of stroke. By employing MCAO future studies will explore the role of ECM mediated cues in the repair of the BBB. By expanding our understanding of the regulatory mechanisms which are perturbed in LAMA2 $^{-/-}$ and DAG1 inducible conditional knockout (iCKO) mice, we may better identify novel pharmacological targets, and potentially enhance the development of therapeutic strategies to improve clinical outcomes following ischemic stroke. In addition, pericyte dysfunction has been implicated in neurodegenerative diseases such as, Multiple Sclerosis, Alzheimer's Disease, CNS trauma, brain

tumors and diabetic retinopathy, highlighting the broad clinical significance of knowledge and potential therapeutic applications that may arise from understanding ECM regulation of pericyte function.

Exploring laminin-dystroglycan mediated BBB repair mechanisms following MCAO

Our findings published in Menezes et al. 2014 indicate that both laminin and dystroglycan regulate pericyte coverage of the cerebral vasculature. Given the observed transient increases in laminin production and the later decrease in pericyte coverage following stroke induction, future studies could examine a possible role for laminin-dystroglycan interactions in repair mechanisms mediated by the adhesion receptor dystroglycan.

Our findings indicate that the absence of LAMA2 and DAG1 expression results in increased permeability of the BBB, which indicates perturbed BBB integrity and function. Future studies should evaluate specific barrier components and steps in BBB maturation to narrow down the role that laminin-dystroglycan signaling plays in the development of the BBB. A particular focus should be on pericytes**,** perivascular mural cells that facilitate the development, maturation and remodeling of blood vessels. The cerebral vasculature is extensively covered by pericytes, which highly express PDGFR-β, a necessary signaling receptor for pericyte recruitment [36]. In a mouse model of pericyte deficiency, the loss of vascular pericyte coverage is highly correlated with vascular leakage at the BBB and substantially decreased laminin α2 immunoreactivity at the gliovascular interface [31]. In addition, the integration of ECM signaling in pericytes, mediated by β1 integrins, is required for proper pericyte development, including cell adhesion, spreading and endothelial cell stability [64]. Furthermore, evidence suggests that pericytes themselves produce laminin-α2 [27, 29], which may facilitate adhesion with dystroglycan expressed on astrocytes and endothelial cells.

Therefore, we hypothesize that the loss of interactions facilitated by laminin, or the adhesion receptor dystroglycan at the gliovascular interface, will perturb pericyte development. We will therefore assess the contribution of laminin-dystroglycan interactions to the regulation of pericyte development, proliferation and survival by utilizing immunohistochemistry to determine pericyte densities (PDGFR-β^+ cells), dying pericytes (PDGFR-β^+/CC3$^+$ cells) and proliferating pericytes (PDGFR-β^+/Ki67$^+$ cells).

The most commonly employed method for replicating cerebral ischemia in controlled laboratory settings is the MCAO stroke model for rodents. This method utilizes a nylon microfilament, inserted through the common carotid artery to transiently occlude the MCA resulting in a controlled region of focal cerebral ischemia [137]. Previous studies that have induced ischemic stroke in an effort to characterize the response of cerebrovascular pericytes have observed increased death of mural cells following ischemic insult [136]. However, in the period following cerebral ischemic insult both increased laminin expression and proliferation of pericytes have been reported [135, 136]. Given the increased expression of laminin and the perivascular localization of astrocytic dystroglycan, which is expressed on the perivascular endfeet, we hypothesize that laminin-dystroglycan interactions may facilitate BBB maintenance and/or repair. To test this hypothesis future studies should perform MCAO in mice that lack astroglial dystroglycan, either constitutively or induced prior to MCAO.

Our recently published data in Menezes et al. 2014, reports that dystroglycan regulates barrier function and pericyte recruitment during postnatal development such that both parameters are compromised in DAG1 CKO mice. To test whether the absence of astrocytic dystroglycan impacts the severity of ischemic insult in adult mice, MCAO can be performed for 30 minutes on DAG1 CKO and wild type mice at approximately three months of age. These mice lack

dystroglycan expression in neurons and glia, but not in BECs. We have evaluated these mice and observed evidence of increased BBB permeability (Fig. III-1A) but did not observe any evidence of spontaneous hemorrhage. Future experiments should quantify the magnitude of infarct volume and cellular death by quantifying the number of cleaved caspase3 (CC3) positive cells in the affected region following MCAO at specific intervals (1, 3, 6, 12, 24, 48 hours, as well as at 7 days) that correspond to previously reported time points associated with cellular death following MCAO as well as a later "repair" time point [135]. Infarct regions could be compared to the contralateral region, which did not sustain infarct from MCAO in DAG1 CKO mice and controls, and comparisons of infarct volume and $CC3^+$ cells will be additionally analyzed between MCAO treated wild type controls and DAG1 CKO mice. If differences in death are observed we can further characterize the dying cells by performing double immunohistochemistry with CD31/PDGFR-β/GFAP and CC3 to determine death in each BBB cell type (e.g., endothelial, pericyte, astrocyte). Through these experiments we could gain a better understanding whether the absence of dystroglycan mediates the magnitude of ischemic insult and BBB disruption following MCAO, and the cell types that are affected.

Since laminin levels are increased following induced stroke, and laminin is the major dystroglycan ligand at the gliovascular interface, [135, 136], we may also seek to better understand whether astrocytic dystroglycan-laminin interactions contribute to the repair of the BBB following ischemic insult. A second series of experiments could utilize MCAO in DAG1 inducible CKO (iCKO) and wild type control mice. Expression of dystroglycan in DAG1 iCKO mice is removed from DAG1 lox/lox mice via tamoxifen inducible nestin cre recombinase (DAG1 fl/fl: nestin-CreERT2). Two injections of tamoxifen prior to MCAO surgery are required to allow sufficient time for recombination and loss of gene expression to occur [138, 139]. As in

the first series of experiments, infarct regions will be compared to contralateral regions in DAG1 CKO mice and controls receiving MCAO. Comparisons will be made between cellular changes in DAG1 iCKO and control mice receiving MCAO. Infarct area and cell numbers will be quantified. To assess pericyte cellular dynamics following MCAO we will use immunohistochemistry to determine pericyte densities (PDGFR-β^+ cells), dying pericytes (PDGFR-β^+/CC3$^+$ cells) and proliferating pericytes (PDGFR-β^+/Ki67$^+$ cells). We will analyze at time points corresponding to previously reported time points associated with pericyte loss and ECM changes following MCAO and subsequent barrier repair [136]. We will also conduct immunohistochemistry and western blotting to determine laminin levels, both to confirm previous observations of elevated laminin following MCAO and to determine if ECM modulation following ischemic insult is dystroglycan-sensitive.

We anticipate that barrier repair mechanisms will be impaired following transient MCAO in the absence of DAG1 expression. In the first series of experiments, we expect that both the infarct volume and number of CC3$^+$ cells will be increased in DAG1 CKO mice compared to controls. In the second series of experiments, we expect to observe increased cell death in DAG1 CKO mice relative to controls, with increased PDGFR-β^+/CC3$^+$ cells and decreased levels of PDGFR-β^+/Ki67$^+$ cells. In addition, increased levels of laminin α2 immunoreactivity in DAG1 CKO and wild type mice are expected following MCAO. Further, less technical alternative approaches such as triphenyltetrazolium chloride (TTC) staining can be utilized to quantify infarct volume following MCAO. Using this method, viable tissue is stained by TTC, whereas infracted tissues do not readily stain, therefore the area of TTC$^-$ tissue can be quantified relative to unaffected regions and control mice receiving MCAO treatment.

Exploring dystroglycan's role in glymphatic system function

In the absence of a lymphatic system within the CNS, metabolic waste from the highly active cellular components of brain and spinal cord is removed by alternative means. The cerebrospinal fluid (CSF) circulation functions as a major sink for the clearance of interstitial (ISF) within the CNS. The CSF clears solutes from neuronal and glial activity as it is reabsorbed across the arachnoid granulations, cranial and spinal nerves, as well as the brain microvasculature [140-146]. The glymphatic system functions by the flux of sub-arachnoid CSF that recirculates through the brain parenchyma through the perivascular space of the cerebral vasculature, thereby exchanging with brain ISF before being cleared through peri-venous pathways [140-142]. Paravascular waste removal from the CNS was studied using fluorescent tracers injected into the CSF mice and observing its movements in wild type mice [141]. By utilizing AQP4 deficient mice, which lack AQP4 along perivascular endfeet, the diffusion of injected tracers was disrupted, limiting diffusion and increasing the time needed for clearance [141]. Moreover, disruption of the glymphatic system, through studies conducted using AQP4 null mutants, found this paravascular transport system to be important in pathological conditions ranging from traumatic brain injury (TBI) through a 60% reduction of glymphatic function and subsequent Tau pathology, Alzheimer's disease via removing amyloid beta (aβ), and stroke by regulating cellular damage caused by cerebral edema [140-142, 147].

How could dystroglycan regulate functional aspects of the BBB beyond cell-cell and cell-matrix organization of the gliovascular interface? One avenue of inquiry to pursue is the role of dystroglycan in the functional aspects of the newly identified "glymphatic" system, which serves

to remove cellular waste from the CNS via AQP4 channels that are regulated by the DGC [140-142]. In Chapter III and the findings published in Menezes et al. 2014 we established dystroglycan as a regulator of barrier formation, physically restricting *paracellular* transport [28]. However, it would be interesting to explore whether dystroglycan serves as a regulator of *paravascular* transport through the CNS, by regulating the DGC and AQP4 polarization.

By utilizing an inducible DAG1 conditional knockout it is possible to remove dystroglycan distributed along perivascular endfeet in adult mice, thereby disrupting the DGC and AQP4 polarization [28]. Experiments utilizing injectable fluorescent tracers and dyes into the CSF can visualize the flow of paravascular transport through the glymphatic system. By removing dystroglycan expression in perivascular endfeet, the diffusion of injected tracers would be expected to be spatially restricted and require extended clearance time to be removed from the CSF. Additionally, tracers such as fluorescently labeled aβ, or experimental designs incorporating TBI or stroke can be utilized to examine functional changes in DAG1 iCKO brains. The experiments described in this section would likely require collaboration with Dr. Maiken Nedergaard (University of Rochester) and Dr. Helene Benveniste (Stony Brook University). Despite the technical challenges posed by these experiments, the possibility of dystroglycan regulating paravascular flow is exciting and could have broad clinical implications to understanding and designing therapeutic strategies to address a variety of pathological conditions.

Materials and methods

Mice

Laminin α2 subunit null mice (LAMA2 -/-) were generated by breeding LAMA2 heterozygous pairs as described previously [148, 149]. Genotyping of LAMA2 mutants was performed on tail DNA to detect both the LAMA2 wild-type allele (5'-CCAGATTGCCTACGTAATTG-3' and 5-CCTCTCCATTTTCTAAAG-3') and the LAMA2 null allele (5'-CTTTCAGATTGCAAGC-3' and 5'-TCGTTTGTTCGGATCCGTCG-3'). Homozygous and heterozygous wild-type littermates of either sex served as age-match controls to homozygous null LAMA2 mutants. The adhesion receptor dystroglycan (DAG) was removed from neural stem cells by crossing mice heterozygous for DAG lox/lox mice and nestin-cre. Nestin-cre mice and DAG1 loxP/loxP mice were described previously [67, 150]. Genotyping was performed on tail DNA to detect DAG1 loxP and nestin-cre alleles. The primers used to detect the dystroglycan loxP allele were: 5'-GGAGAGGATCAATCATGG-3' and 5'-CAACTGCTGCATCTCTAC-3'. The primers used to detect nestin-cre alleles were: 5'-GACGGAAATCCATCGCTCACCAG-3' and 5'-GACATGTTCAGGGATCGCCAGGCG-3'. Dystroglycan conditional knockouts were homozygous DAG1 loxP and positive for nestin-cre. Nestin-cre negative littermates were used as age-matched controls. Mice of either sex were utilized in experimental and control conditions. All experimental procedures were performed in compliance with the NIH Guide for the Care and Use of Laboratory Animals and approved by the State University of New York at Stony Brook University IACUC.

Antibodies

The following rabbit polyclonal IgG antibodies were used: α-SMA (ABCAM); AQP4 (Millipore); CD31 i.e. PECAM-1 (ABCAM); Collagen IV (Sigma); GFAP (DAKO); Glut-1 (Millipore); Iba-1 (Wako); laminin-1 (Sigma); VE-Cadherin (ABCAM). Antibodies against laminin α4-subunit (Clone 377b) and laminin α5-subunit (Clone 504) were kindly provided by Dr. L. Sorokin (Institute of Physiological Chemistry and Pathbiochemistry; Münster University). The following rat monoclonal IgG antibodies were used: CD45 (BD Pharmingen); β1-Integrin (Millipore); laminin α1-subunit (clone 4H82, Sigma); laminin α2-subunit (clone A5, Millipore); MECA32, also called plasmalemma vesicle associated protein (PLVAP) (BD Pharmingen and ABCAM). The Armenian hamster polyclonal IgG antibody against CD3ε was kindly provided by Dr. Nicholas Carpino (Department of Molecular Genetics & Microbiology, Stony Brook University). The following mouse monoclonal IgG antibodies were used: β-actin (Sigma), β-Dystroglycan (ABCAM), GFAP (Sigma), p115 (BD Biosciences). The following additional antibodies were used: chicken anti-cow GFAP polyclonal IgY (ABCAM) and goat anti-mouse CD140b i.e. PDGFR-β polyclonal IgG (Neuromics).The following monoclonal blocking antibodies were used: IIH6 i.e. α-Dystroglycan (mouse, Millipore), Ha 2/5 i.e. β1-Integrin (hamster, BD Pharmingen). The following IgG control antigens were used: mouse (κ isotype, BioLegend), hamster (λ1 isotype, BD Pharmingen).

Fluorescent immunohistochemistry using frozen sections

Cerebral cortices from wild-type, DAG1 CKO or LAMA2 -/- littermates at postnatal days 1, 8 were frozen and embedded in TissueTek OCT. Mice at postnatal day 15 and beyond were anesthetized with Avertin and perfused with saline to remove residual blood from the cerebral

vasculature. Frozen tissues were cryosectioned to a thickness of 20 to 35 μm. Sections were fixed in acetone for 10 min at -20° C, then washed with phosphate buffered saline (PBS). Sections were blocked for 1 hour in PBS containing 10 % donkey serum (DS), then incubated overnight with primary antibodies in block at 4°C. Sections were then washed with PBS, followed by incubation for 1 hour at room temperature with either Cy3 or dylight488 conjugated secondary antibodies in blocking solution. Sections were then washed with PBS and counterstained with 10 μg/mL DAPI in PBS and mounted using SlowFade Gold.

Fluorescent immunohistochemistry using paraformaldehyde – fixed sections

Cerebral cortices from wild-type, DAG1 CKO or LAMA2 -/- littermates at postnatal days 1 and 8 were fixed with 4% paraformaldehyde (PFA) by submersion for 16 to 24 hours. Mice postnatal day 15 and beyond were anesthetized and perfused intracardially with saline, followed by filtered 4% PFA. Brains were removed and post-fixed for 2 hours in 4% PFA, washed with PBS, then equilibrated in a gradient of 20% followed by 30% sucrose at 4° C. Brains were frozen in TissueTek OCT using a liquid nitrogen bath, and coronal cryostat sections of 20 to 35 μm were prepared. Sections were blocked in 10% DS with 0.2-0.5% Triton-X-100 for 1 hour before incubating overnight with primary antibodies at 4°C. Sections were then washed and incubated with either Cy3 or Dylight488 conjugated secondary antibodies in blocking solution for 1 hour, followed by DAPI counter stain, and mounted with SlowFade Gold. To evaluate Glut-1 immunoreactivity, postnatal day 21 sections were post-fixed with 2:1 ethanol acetic acid for 20 minutes at -20º C prior to immunostaining as described. Evaluation of the vasculature (CD31) and gliovascular interface (GFAP and AQP4) was performed with sections heated in Antigen Retrieval Solution ph=6 (DAKO) for 30 minutes, followed by PBS washes prior to blocking.

Analysis of astrocyte development

Immunohistochemistry with glial fibrillary acid protein (GFAP) was performed to quantify astrocytes within the cortex of LAMA2 -/- mice and wild-type littermates. PFA-fixed coronal sections were pretreated in PBS for 10 minutes at room temperature before heating at 95º to 99º C for 25 min in 1x Target Retrieval Solution citrate buffer (ph 6.0, Dako). Sections were then cooled at room temperature for 15 minutes. Prior to blocking with 10% Donkey serum with 0.5% Triton-X-100 for 1 hour, sections were washed with PBS to remove residual antigen retrieval solution. Immunohistochemistry for GFAP was performed overnight at 4º C. Following primary antibody incubation, slides were washed with PBS then incubated with Dy-Light 488 secondary antibodies for 1 hour, before counterstaining with DAPI and mounting with SlowFade Gold. Sections were imaged using a Zeiss 200M epifluorescence microscope or Zeiss 510 Meta confocal microscope. $GFAP^+$ cell bodies within the cortex were quantified in matching sections of wild-type and LAMA2 -/- using Axiovision Rel. 4.8 software (Zeiss). Number of $GFAP^+$ cells per field and area of GFAP immunoreactivity per field in the cortex was analyzed on a minimum of three matched sections, five images per region of interest were acquired for each LAMA2 -/- and WT pairs (n=3). Equal intensity thresh-holding was applied to maximum image projections in each region for mutants and wild type controls to obtain area of GFAP coverage. Area of total GFAP immunoreactivity coverage was then normalized to total $GFAP^+$ cells per field of view. Protein levels of GFAP were quantified using whole cortex lysates obtained from LAMA2 -/- and wild type littermate controls at postnatal day 21.

Analysis of gross vascular morphology

Blood vessels were visualized by utilizing collagen IV immunohistochemistry and imaged using an LSM Meta 510 microscope (Carl Zeiss). For analysis of vascular density and complexity, five corresponding areas in three pairs of LAMA2 -/- and wild type mice were analyzed at postnatal day 21. Blood vessel area was quantified in maximum image projections and normalized to the total vessel length per field. Vascular complexity was quantified by counting the number of branch points along each vessel per field. The number of branch points was standardized to 100 μm segments of the vasculature.

Analysis of α-SMA vascular coverage

To quantify the degree of α-smooth muscle actin coverage along VSMCs, we utilized α-SMA immunohistochemistry in combination with pan-laminin immunohistochemistry, to visualize VSMCs and vascular basal lamina, respectively. Frozen cortical sections (25 μm) of wild-type and LAMA 2-/- mice at postnatal days 21-22 were fixed in acetone at -20º C for 10 minutes followed by several washes with PBS. Sections were then blocked with 10% Donkey Serum with 0.2% Triton-X-100 at room temperature for 1 hour. Primary antibody incubation was performed at 4º C overnight. Area of α-SMA immunoreactivity relative to the total area of vascular pan-laminin immunoreactivity per field in the cortex and striatum were analyzed on a minimum of three matched sections, five images per region of interest were acquired for each LAMA2 -/- and WT pairs (n=3). Equal intensity thresh-holding was applied to maximum image projections in each region for mutants and wild type controls to obtain area of α-SMA coverage. Intensity thresh-holding of pan-Laminin immunoreactivity was adjusted appropriately to reflect total vascular coverage per field. Area of total α-SMA immunoreactivity coverage was then normalized to total vascular coverage per field of view.

Analysis of Glut-1 vascular coverage

To quantify the degree of the glucose transporter, Glut-1 coverage along the vasculature, we utilized Glut-1 immunohistochemistry in combination with pan-Laminin immunohistochemistry, to visualize Glut-1 transporters and blood vessels, respectively. Frozen cortical sections (25 μm) of wild-type and LAMA 2-/- or DAG1 CKO mice at postnatal days 21-22 were fixed in acetone at -20º C for 10 minutes followed by several washes with PBS. Sections were then blocked with 10% Donkey Serum at room temperature for 1 hour. Primary antibody incubation was performed at 4º C overnight. Area of Glut-1 immunoreactivity relative to the total area of vascular pan-Laminin immunoreactivity per field in the cortex were analyzed on a minimum of three matched sections, five images per region of interest were acquired for each LAMA2 -/- or DAG1 CKO and WT pairs (n=3). Equal intensity thresh-holding was applied to maximum image projections in each region for mutants and wild type controls to obtain area of Glut-1 coverage. Intensity thresh-holding of pan-Laminin immunoreactivity was adjusted appropriately to reflect total vascular coverage per field. Area of total Glut-1 immunoreactivity coverage was then normalized to total vascular coverage per field of view.

Analysis of MECA32 vascular coverage

To quantify the degree of MECA32 coverage along the vasculature, we utilized MECA32 immunohistochemistry in combination with pan-Laminin immunohistochemistry, to visualize MECA32 expression and blood vessels, respectively. Frozen cortical sections (25 μm) of wild-type and LAMA 2-/- mice at postnatal days 21-22 were fixed in acetone at -20º C for 10 minutes followed by several washes with PBS. Sections were then blocked with 10% Donkey Serum with 0.5% Triton-X-100 at room temperature for 1 hour. Primary antibody incubation was

performed at 4º C overnight. Area of MECA32 immunoreactivity relative to the total area of vascular pan-Laminin immunoreactivity per field in the cortex, striatum and hippocampus were analyzed on a minimum of three matched sections, five images per were acquired for each LAMA2 -/- and WT pairs (n=3). MECA32 immunoreactivity was confirmed in both LAMA2 -/- and WT mice by acquiring a representative field from the circumventricular region of the brainstem that expresses MECA32. Equal intensity thresh-holding was applied to maximum image projections in each region for mutants and wild type controls to obtain area of MECA32 coverage. Intensity thresh-holding of pan-laminin immunoreactivity was adjusted appropriately to reflect total vascular coverage per field. Area of total MECA32 immunoreactivity coverage was then normalized to total vascular coverage per field of view.

Blood-brain barrier permeability assay

Postnatal day 21 mice were either injected with 0.2 micron filtered 2% Evans blue in saline (150 µl / 10g of body weight) intraperitoneally or anesthetized and perfused with Evans blue intracardially. Following an acute 30-minute dye circulation, mice were anesthetized and perfused with 150 µl of saline. To verify systemic dye distribution kidney tissue was analyzed to confirm successful circulation. Analysis of cortical extravasation of Evans blue was performed by dissecting and weighing cerebral cortices following dye circulation and snap freezing cortices in liquid nitrogen, storing samples at -80°C. Evans blue dye extraction for all samples was processed in parallel, performed by immersing cortices (n=4) in 500 µl of formamide in a shaking heat block at 65° C for 24 hours. Samples were centrifuged at 13.2k RPM for 30 minutes, and the supernatant was removed for analysis. Absorbance at 620 nm was measured using a florescent plate reader. Visualization of dye extravasation in cerebral cortices and

cerebella of fresh tissue was obtained by mounting dried tissue with DAPI Fluromount (SouthernBioTech) and imaging immediately using an inverted Zeiss Axioplan epifluorescence microscope.

Brain water content

Mice approximately three weeks of age were euthanized, and their brains were rapidly dissected. Isolated cerebral cortices were weighed to obtain wet mass and then snap frozen in liquid nitrogen and stored. A total of n=9 mice were processed concurrently in a vacuum oven (Savant Speed Vac SC110) for 16 hours at -1,000 mbar (Savant VP Two Stage Vacuum Pump) to completely desiccate cortices. The percentage of brain water content was calculated by: (wet mass – dry mass) x 100/ (wet mass).

Analysis of iba-1 positive microglia

Immunohistochemistry with monocyte-specific antigens was performed to quantify microglia within the striatum of LAMA2 -/- mice and wild-type littermates. PFA-fixed coronal sections were pretreated in PBS for 10 minutes at room temperature before heating at 95º to 99º C for 25 min in 1x Target Retrieval Solution citrate buffer (ph 6.0, Dako). Sections were then cooled at room temperature for 15 minutes. Prior to blocking with 10% Donkey serum with 0.5% Triton-X-100 for 1 hour, sections were washed with PBS to remove residual antigen retrieval solution. Immunohistochemistry for Iba-1, a calcium binding protein found in microglia, was performed overnight at 4º C. Following primary antibody incubation, slides were washed with PBS then incubated with Dy-Light 488 secondary antibodies for 1 hour, before counterstaining with DAPI and mounting with SlowFade Gold. Sections were imaged using a

Zeiss 200M epiflurescence microscope or Zeiss 510 Meta confocal microscope. Iba-1^+ cells within the striatum were quantified in matching sections of wild-type and LAMA2 -/- using Axiovision Rel. 4.8 software (Carl Zeiss, Germany). Number of Iba-1^+ cells per field in the striatum were analyzed on a minimum of three matched sections, five images per region of interest were acquired for each LAMA2 -/- and WT pairs. Qualitative analysis of Iba-1^+ cells was determined by morphological characteristics of cell bodies and retracted processes consistent with activated microglial phenotypes.

Analysis of β-Dystroglycan immunoreactivity on astrocytic endfeet

To quantify the relationship between LAMA2 and the attachment of astrocytic endfeet via β-dystroglycan, we utilized β-dystroglycan immunohistochemistry in combination with GFAP immunohistochemistry. GFAP endfeet making contact with β-dystroglycan positive vessels, extending back to an astrocyte cell body were counted as β-dystroglycan positive (+) astrocytes. Whereas, GFAP processes that extended from an astrocyte cell body, but not in contact a β-dystroglycan immunoreactive vessel were counted as β-dystroglycan negative (-). Data was obtained from a minimum of three matched sections, 3 images (20x magnification) per region of interest were acquired for each LAMA2 -/- and WT pairs (n=3).

Analysis of β1-integrin vascular coverage

To quantify the degree of β1-integrin coverage along the vasculature, we utilized β1-Integrin immunohistochemistry in combination with collagen IV immunohistochemistry, to visualize the adhesion receptor β1-integrin and blood vessels, respectively. Frozen cortical sections (25 μm) of wild-type and LAMA 2-/- or DAG1 CKO mice at postnatal days 21-22 were

fixed in acetone at -20º C for 10 minutes followed by several washes with PBS. Sections were then blocked with 10% Donkey Serum with 0.5% Triton-X-100 at room temperature for 1 hour. Primary antibody incubation was performed at 4º C overnight. Area of β1-integrin immunoreactivity relative to the total area of vascular collagen IV immunoreactivity per field in the cortex were analyzed on a minimum of three matched sections, five images were acquired for each LAMA2 -/- and WT pairs (n=3). Equal intensity thresh-holding was applied to maximum image projections in each region for mutants and wild type controls to obtain area of β1-integrin coverage. Intensity thresh-holding of collagen IV immunoreactivity was adjusted appropriately to reflect total vascular coverage per field. Area of total β1-integrin immunoreactivity coverage was then normalized to total vascular coverage per field of view.

Analysis of AQP4 clusters along astrocytic endfeet

To quantify the degree of AQP4 coverage along astrocytic endfeet, we utilized AQP4 immunohistochemistry in combination with GFAP immunohistochemistry, to visualize the osmotic regulatory channel AQP4 and astrocyte endfeet, respectively. PFA-fixed coronal sections were pretreated in PBS for 10 minutes at room temperature before heating at 95º to 99º C for 25 min in 1x Target Retrieval Solution citrate buffer (ph 6.0, Dako). Sections were then cooled at room temperature for 15 minutes. Prior to blocking with 10% Donkey serum with 0.5% Triton-X-100 for 1 hour, sections were washed with PBS to remove residual antigen retrieval solution. Sections were then blocked with 10% Donkey Serum with 0.5% Triton-X-100 at room temperature for 1 hour. Primary antibody incubation was performed at 4º C overnight. Area of AQP4 immunoreactivity relative to the total length vessel length, ensheathed by circumferential astrocytic endfeet, per field in the cortex were analyzed on a minimum of three matched sections,

five images per region of interest were acquired for each LAMA2 -/- or DAG1 CKO and WT pairs (n=3). Equal intensity thresh-holding was applied to maximum image projections in each region for mutants and wild type controls to obtain area of AQP4 coverage. The total vessel length per field in each region for mutants and wild type controls was calculated, area of total AQP4 immunoreactivity coverage was then normalized to total vascular length per field of view.

Analysis of pericyte vascular coverage

To quantify the degree of pericyte coverage along the vasculature, we utilized PDGFR-β immunohistochemistry in combination with collagen IV immunohistochemistry, to visualize pericytes and blood vessels, respectively. Frozen cortical sections (25 μm) of wild-type and LAMA 2-/- mice at postnatal days 21-22 were fixed in acetone at -20º C for 10 minutes followed by several washes with PBS. Sections were then blocked with 10% Donkey Serum with 0.5% Triton-X-100 at room temperature for 1 hour. Primary antibody incubation was performed at 4º C overnight. Area of PDGFR-β immunoreactivity relative to the total area of vascular collagen IV immunoreactivity per field in the frontal cortex, striatum and hippocampus were analyzed on a minimum of three matched sections, five images per region of interest were acquired for each LAMA2 -/- and WT pairs. Equal intensity thresh-holding was applied to maximum image projections in each region for mutants and wild type controls to obtain area of PDGFR-β coverage. Intensity thresh-holding of collagen IV immunoreactivity was adjusted appropriately to reflect total vascular coverage per field. Area of total PDGFR-β immunoreactivity coverage was then normalized to total vascular coverage per field of view.

Analysis of laminin vascular coverage

To quantify the specific endothelial laminin chain coverage along the vasculature, we utilized laminin α4, α5 and γ1 immunohistochemistry. Frozen cortical sections (25 μm) of wild-type and LAMA 2-/- mice at postnatal days 21-22 were fixed in acetone at -20º C for 10 minutes followed by several washes with PBS. Sections were then blocked with 10% Donkey Serum with 0.5% Triton-X-100 at room temperature for 1 hour. Primary antibody incubation was performed at 4º C overnight. Area of either laminin α4, α5 or γ1 immunoreactivity relative to the total area of vascular immunoreactivity per field in the cortex were analyzed on a minimum of three matched sections, five images per region of interest were acquired for each LAMA2 -/- and WT pairs (n=3). Equal intensity thresh-holding was applied to maximum image projections in each region for mutants and wild type controls to obtain area of laminin coverage. Then, intensity thresh-holding was adjusted to determine total vascular (laminin) coverage per field. Area of total endothelial laminin immunoreactivity coverage was then normalized to total vascular coverage per field of view.

Western blot analysis

Cerebral cortices were removed, dissected free of meninges and frozen in liquid nitrogen from wild-type and LAMA2-/- littermates at postnatal days 1, 8, 15 and 21. Tissues were pulverized immediately preceding lysis followed by lysis in 1% SDS, 20 mM Tris pH 7.4 with protease and phosphatase inhibitor cocktails (Calbiochem) at 95º C for 10 min, with occasional trituration. Supernatant was collected following centrifugation at 16.1 RCF for 10 minutes and protein concentration was determined (Bio-Rad). Laemmli solubilizing buffer with 2% β-mercaptoethanol was added to lysates and incubated at 95º C for 5 minutes. Proteins were then

separated by SDS-PAGE using 7.5, 10, or 12% acrylamide minigels and transferred to 0.45 μm nitrocellulose. Membranes were blocked in Tris-buffered saline with 0.1% Tween-20 (TBS-T) containing either 1% nonfat milk or 4% bovine serum albumin for 1 hour, followed by primary antibody incubation overnight in blocking buffer at 4º C. Membranes were washed in TBS-T, incubated for 1 hour with fluorescent-conjugated antibodies diluted at 1:5,000 in blocking buffer, washed with TBS-T and then visualized using a LICOR Odyssey Classic. Alternatively, membranes were washed with TBS-T, incubated with anti-biotin secondary antibodies diluted at 1: 10,000 in blocking buffer followed by anti-streptavidin antibodies diluted at 1: 5,000. Relative protein level quantifications were determined using the Odyssey Infrared Imaging System (Ver. 3.0) analysis program.

Transmission electron microscopy

Postnatal day twenty-two littermate mice were processed for electron microscopy by intracardially perfusion with 4% paraformaldehyde/ 2.5% glutaraldehyde in 0.1 M PBS. Brains were removed and post-fixed overnight at 4º C. Brains were cut along the coronal plane on a Leica VT-1000 Vibratome at a thickness of 50-60 μm. Samples were processed as previously described [149]. Processed samples were viewed using a Tecnai^{TM} Spirit BioTwin G^2 transmission electron microscope (FEI Company). Images were acquired with an AMT XR-60 CCD Digital Camera System (Advanced Microscopy Techniques Corp.). The basal lamina ultrastructure of the gliovascular interface and tight junction morphology in the hippocampus of LAMA2 -/- and wild type control littermate mice was analyzed and compared on acquired images using Adobe Photoshop 5.5. Quantification of discontinuous regions of gliovascular basal lamina in LAMA2 -/- and wild-type litter mate controls were determined by counting the

number of breaches per length of basal lamina in a minimum of 10 vessel fields per genotype (n=4). Discontinuous basal lamina regions were identified and expressed as the number of total number of breaches over the total length observed.

Astrocyte cultures

For experiments including dystroglycan (IIH6) and integrin β1 (HA 2/5) blocking antibodies, primary cortical astrocyte cultures were prepared from postnatal day 0-2 rat cortices (Sprague-Dawley, Harlan) and cultured at 37º C, 7.5% CO_2 in poly-D-lysine (PDL) coated flasks with high-glucose Dulbecco's modified Eagle's medium (DMEM) containing 10% fetal calf serum (FCS) and Penicillin/Streptomycin. Media was changed every 3-4 days for two-weeks to obtain mixed glial cultures containing oligodendrocyte progenitor cells (OPCs) and microglia on astrocyte monolayers. OPCs and microglia were removed from the astrocyte monolayer by physical agitation for approximately 16 hours on an orbital shaker. Remaining astrocytes were removed from the flasks using trypsin-EDTA and resuspended in modified Sato's medium containing 0.5% FCS (differentiation medium) and plated on Permanox 8-well chamber slides (NalgeNunc) coated with 10 μg/mL PDL at a density of 10,000 cells/ well. Four days after seeding, the cells were incubated with IIH6, HA 2/5 or isotype control antibodies in differentiation medium for 2 hours preceding 7 hours treatment with 20 nM murine laminin-111 (Sigma-Aldrich). Cells were then fixed with methanol for 5 min at -20º C.

Primary cortical astrocytes from postnatal day 0-2 wild type and LAMA2 -/- mice were prepared as described above. Genotyping was performed to identify homozygous wild-type and LAMA2 -/- cultures derived from individual pups. Astrocytes were resuspended in differentiation media and grown for four days in eight-well chamber slides coated with either

PDL or with Laminin-211 (purified human merosin; Millipore Corporation). Laminin-211 slides were prepared by pre-coating with PDL at 37º C for 1 hour, washing twice with water, then incubating with laminin-211 at 37º C for 4 hours, followed by 3 washes in PBS.

Analysis of aquaporin 4 clusters

The surface area of aquaporin 4 (AQP4) clusters and the total area of GFAP immunoreactivity were determined on images following intensity thresholding using the NIH ImageJ Processing and Analysis Program. Cluster areas were defined as areas of intense AQP4 immunoreactivity as determined by uniformly applied intensity thresh-holding. The area occupied by these intensely AQP4 immunoreactive regions, relative to total GFAP area coverage, was calculated per field. Within each experiment (5 fields per group, blocking experiments; 2 wells/ group, wild-type/ LAMA2 -/- experiments: min 3 wells/ group, n=3), images were acquired utilizing identical parameters on an inverted Zeiss Axioplan epifluorescence microscope fitted with a 10x eyepiece and 20x (0.5 NA) objective. High-magnification AQP4 images were captured with a 63x oil immersion objective. All images were acquired using a Zeiss Axiocam MRM digital camera controlled by Zeiss Axiovision software.

Statistical Analysis

Statistical significance of brain water content, cortical Evans Blue dye extravasation, GFAP/iba-1 positive cell density, GFAP area, vascular coverage of pericyte (PDGFR-β)/ α-SMA/ β1-integrin/MECA32, vascular density complexity or density and protein quantification by western immunoblotting was determined using the Student's two-tailed t-test. Statistical significance of AQP4 cluster analysis was determined using the one-way Holm-Sidak ANOVA

for pair-wise comparisons or Student's two-tailed t-test where indicated. Statistical significance of TEM analysis was determined using the Mann-Whitney Rank Sum test. All analysis was conducted using SigmaPlot 11.0 (Systat Software Inc). Bars represent the mean values, with error bars depicting standard error of the mean (SEM).

References

1. Redzic, Z., *Molecular biology of the blood-brain and the blood-cerebrospinal fluid barriers: similarities and differences.* Fluids Barriers CNS, 2011. **8**(1): p. 3.
2. Baeten, K.M. and K. Akassoglou, *Extracellular matrix and matrix receptors in blood-brain barrier formation and stroke.* Dev Neurobiol, 2011. **71**(11): p. 1018-39.
3. Abbott, N.J., L. Ronnback, and E. Hansson, *Astrocyte-endothelial interactions at the blood-brain barrier.* Nat Rev Neurosci, 2006. **7**(1): p. 41-53.
4. Abbott, N.J., et al., *Structure and function of the blood-brain barrier.* Neurobiol Dis, 2010. **37**(1): p. 13-25.
5. Obermeier, B., R. Daneman, and R.M. Ransohoff, *Development, maintenance and disruption of the blood-brain barrier.* Nat Med, 2013. **19**(12): p. 1584-96.
6. Zlokovic, B.V., *The blood-brain barrier in health and chronic neurodegenerative disorders.* Neuron, 2008. **57**(2): p. 178-201.
7. Carvey, P.M., B. Hendey, and A.J. Monahan, *The blood-brain barrier in neurodegenerative disease: a rhetorical perspective.* J Neurochem, 2009. **111**(2): p. 291-314.
8. Stewart, P.A. and M.J. Wiley, *Developing nervous tissue induces formation of blood-brain barrier characteristics in invading endothelial cells: a study using quail--chick transplantation chimeras.* Dev Biol, 1981. **84**(1): p. 183-92.
9. Forster, C., *Tight junctions and the modulation of barrier function in disease.* Histochem Cell Biol, 2008. **130**(1): p. 55-70.
10. Huber, J.D., R.D. Egleton, and T.P. Davis, *Molecular physiology and pathophysiology of tight junctions in the blood-brain barrier.* Trends Neurosci, 2001. **24**(12): p. 719-25.
11. Wolburg, H. and A. Lippoldt, *Tight junctions of the blood-brain barrier: development, composition and regulation.* Vascul Pharmacol, 2002. **38**(6): p. 323-37.
12. Harhaj, N.S. and D.A. Antonetti, *Regulation of tight junctions and loss of barrier function in pathophysiology.* Int J Biochem Cell Biol, 2004. **36**(7): p. 1206-37.
13. Kniesel, U. and H. Wolburg, *Tight junctions of the blood-brain barrier.* Cell Mol Neurobiol, 2000. **20**(1): p. 57-76.
14. Sofroniew, M.V. and H.V. Vinters, *Astrocytes: biology and pathology.* Acta Neuropathol, 2010. **119**(1): p. 7-35.
15. Zhang, Y. and B.A. Barres, *Astrocyte heterogeneity: an underappreciated topic in neurobiology.* Curr Opin Neurobiol, 2010. **20**(5): p. 588-94.
16. Allaman, I., M. Belanger, and P.J. Magistretti, *Astrocyte-neuron metabolic relationships: for better and for worse.* Trends Neurosci, 2011. **34**(2): p. 76-87.
17. Nguyen, J.V., et al., *Myelination transition zone astrocytes are constitutively phagocytic and have synuclein dependent reactivity in glaucoma.* Proc Natl Acad Sci U S A, 2011. **108**(3): p. 1176-81.
18. Janzer, R.C. and M.C. Raff, *Astrocytes induce blood-brain barrier properties in endothelial cells.* Nature, 1987. **325**(6101): p. 253-7.
19. Gee, J.R. and J.N. Keller, *Astrocytes: regulation of brain homeostasis via apolipoprotein E.* Int J Biochem Cell Biol, 2005. **37**(6): p. 1145-50.
20. Hayashi, Y., et al., *Induction of various blood-brain barrier properties in non-neural endothelial cells by close apposition to co-cultured astrocytes.* Glia, 1997. **19**(1): p. 13-26.

21. Sun, D., C. Lytle, and M.E. O'Donnell, *IL-6 secreted by astroglial cells regulates Na-K-Cl cotransport in brain microvessel endothelial cells.* Am J Physiol, 1997. **272**(6 Pt 1): p. C1829-35.
22. Igarashi, Y., et al., *Glial cell line-derived neurotrophic factor induces barrier function of endothelial cells forming the blood-brain barrier.* Biochem Biophys Res Commun, 1999. **261**(1): p. 108-12.
23. Sobue, K., et al., *Induction of blood-brain barrier properties in immortalized bovine brain endothelial cells by astrocytic factors.* Neurosci Res, 1999. **35**(2): p. 155-64.
24. Alvarez, J.I., et al., *The Hedgehog pathway promotes blood-brain barrier integrity and CNS immune quiescence.* Science, 2011. **334**(6063): p. 1727-31.
25. Milsted, A., et al., *Astrocyte cultures derived from human brain tissue express angiotensinogen mRNA.* Proc Natl Acad Sci U S A, 1990. **87**(15): p. 5720-3.
26. Wosik, K., et al., *Angiotensin II controls occludin function and is required for blood brain barrier maintenance: relevance to multiple sclerosis.* J Neurosci, 2007. **27**(34): p. 9032-42.
27. Chen, Z.L., et al., *Ablation of astrocytic laminin impairs vascular smooth muscle cell function and leads to hemorrhagic stroke.* J Cell Biol, 2013. **202**(2): p. 381-95.
28. Menezes, M.J., et al., *The extracellular matrix protein laminin alpha2 regulates the maturation and function of the blood-brain barrier.* J Neurosci, 2014. **34**(46): p. 15260-80.
29. Daneman, R., et al., *The mouse blood-brain barrier transcriptome: a new resource for understanding the development and function of brain endothelial cells.* PLoS One, 2010. **5**(10): p. e13741.
30. Allt, G. and J.G. Lawrenson, *Pericytes: cell biology and pathology.* Cells Tissues Organs, 2001. **169**(1): p. 1-11.
31. Armulik, A., et al., *Pericytes regulate the blood-brain barrier.* Nature, 2010. **468**(7323): p. 557-61.
32. Winkler, E.A., R.D. Bell, and B.V. Zlokovic, *Central nervous system pericytes in health and disease.* Nat Neurosci, 2011. **14**(11): p. 1398-405.
33. Lindahl, P., et al., *Pericyte loss and microaneurysm formation in PDGF-B-deficient mice.* Science, 1997. **277**(5323): p. 242-5.
34. Hellstrom, M., et al., *Lack of pericytes leads to endothelial hyperplasia and abnormal vascular morphogenesis.* J Cell Biol, 2001. **153**(3): p. 543-53.
35. Tallquist, M.D., W.J. French, and P. Soriano, *Additive effects of PDGF receptor beta signaling pathways in vascular smooth muscle cell development.* PLoS Biol, 2003. **1**(2): p. E52.
36. Lindblom, P., et al., *Endothelial PDGF-B retention is required for proper investment of pericytes in the microvessel wall.* Genes & Development, 2003. **17**(15): p. 1835-1840.
37. Li, F., et al., *Endothelial Smad4 maintains cerebrovascular integrity by activating N-cadherin through cooperation with Notch.* Dev Cell, 2011. **20**(3): p. 291-302.
38. Yurchenco, P.D., P.S. Amenta, and B.L. Patton, *Basement membrane assembly, stability and activities observed through a developmental lens.* Matrix Biol, 2004. **22**(7): p. 521-38.
39. Yurchenco, P.D. and B.L. Patton, *Developmental and pathogenic mechanisms of basement membrane assembly.* Curr Pharm Des, 2009. **15**(12): p. 1277-94.

40. Barber, A.J. and E. Lieth, *Agrin accumulates in the brain microvascular basal lamina during development of the blood-brain barrier.* Dev Dyn, 1997. **208**(1): p. 62-74.
41. Lukes, A., et al., *Extracellular matrix degradation by metalloproteinases and central nervous system diseases.* Mol Neurobiol, 1999. **19**(3): p. 267-84.
42. Fukuda, S., et al., *Focal cerebral ischemia induces active proteases that degrade microvascular matrix.* Stroke, 2004. **35**(4): p. 998-1004.
43. Agrawal, S., et al., *Dystroglycan is selectively cleaved at the parenchymal basement membrane at sites of leukocyte extravasation in experimental autoimmune encephalomyelitis.* J Exp Med, 2006. **203**(4): p. 1007-19.
44. Baumann, E., et al., *Post-ischemic hypothermia attenuates loss of the vascular basement membrane proteins, agrin and SPARC, and the blood-brain barrier disruption after global cerebral ischemia.* Brain Res, 2009. **1269**: p. 185-97.
45. Cardoso, F.L., D. Brites, and M.A. Brito, *Looking at the blood-brain barrier: molecular anatomy and possible investigation approaches.* Brain Res Rev, 2010. **64**(2): p. 328-63.
46. Miner, J.H. and P.D. Yurchenco, *Laminin functions in tissue morphogenesis.* Annu Rev Cell Dev Biol, 2004. **20**: p. 255-84.
47. Hallmann, R., et al., *Expression and function of laminins in the embryonic and mature vasculature.* Physiol Rev, 2005. **85**(3): p. 979-1000.
48. Durbeej, M., *Laminins.* Cell Tissue Res, 2010. **339**(1): p. 259-68.
49. Miner, J.H., *Laminins and their roles in mammals.* Microsc Res Tech, 2008. **71**(5): p. 349-56.
50. Domogatskaya, A., S. Rodin, and K. Tryggvason, *Functional diversity of laminins.* Annu Rev Cell Dev Biol, 2012. **28**: p. 523-53.
51. Yurchenco, P.D., *Basement membranes: cell scaffoldings and signaling platforms.* Cold Spring Harb Perspect Biol, 2011. **3**(2).
52. Aumailley, M., et al., *A simplified laminin nomenclature.* Matrix Biol, 2005. **24**(5): p. 326-32.
53. Scheele, S., et al., *Laminin isoforms in development and disease.* J Mol Med (Berl), 2007. **85**(8): p. 825-36.
54. Yurchenco, P.D., Y.S. Cheng, and H. Colognato, *Laminin forms an independent network in basement membranes.* J Cell Biol, 1992. **117**(5): p. 1119-33.
55. Colognato, H., D.A. Winkelmann, and P.D. Yurchenco, *Laminin polymerization induces a receptor-cytoskeleton network.* J Cell Biol, 1999. **145**(3): p. 619-31.
56. Timpl, R., et al., *Structure and function of the laminin-nidogen complex.* Ann N Y Acad Sci, 1990. **580**: p. 311-23.
57. Erickson, A.C. and J.R. Couchman, *Still more complexity in mammalian basement membranes.* J Histochem Cytochem, 2000. **48**(10): p. 1291-306.
58. Chung, A.E., et al., *Biological functions of entactin.* Kidney Int, 1993. **43**(1): p. 13-9.
59. Halfter, W., et al., *A critical function of the pial basement membrane in cortical histogenesis.* J Neurosci, 2002. **22**(14): p. 6029-40.
60. Willem, M., et al., *Specific ablation of the nidogen-binding site in the laminin gamma1 chain interferes with kidney and lung development.* Development, 2002. **129**(11): p. 2711-22.
61. Yousif, L.F., J. Di Russo, and L. Sorokin, *Laminin isoforms in endothelial and perivascular basement membranes.* Cell Adh Migr, 2013. **7**(1): p. 101-10.

62. Sixt, M., et al., *Endothelial cell laminin isoforms, laminins 8 and 10, play decisive roles in T cell recruitment across the blood-brain barrier in experimental autoimmune encephalomyelitis.* J Cell Biol, 2001. **153**(5): p. 933-46.
63. Sorokin, L., et al., *Expression of novel 400-kDa laminin chains by mouse and bovine endothelial cells.* Eur J Biochem, 1994. **223**(2): p. 603-10.
64. Abraham, S., et al., *Integrin beta1 subunit controls mural cell adhesion, spreading, and blood vessel wall stability.* Circ Res, 2008. **102**(5): p. 562-70.
65. del Zoppo, G.J. and R. Milner, *Integrin-matrix interactions in the cerebral microvasculature.* Arterioscler Thromb Vasc Biol, 2006. **26**(9): p. 1966-75.
66. Moore, C.J. and S.J. Winder, *Dystroglycan versatility in cell adhesion: a tale of multiple motifs.* Cell Commun Signal, 2010. **8**: p. 3.
67. Moore, S.A., et al., *Deletion of brain dystroglycan recapitulates aspects of congenital muscular dystrophy.* Nature, 2002. **418**(6896): p. 422-5.
68. Thyboll, J., et al., *Deletion of the laminin alpha4 chain leads to impaired microvessel maturation.* Mol Cell Biol, 2002. **22**(4): p. 1194-202.
69. Wu, C., et al., *Endothelial basement membrane laminin alpha5 selectively inhibits T lymphocyte extravasation into the brain.* Nat Med, 2009. **15**(5): p. 519-27.
70. Jucker, M., et al., *Laminin alpha 2 is a component of brain capillary basement membrane: reduced expression in dystrophic dy mice.* Neuroscience, 1996. **71**(4): p. 1153-61.
71. Yoshioka, M., et al., *Seizure-genotype relationship in Fukuyama-type congenital muscular dystrophy.* Brain Dev, 2008. **30**(1): p. 59-67.
72. Allamand, V. and P. Guicheney, *Merosin-deficient congenital muscular dystrophy, autosomal recessive (MDC1A, MIM#156225, LAMA2 gene coding for alpha2 chain of laminin).* Eur J Hum Genet, 2002. **10**(2): p. 91-4.
73. Buteica, E., et al., *Merosin-deficient congenital muscular dystrophy type 1A.* Rom J Morphol Embryol, 2008. **49**(2): p. 229-33.
74. Fujii, Y., et al., *Sequential neuroradiological and neurophysiological studies in a Japanese girl with merosin-deficient congenital muscular dystrophy.* Brain Dev, 2011. **33**(2): p. 140-4.
75. Miyagoe-Suzuki, Y., M. Nakagawa, and S. Takeda, *Merosin and congenital muscular dystrophy.* Microsc Res Tech, 2000. **48**(3-4): p. 181-91.
76. Caro, P.A., et al., *MR imaging findings in children with merosin-deficient congenital muscular dystrophy.* AJNR Am J Neuroradiol, 1999. **20**(2): p. 324-6.
77. Yao, Y., et al., *Astrocytic laminin regulates pericyte differentiation and maintains blood brain barrier integrity.* Nat Commun, 2014. **5**: p. 3413.
78. Zaccaria, M.L., et al., *Dystroglycan distribution in adult mouse brain: a light and electron microscopy study.* Neuroscience, 2001. **104**(2): p. 311-24.
79. Waite, A., S.C. Brown, and D.J. Blake, *The dystrophin-glycoprotein complex in brain development and disease.* Trends Neurosci, 2012. **35**(8): p. 487-96.
80. Lien, C.F., et al., *Absence of glial alpha-dystrobrevin causes abnormalities of the blood-brain barrier and progressive brain edema.* J Biol Chem, 2012. **287**(49): p. 41374-85.
81. Nico, B., et al., *Altered blood-brain barrier development in dystrophic MDX mice.* Neuroscience, 2004. **125**(4): p. 921-35.
82. Blake, D.J., et al., *Different dystrophin-like complexes are expressed in neurons and glia.* J Cell Biol, 1999. **147**(3): p. 645-58.

83. Rurak, J., et al., *Distribution of potassium ion and water permeable channels at perivascular glia in brain and retina of the Large(myd) mouse.* J Neurochem, 2007. **103**(5): p. 1940-53.
84. Noel, G., D.K. Tham, and H. Moukhles, *Interdependence of laminin-mediated clustering of lipid rafts and the dystrophin complex in astrocytes.* J Biol Chem, 2009. **284**(29): p. 19694-704.
85. Hynes, R.O., *Integrins: versatility, modulation, and signaling in cell adhesion.* Cell, 1992. **69**(1): p. 11-25.
86. Hynes, R.O., *Integrins: bidirectional, allosteric signaling machines.* Cell, 2002. **110**(6): p. 673-87.
87. Paulus, W., et al., *Characterization of integrin receptors in normal and neoplastic human brain.* Am J Pathol, 1993. **143**(1): p. 154-63.
88. Tagaya, M., et al., *Rapid loss of microvascular integrin expression during focal brain ischemia reflects neuron injury.* J Cereb Blood Flow Metab, 2001. **21**(7): p. 835-46.
89. Milner, R. and I.L. Campbell, *Developmental regulation of beta1 integrins during angiogenesis in the central nervous system.* Mol Cell Neurosci, 2002. **20**(4): p. 616-26.
90. Engelhardt, B. and L. Sorokin, *The blood-brain and the blood-cerebrospinal fluid barriers: function and dysfunction.* Semin Immunopathol, 2009. **31**(4): p. 497-511.
91. Balabanov, R., et al., *CNS microvascular pericytes express macrophage-like function, cell surface integrin alpha M, and macrophage marker ED-2.* Microvasc Res, 1996. **52**(2): p. 127-42.
92. Grazioli, A., et al., *Defective blood vessel development and pericyte/pvSMC distribution in alpha 4 integrin-deficient mouse embryos.* Dev Biol, 2006. **293**(1): p. 165-77.
93. Wagner, S., et al., *Rapid disruption of an astrocyte interaction with the extracellular matrix mediated by integrin alpha 6 beta 4 during focal cerebral ischemia/reperfusion.* Stroke, 1997. **28**(4): p. 858-65.
94. Wang, J. and R. Milner, *Fibronectin promotes brain capillary endothelial cell survival and proliferation through alpha5beta1 and alphavbeta3 integrins via MAP kinase signalling.* J Neurochem, 2006. **96**(1): p. 148-59.
95. Taddei, A., et al., *Endothelial adherens junctions control tight junctions by VE-cadherin-mediated upregulation of claudin-5.* Nat Cell Biol, 2008. **10**(8): p. 923-34.
96. Gavard, J. and J.S. Gutkind, *VE-cadherin and claudin-5: it takes two to tango.* Nat Cell Biol, 2008. **10**(8): p. 883-5.
97. Osada, T., et al., *Interendothelial claudin-5 expression depends on cerebral endothelial cell-matrix adhesion by beta(1)-integrins.* J Cereb Blood Flow Metab, 2011. **31**(10): p. 1972-85.
98. Robel, S., et al., *Conditional deletion of beta1-integrin in astroglia causes partial reactive gliosis.* Glia, 2009. **57**(15): p. 1630-47.
99. Holt, K.H., et al., *Biosynthesis of dystroglycan: processing of a precursor propeptide.* FEBS Lett, 2000. **468**(1): p. 79-83.
100. Ervasti, J.M. and K.P. Campbell, *A role for the dystrophin-glycoprotein complex as a transmembrane linker between laminin and actin.* J Cell Biol, 1993. **122**(4): p. 809-23.
101. Milner, R., et al., *The rapid decrease in astrocyte-associated dystroglycan expression by focal cerebral ischemia is protease-dependent.* J Cereb Blood Flow Metab, 2008. **28**(4): p. 812-23.

102. Del Zoppo, G.J., et al., *Vascular matrix adhesion and the blood-brain barrier.* Biochem Soc Trans, 2006. **34**(Pt 6): p. 1261-6.
103. Vajda, Z., et al., *Delayed onset of brain edema and mislocalization of aquaporin-4 in dystrophin-null transgenic mice.* Proc Natl Acad Sci U S A, 2002. **99**(20): p. 13131-6.
104. Nico, B., et al., *Severe alterations of endothelial and glial cells in the blood-brain barrier of dystrophic mdx mice.* Glia, 2003. **42**(3): p. 235-51.
105. Noell, S., et al., *Evidence for a role of dystroglycan regulating the membrane architecture of astroglial endfeet.* Eur J Neurosci, 2011. **33**(12): p. 2179-86.
106. Dmytrenko, L., et al., *The impact of alpha-syntrophin deletion on the changes in tissue structure and extracellular diffusion associated with cell swelling under physiological and pathological conditions.* PLoS One, 2013. **8**(7): p. e68044.
107. Anderova, M., et al., *Altered astrocytic swelling in the cortex of alpha-syntrophin-negative GFAP/EGFP mice.* PLoS One, 2014. **9**(11): p. e113444.
108. Eilert-Olsen, M., et al., *Deletion of aquaporin-4 changes the perivascular glial protein scaffold without disrupting the brain endothelial barrier.* Glia, 2012. **60**(3): p. 432-40.
109. Sandoval, K.E. and K.A. Witt, *Blood-brain barrier tight junction permeability and ischemic stroke.* Neurobiol Dis, 2008. **32**(2): p. 200-19.
110. Liotta, L.A., et al., *Effect of plasminogen activator (urokinase), plasmin, and thrombin on glycoprotein and collagenous components of basement membrane.* Cancer Res, 1981. **41**(11 Pt 1): p. 4629-36.
111. Li, L., et al., *Upregulation of fibronectin and the alpha5beta1 and alphavbeta3 integrins on blood vessels within the cerebral ischemic penumbra.* Exp Neurol, 2012. **233**(1): p. 283-91.
112. Li, L., et al., *In the hypoxic central nervous system, endothelial cell proliferation is followed by astrocyte activation, proliferation, and increased expression of the alpha 6 beta 4 integrin and dystroglycan.* Glia, 2010. **58**(10): p. 1157-67.
113. Steiner, E., et al., *Loss of astrocyte polarization upon transient focal brain ischemia as a possible mechanism to counteract early edema formation.* Glia, 2012. **60**(11): p. 1646-59.
114. Bozzi, M., et al., *Enzymatic processing of beta-dystroglycan recombinant ectodomain by MMP-9: identification of the main cleavage site.* IUBMB Life, 2009. **61**(12): p. 1143-52.
115. Masocha, W., et al., *Cerebral vessel laminins and IFN-gamma define Trypanosoma brucei brucei penetration of the blood-brain barrier.* J Clin Invest, 2004. **114**(5): p. 689-94.
116. Girardin, F., *Membrane transporter proteins: a challenge for CNS drug development.* Dialogues Clin Neurosci, 2006. **8**(3): p. 311-21.
117. Daneman, R., et al., *Pericytes are required for blood-brain barrier integrity during embryogenesis.* Nature, 2010. **468**(7323): p. 562-6.
118. Reese, T.S. and M.J. Karnovsky, *Fine structural localization of a blood-brain barrier to exogenous peroxidase.* J Cell Biol, 1967. **34**(1): p. 207-17.
119. Colognato, H. and P.D. Yurchenco, *Form and function: the laminin family of heterotrimers.* Dev Dyn, 2000. **218**(2): p. 213-34.
120. Jimenez-Mallebrera, C., et al., *Congenital muscular dystrophy: molecular and cellular aspects.* Cell Mol Life Sci, 2005. **62**(7-8): p. 809-23.
121. Shue, E.H., et al., *Plasmalemmal vesicle associated protein-1 (PV-1) is a marker of blood-brain barrier disruption in rodent models.* BMC Neurosci, 2008. **9**: p. 29.

122. Ioannidou, S., et al., *An in vitro assay reveals a role for the diaphragm protein PV-1 in endothelial fenestra morphogenesis.* Proc Natl Acad Sci U S A, 2006. **103**(45): p. 16770-5.
123. Schulz, M. and B. Engelhardt, *The circumventricular organs participate in the immunopathogenesis of experimental autoimmune encephalomyelitis.* Cerebrospinal Fluid Res, 2005. **2**: p. 8.
124. Yu, D., et al., *Early cerebrovascular inflammation in a transgenic mouse model of Alzheimer's disease.* Neurobiol Aging, 2012. **33**(12): p. 2942-7.
125. Cannella, B., A.H. Cross, and C.S. Raine, *Adhesion-related molecules in the central nervous system. Upregulation correlates with inflammatory cell influx during relapsing experimental autoimmune encephalomyelitis.* Lab Invest, 1991. **65**(1): p. 23-31.
126. Engelhardt, B., F.K. Conley, and E.C. Butcher, *Cell adhesion molecules on vessels during inflammation in the mouse central nervous system.* J Neuroimmunol, 1994. **51**(2): p. 199-208.
127. Komarova, Y. and A.B. Malik, *Regulation of endothelial permeability via paracellular and transcellular transport pathways.* Annu Rev Physiol, 2010. **72**: p. 463-93.
128. Hallmann, R., et al., *Novel mouse endothelial cell surface marker is suppressed during differentiation of the blood brain barrier.* Dev Dyn, 1995. **202**(4): p. 325-32.
129. Wang, S., et al., *Venular basement membranes contain specific matrix protein low expression regions that act as exit points for emigrating neutrophils.* J Exp Med, 2006. **203**(6): p. 1519-32.
130. Voisin, M.B., D. Probstl, and S. Nourshargh, *Venular basement membranes ubiquitously express matrix protein low-expression regions: characterization in multiple tissues and remodeling during inflammation.* Am J Pathol, 2010. **176**(1): p. 482-95.
131. Sparks, D.L., et al., *Alterations of Alzheimer's disease in the cholesterol-fed rabbit, including vascular inflammation. Preliminary observations.* Ann N Y Acad Sci, 2000. **903**: p. 335-44.
132. Amiry-Moghaddam, M., et al., *Delayed K+ clearance associated with aquaporin-4 mislocalization: phenotypic defects in brains of alpha-syntrophin-null mice.* Proc Natl Acad Sci U S A, 2003. **100**(23): p. 13615-20.
133. Amiry-Moghaddam, M., et al., *An alpha-syntrophin-dependent pool of AQP4 in astroglial end-feet confers bidirectional water flow between blood and brain.* Proc Natl Acad Sci U S A, 2003. **100**(4): p. 2106-11.
134. Guadagno, E. and H. Moukhles, *Laminin-induced aggregation of the inwardly rectifying potassium channel, Kir4.1, and the water-permeable channel, AQP4, via a dystroglycan-containing complex in astrocytes.* Glia, 2004. **47**(2): p. 138-49.
135. Ji, K. and S.E. Tsirka, *Inflammation modulates expression of laminin in the central nervous system following ischemic injury.* J Neuroinflammation, 2012. **9**: p. 159.
136. Fernandez-Klett, F., et al., *Early loss of pericytes and perivascular stromal cell-induced scar formation after stroke.* J Cereb Blood Flow Metab, 2013. **33**(3): p. 428-39.
137. Ohab, J.J. and S.T. Carmichael, *Poststroke neurogenesis: emerging principles of migration and localization of immature neurons.* Neuroscientist, 2008. **14**(4): p. 369-80.
138. Hayashi, S. and A.P. McMahon, *Efficient recombination in diverse tissues by a tamoxifen-inducible form of Cre: a tool for temporally regulated gene activation/inactivation in the mouse.* Dev Biol, 2002. **244**(2): p. 305-18.

139. Battiste, J., et al., *Ascl1 defines sequentially generated lineage-restricted neuronal and oligodendrocyte precursor cells in the spinal cord.* Development, 2007. **134**(2): p. 285-93.
140. Begley, D.J., *Brain superhighways.* Sci Transl Med, 2012. **4**(147): p. 147fs29.
141. Iliff, J.J., et al., *A paravascular pathway facilitates CSF flow through the brain parenchyma and the clearance of interstitial solutes, including amyloid beta.* Sci Transl Med, 2012. **4**(147): p. 147ra111.
142. Yang, L., et al., *Evaluating glymphatic pathway function utilizing clinically relevant intrathecal infusion of CSF tracer.* J Transl Med, 2013. **11**: p. 107.
143. Bradbury, M.W., H.F. Cserr, and R.J. Westrop, *Drainage of cerebral interstitial fluid into deep cervical lymph of the rabbit.* Am J Physiol, 1981. **240**(4): p. F329-36.
144. Szentistvanyi, I., et al., *Drainage of interstitial fluid from different regions of rat brain.* Am J Physiol, 1984. **246**(6 Pt 2): p. F835-44.
145. Johnston, M., *The importance of lymphatics in cerebrospinal fluid transport.* Lymphat Res Biol, 2003. **1**(1): p. 41-4; discussion 45.
146. Abbott, N.J., *Evidence for bulk flow of brain interstitial fluid: significance for physiology and pathology.* Neurochem Int, 2004. **45**(4): p. 545-52.
147. Iliff, J.J., et al., *Impairment of glymphatic pathway function promotes tau pathology after traumatic brain injury.* J Neurosci, 2014. **34**(49): p. 16180-93.
148. Miyagoe, Y., et al., *Laminin alpha2 chain-null mutant mice by targeted disruption of the Lama2 gene: a new model of merosin (laminin 2)-deficient congenital muscular dystrophy.* FEBS Lett, 1997. **415**(1): p. 33-9.
149. Relucio, J., et al., *Laminin regulates postnatal oligodendrocyte production by promoting oligodendrocyte progenitor survival in the subventricular zone.* Glia, 2012. **60**(10): p. 1451-67.
150. Tronche, F., et al., *Disruption of the glucocorticoid receptor gene in the nervous system results in reduced anxiety.* Nat Genet, 1999. **23**(1): p. 99-103.